Manufacturing Highly Expanded Thermoplastic Polyurethane Foams Using Novel Injection Molding Foaming Technologies

By

HRISHIKESH ASHOKRAO KHARBAS

A dissertation submitted in partial fulfillment of the requirements for the degree of

Doctor of Philosophy

Mechanical Engineering

University of Wisconsin–Madison, Madison, WI, USA

2016

Date of final oral examination: 26th April 2016

This dissertation is approved by the following members of the Final Oral Committee:

Lih-Sheng Turng, Professor, Mechanical Engineering

Tim Osswald, Professor, Mechanical Engineering

Frank Pfefferkorn, Associate Professor, Mechanical Engineering

Natalie Rudolph, Assistant Professor, Mechanical Engineering

Robert Rowlands, Professor, Mechanical Engineering

ABSTRACT

This thesis summarizes the studies undertaken to achieve the objective of manufacturing injection-molded thermoplastic polyurethane (TPU) foams with high density reductions, desirable microstructures, and customizable properties. TPU foams are quickly gaining market share in numerous applications in the sports and recreation as well as manufacturing industries. This is because TPU foams can be easily manufactured in a variety of densities, hardnesses, and mechanical properties, ranging from highly resilient to highly compressible foams, with different processing methods, such as injection molding, casting, and extrusion. Typically, TPUs are being foamed to a minimum density of 0.40 g/cm^3 (400 kg/m^3). It is the aim of this thesis to expand the understanding and processing knowledge of manufacturing TPU foams with densities as low as 0.25 g/cm^3 (250 kg/m^3), while maintaining desirable microstructures. It is also an aim of this thesis to develop a novel process to control foam properties locally in injection molded TPU foams. In the journey toward achieving the aforementioned objectives, five studies were conducted and are presented in this manuscript.

An experimental study evaluating the CBA and PBA foaming of TPU has been undertaken. A novel foam injection molding process using CO_2 + N_2 as co-blowing agents to exploit the synergistic benefits of co-blowing agents was also evaluated in this study. It was found that PBA foaming can be vastly advantageous for foaming TPU by enabling large reductions in bulk densities without the harmful effects of chemical residue. This novel process of using co-blowing agents yielded the lowest bulk density while achieving the highest cell density and finest average cell size.

To resolve the issue of low melt strength at higher temperatures, which leads to cell coalescence and undesirable microstructures, the use of a physical cross-linking agent was considered. It was proposed that a physical cross-linking agent could increase the melt strength of the TPU at higher temperatures, thus enabling aggressive foaming strategies to give enhanced density reductions. It is shown here that extremely low-density TPU foams of bulk density 0.16 g/cm^3 (160 kg/m^3) can be achieved consistently.

In Chapter 3, nanoclay as a reinforcing filler was employed to increase the melt viscosity and to trigger heterogeneous nucleation in the TPU matrix, thereby improving the foamability of TPU while achieving a homogenous microstructure with low average cell size and high cell density. It is generally known that TPU's rebound resilience values decrease with decreasing foam density. It was observed that rebound resilience values could increase significantly if a tunable alignment of microcells can be produced within the part, even while reducing bulk densities. Through the action of mold inserts, the expanding microcells will thereby stretch and align with the intercellular TPU walls and individual molecules in the direction of mold opening. With aligned microcells, the softness of the foams improved significantly, while achieving lower hysteresis loss ratios or energy loss (dissipation).

In Chapter 5, a core retraction mold capable of increasing cavity volume was designed and manufactured to enable further study of the phenomenon observed in Chapter 4, with better parameter control. Polypropylene (PP) was the material chosen to validate the capabilities of the mold and the applicability of this technology to materials other than TPU. Core retraction was used with the conventional microcellular injection molding (MIM) process to foam thick PP

parts with high density reductions of 30% and 55%. The cavity volume was modified by changing the retraction distance, which resulted in varying density reductions. The lowest densities were achieved with a core retraction-aided microcellular injection molding (CR-MIM) process, the results of which could not have been achieved by the conventional MIM process alone. It was shown that the CR-MIM process yielded a better microstructure and a higher tensile modulus than the conventional MIM process. Use of core retraction also yielded more consistent densities and tensile properties at different distances from the gate location. It was shown that by using delay times and holding pressures, cell nucleation and cell growth can be delayed to a more suitable time and melt temperature.

Mechanical and energy absorption properties of TPU foam can be varied with the density and microstructure of the foam. In Chapter 6, a new process is developed using core retraction and out-of-mold foaming to develop injection molded parts of varying cross-sections with varying mechanical properties. It was shown that, using this process, very low density foams of less than 0.25 g/cm^3 can be produced while maintaining uniform and good microstructures. It was also shown that this technology can be effectively used to vary microstructures, densities, and mechanical properties within an injection molded part locally, depending on the application.

In summary, the aforementioned approaches have helped to advance the knowledge of manufacturing TPU foams and other regular thermoplastics with customizable microstructures and mechanical properties for various specific applications.

ACKNOWLEDGEMENTS

First and foremost, I would like to express my appreciation to my advisor, Professor Lih-Sheng (Tom) Turng, without whose guidance, support, and encouragement this work would not have been possible. His dedication toward my research work and also toward my personal growth has been a constant sense of encouragement and motivation for me. He is one of the main reasons that I was able to gather enough courage to take a break from my career in industry and return to glorious Madison to pursue my Ph.D. All that Professor Turng has done for me over the past many years is far too much to expect from a professor or even a close friend. I am indebted to him for all my life.

I would like to thank Professor Tim A. Osswald, Professor Frank Pfefferkorn, Professor Robert Rowlands, and Professor Natalie Rudolph for serving on my defense committee. Their valuable ideas, advice, and instruction in the fields of polymers and other related fields of engineering will be helpful for my future work and study.

I would also like to acknowledge the support of Mihai Manitiu and Guenter Scholz at BASF Corporation, Jay Constantinou and Ryan Mace at Nike Corporation, and Mark Hartwick at Hoffer Plastics for their invaluable inputs to my research. My research would not have been possible without the brainstorming, help, and suggestions from my friends Tom Ellingham, Jason McNulty, Xiaofei Sun, Cyrus Thompson, Reba Shotwell, Xinchao Wang, Yiyan Peng, and other Bionates and PEC members. I would like to thank Chris Lacey for the patient editing of my publications and this document. Part of this research is supported by the Wisconsin Institute for

Discovery (WID) and the Polymer Engineering Center Industrial Consortium at the University of Wisconsin–Madison.

I am thankful to my family for their continued support and encouragement. Their commitment to do all that is needed to allow me the freedom to pursue my dreams is a big enabler for me. A special note of thanks to my wife, Punita, my children, and my parents for cheering me on through my efforts.

Last but not the least, I would like to thank my team at Amul Parlours, including my cousins, Shweta and Kannaiah, for being up to the challenge of managing the business without my physical presence. This would not have been possible without them.

DEDICATION

To my family for their love, support, and patience.

TABLE OF CONTENTS

LIST OF FIGURES

LIST OF TABLES

NOMENCLATURE

CBA	Chemical blowing agent
CFC	Chlorofluorocarbons
CO_2	Carbon dioxide
CR-MIM	Core retraction-assisted microcellular injection molding
DSC	Differential scanning calorimetry
HCFC	Hydrochlorofluorocarbons
HLR	Hysteresis loss ratio
HS	Hard segment
LDPE	Low density polyethylene
MIM	Microcellular injection molding
N_2	Nitrogen
PBA	Physical blowing agent
PC	Polycarbonate
PP	Polypropylene
PVA	Polyvinyl alcohol
RIM	Reaction injection molding
SCF	Supercritical fluid
$scCO_2$	Supercritical carbon dioxide
SEM	Scanning electron microscope
SIFT	Supercritical fluid-laden pellets injection molding foaming technology
SIM	Sacrificial injection molding

SS	Soft segment
T_g	Glass transition temperature
TGA	Thermogravimetric analysis
TPU	Thermoplastic polyurethane

1 LITERATURE SURVEY

1.1 Background

The plastics industry is one of the largest manufacturing industries in the United States, accounting for more than $465 billion in annual shipments and 1.4 million jobs [1]. The total plastics consumption in the world has risen from 7 million tons in 1960 to 300 million tons in 2010, and is conservatively estimated to grow at 5.4% every year. Since 1976, plastics have been the most widely used materials in the U.S., surpassing steel, copper, and aluminum combined by volume. Plastics play an indispensable role in a wide variety of markets, ranging from packaging and building/construction to transportation, consumer and institutional products, furniture and furnishings, electronics, and more. Today, plastics are broadly integrated into our lifestyle and make a major, irreplaceable contribution to virtually all product areas. Plastics continue to replace conventional materials in old applications and find newer applications because of their low cost and processing benefits. While plastics have become ubiquitous, petroleum resources remain finite, and the cost of fossil-based plastics will continue to increase. As the need for thermoplastic resins for domestic consumption increases, there is a great demand for plastic processing technologies that can help provide environmental friendly solutions to reduce plastics consumption per product while maintaining product quality and properties. Among all of the plastics processing methods, injection molding and extrusion account for more than two-thirds of all polymer processes [2]. Special injection molding and extrusion processes that reduce material consumption are highly desirable from the viewpoint of not only reducing production costs but also helping sustain natural resources while saving the environment.

Due to the increasing demand for light-weight, insulating, and shock absorbing materials, polymeric foams were invented and have now become an important part of polymer production. Research on polymeric foams in the context of materials, blowing agents, equipment, and processing methodologies has been conducted in academia and industry for the last 100 years. It is reported that the global polymeric foam market is expected to reach 18 million tons by 2015 [3]. Polymer foams are typically produced using chemical blowing agents (CBAs) or physical blowing agents (PBAs). Earlier, a lot of PBAs such as chlorofluorocarbons (CFCs) and hydrochlorofluorocarbons (HCFCs), which were essentially low boiling point liquids, were used for this purpose. Following environmental concerns of their harmful effects on the ozone layer, they were discontinued and slowly phased out. Chemical foaming involves the use of CBAs, which decompose at processing temperatures and release gases such as CO_2 and N_2 [4]. The gas(es) released lead to nucleation and growth of the cell structure. On the other hand, during the physical foaming process, no chemical reaction occurs. The foaming occurs because of phase change and separation from the polymer matrix due to the introduction of thermodynamic instability [5] [6]. Each method has its inherent benefits and processing challenges, which are discussed later in this thesis.

1.2 Chemical Foaming Process

Chemical foaming is the most widely used method of foaming plastics because of its simplicity, ease of use, lack of machinery modification, and low capital investment. Almost all CBAs are solids and can be mixed with the polymer in the desired amount and stored at room temperature [7]. CBAs are thermally unstable and will decompose or dissolve at the processing

temperatures of the polymer, yielding one or more gases [8] [9]. The gas(es) produced will nucleate due to thermodynamic instability and give a cellular structure to the polymer matrix. The desirable properties of a CBA [10] include the following: (1) a decomposition temperature within the processing range of the polymer for which it is being used, (2) a steady decomposition rate, (3) safe and stable at normal room temperature, (4) easily mixable with a uniform distribution, (5) high gas yield per unit weight, (6) non-corrosive for tools, and (7) prevents heat built up and degradation of the polymer matrix. Chemical blowing agents can be placed into two categories: endothermic and exothermic. Endothermic CBAs absorb heat during decomposition, while exothermic CBAs generate heat during the blowing process. Most endothermic CBAs generate CO_2 gas upon decomposition, which is safe, stable, and improves the processability of the polymer due to the inherent plasticizing effect of low molecular weight CO_2. Moreover, as the heat is absorbed during the blowing process, it helps reduce the cooling time during the injection molding process, thereby reducing processing time and increasing productivity. The most commonly used endothermic CBA is sodium bicarbonate, which decomposes at 140°C and generates CO_2 and water as it decomposes [11]. Endothermic CBAs are widely used in many injection molding applications and in extruding rigid PVC foam profiles where the endothermic nature and controlled rate of decomposition of these blowing agents help in forming a desirable solid skin layer on the exterior of the profile.

Exothermic CBAs generate heat upon decomposition, and usually have a higher yield of gas per weight of CBA. Most of the exothermic CBAs are derived from dydrazine, such as sulphonyldydrazines, pure and modified azodicarbonamide, tetrazoles, and dihydrooxadiazinones [11]. The major gas released upon decomposition is N_2, with sometimes small amounts of other gases

such as CO, CO_2, and ammonia (NH_3). Recently, combinations of endothermic and exothermic CBAs have been tried in an effort to take advantage of the desirable characteristics of both components—the higher yield and expansion of exothermic CBAs and the cooling and stabilizing characteristics of the endothermic CBAs—yielding better microstructures of foamed parts.

However, chemical foaming has a lot of drawbacks that limit its application. For one thing, CBAs are polymer and application specific, with major constraints of decomposition temperature and undesirable reactions with a specific polymer matrix. Extra heat generated in the blowing process can cause some polymers to degrade. Almost certainly, a residue is left behind in the chemical reaction that ensues, which can act as nucleating sites for the gas to evolve and grow, but at the end of the process. This is usually undesirable as it tends to reduce the integrity and strength of the polymer and can have harmful effects on mold surfaces [12]. Furthermore, the use of CBAs usually leads to a less than desirable microstructure [13] and significantly increases the raw material input cost of the product [14].

1.3 Physical Foaming Process

In the physical foaming process, the polymer and a physical blowing agent (PBA) are initially mixed to form a homogenous mixture in which the PBA is dissolved completely or partially in the polymer matrix. When a thermodynamic instability, such as a temperature or pressure change, is applied to the solution, the solubility and miscibility of these two components with each other are reduced. As a result, phase change and phase separation are induced, which lead to cell nucleation and growth processes. Cell nucleation and growth occur at elevated temperatures, which are above the glass transition temperature (T_g) of the polymer. In this pro-

cess, no chemical reaction occurs. There are many types of PBAs which have been successfully applied in this process, and they can be divided into two types: organic and inorganic.

Organic PBAs were used widely in the past because they were easily miscible, cheaper, and easier to control. Organic PBAs are typically low boiling organic liquids, such as pentane, HFCs, HCFCs, and hydrocarbons such as isobutene. One big drawback of this type of PBA is the emission of harmful substances to the environment. Previously, chlorofluorocarbons (CFCs) were used extensively, but were eventually replaced by HCFCs due to serious concerns about the ozone depleting potential of CFCs [15]. However, although the effects are less than those caused by CFCs, HCFCs are also harmful to the earth's ozone layer, and were eventually phased out in Europe for the production of foams in 2004 [15]. Meanwhile, the Montreal Protocol indicates that the use of HCFCs in all applications be reduced in stages, and will be completely phased out by 2020 in developed countries [16]. While other organic blowing agents do not have as much impact on the ozone layer, many of them have other safety or environmental issues. Because of the detrimental effects associated with their use, coupled by the scale at which they were used especially in the foaming of polyurethanes, research and development attention has shifted toward using inorganic PBAs to produce polymeric foams. Although the solubility and plastication effects are much lower than in organic PBAs, inorganic PBAs are more environmentally safe. Inorganic PBAs that have been successfully applied in foaming processes include carbon dioxide (CO_2), nitrogen (N_2), argon (Ar), helium (He), and water [17] [18] [19]. CO_2 is the most versatile inorganic PBA because it has many unique properties such as being nonflammable, nontoxic, relatively inexpensive, has an easy to reach supercritical state (critical temperature, 31.1 °C and critical pressure, 7.38 MPa), and has relatively large solubility in

polymers [20, 21]. Dissolving CO_2 into polymers affects their properties in both their melt and solid states due to its plastication effect. It depresses the glass transition temperature and the crystallization temperature [6], as well as the viscosity and surface tension of the polymer melt [22-24]. Besides CO_2, N_2 is also very widely used. It is the least expensive physical foaming agent, and it is also inert and nontoxic. N_2 has a lower solubility as compared to CO_2. This suggests that smaller amounts of N_2 are needed to achieve a higher degree of super-saturation and foaming [14, 25]. Also, the specific volume of N_2 is higher than CO_2, which, in turn, results in a higher expansion ratio per weight % of the blowing agent [26].

Besides CO_2 and N_2, water (H_2O) has also been used as a PBA in some studies [17, 27]. Microcellular injection molding was also carried out using water as the blowing agent on polycarbonate (PC), and a 10% weight reduction was achieved with a better surface quality compared with using nitrogen [17]. However, its low solubility in polymers, corrosive nature with steel, and the moisture degradation tendency of most polymers prevents its more widespread use as an effective PBA. Noble gases, including Ar and He, were also reported in some studies as PBAs [18]. However, they are quite expensive, and their solubility in the polymer is very low compared with N_2 and CO_2. Since N_2 and CO_2 are most widely used and have the most outstanding processability and resulting foam morphologies, the following discussions in this study only focus on N_2 and CO_2 as the PBAs.

1.4 Microcellular Foaming Processes

Microcellular foaming is a major innovation in plastics technology and has the potential to significantly affect the plastics industry. Conceived in the 1980's at MIT by Prof. Nam Suh [28],

microcellular foaming uses supercritical fluids such as physical blowing agents and is capable of creating foams with an average cell size of 100 μm or less. Since its inception, a lot of research focused on this novel foaming method has yielded results, and new batch foaming processes have proven that nanoscale cells are possible [29]. Microcellular foaming has been done in batch processes and continuous processes. Microcellular foaming in injection molding and extrusion has been gathering widespread interest from companies in all manufacturing sectors because of some obvious benefits of weight reduction [30], better dimensional control [31], and acoustic and heat transfer damping characteristics. This research will concentrate on the developments of microcellular foaming for injection molding applications, which have the potential of significantly affecting the plastics industry. The processing attributes of this technology opens up the avenue for newer applications with plastics and widens the processing window for manufacturing with polymers. This breakthrough foam process enhances product design, improves processing efficiency, and reduces product cost. Some of the benefits of microcellular foaming in injection molding are mentioned below.

Trexel Inc. incorporated the idea of microcellular foaming in an injection process known as microcellular injection molding (MIM) and commercialized it as the MuCell process [2]. Upgrading this batch foaming process to adapt to semi-continuous and continuous processes such as injection molding and extrusion is the single most important breakthrough for the foaming industry in the past 30 years. MIM continues to attract attention because of the benefits of improved dimensional stability, while realizing reductions in part weight and energy costs, when compared with conventional injection molding. Despite the considerable advantages offered by this process, microcellular injection molding is by no means a panacea for all molding problems or

superior to its conventional counterpart in all aspects. Among other concerns of microstructure consistency, process control, and surface finish, huge capital investment in machinery and licensing fees is one of the main setbacks for implementation. MIM requires a special supercritical fluid (SCF) delivery and dosage system, and a specially designed screw-barrel for every machine, which is extremely costly and requires significant changes to the machine [32, 33].

1.4.1 Advantages

Weight Reduction

Recently, there has been an increasing need for lightweight, high performance parts in industry. As compared to conventional injection molding, microcellular injection molding (MIM) can achieve weight reductions as high as 50% [18]. Microcellular injection molding technology has been demonstrated to work with a myriad of commercial and engineering polymers. This technology can bring about significant savings by producing lightweight parts with reduced material consumption.

Cycle Time Reductions and Dimensional Stability

The endothermic process of cell nucleation and growth results in rapid cooling and solidification of the polymer melt [30] and thus reduces the total time for cooling that the part needs before it is ejected from the mold. Furthermore, because of the weight savings, there is a lesser amount of plastic to cool, which further reduces the cooling time. Sink marks are common surface defects formed on injection molded parts because of the shrinkage of the plastic melt after cooling, while warpage is the bending or deformation of the part resulting in dimensional

instability during assembly. In general, warpage is caused by uneven shrinkage in an injection molded part and is caused by a myriad of factors such as unbalanced filling and cooling, poor part and mold designs, and anisotropy in molecular and fiber orientations. In microcellular injection molding, the internal pressure of the nucleating gas compensates for any shrinkage. A uniform microstructure throughout the part can make shrinkage in the entire part uniform and thus reduce warpage. Since the internal pressure arising from foaming eliminates the sink marks and improves the dimensional stability of the molded parts, little or no packing pressure is needed to pack out the mold. As a result, pack and hold time can be reduced or entirely eliminated. Cycle time savings as high as 50% have been reported for some applications [18].

Reduced Energy Requirements for Injection and Clamping

As the gas fills the interstitial spaces between the polymer molecules, it effectively reduces the viscosity of the polymer [13, 34, 35]. The reduced viscosity of the polymer melt allows for injection of the polymer inside the mold at significantly lower pressures. As discussed earlier, the packing pressure and time are also reduced in microcellular injection molding. Because of the lower injection pressures, the requirements on clamping are significantly reduced. Microcellular injection molding can lead to up to a 48% reduction in injection pressures and a 30% reduction in clamp pressures [36].

Improvements in Physical Properties

As the gas forms a homogenous mixture with the polymer, it reduces the glass transition temperature of the polymer melt [35, 37, 38]. Therefore, processing temperatures of materials can be reduced significantly. This opens a window to process temperature-sensitive additives in

high-melt-temperature polymers such as polycarbonate (PC) and polyamides (PA). Furthermore, the microcells serve as crack arrestors by blunting crack tips, thereby greatly enhancing part toughness, fatigue life, and impact strength [37].

1.4.2 Process Physics

Microcellular injection molding (MIM) is comprised of three steps; namely, (1) dissolution of gas in the polymer matrix, (2) nucleation of microcells, and (3) growth and coalescence of microcells to form the final foam structure. These steps are described as follows.

Dissolution of Gas in the Polymer Matrix

The dissolution of gas in the polymer can be achieved by saturating the polymer with SCF, either during the injection molding cycle or before the material is introduced into the screw barrel system. Most of the current technologies that are capable of MIM differ in their approach to adding and mixing the SCF with the polymer. The melt is deliberately maintained at high pressure to ensure that the gas remains in solution with the polymer. The saturation of the polymer by the gas is usually accomplished by vigorous mixing and diffusion. The diffusion coefficients in various polymers are on the order of 1×10^{-5} to 1×10^{-7} cm^2/s for nitrogen and carbon dioxide, respectively [37]. Table 1.1 lists the estimated diffusion coefficients of nitrogen and carbon dioxide gases in commonly used polymers. Table 1.2 enumerates the estimated diffusion times determined by Park [24] at various striation thicknesses and diffusion coefficients without shear for the purposes of the batch foaming process.

Table 1.1: Estimated diffusion coefficients (D) of gases in common polymers at elevated temperatures [37].

Polymer	D of CO_2 (cm^2/s)		D of N_2 (cm^2/s)	
	at 188 °C	at 200 °C	at 188 °C	at 200 °C
PS	—	1.3×10^{-5}	—	1.5×10^{-5}
PP	4.2×10^{-5}	—	3.5×10^{-5}	—
PE	—	2.6×10^{-6}	—	8.8×10^{-7}
HDPE	5.7×10^{-5}	2.4×10^{-5}	6.0×10^{-5}	2.5×10^{-5}
LDPE	—	1.1×10^{-4}	—	1.5×10^{-4}
PTFE	—	7.0×10^{-6}	—	8.3×10^{-6}
PVC	—	3.8×10^{-5}	—	4.3×10^{-5}

Table 1.2: Estimated diffusion times by Park [24] at various striation thicknesses and diffusion coefficients.

Striation Thickness (S)	Diffusion Coefficient (D)			
	10^{-5} cm^2/s	10^{-6} cm^2/s	10^{-7} cm^2/s	10^{-8} cm^2/s
1 μm	1 x 10^{-3} sec	0.01 sec	0.1 sec	1 sec
10 μm	0.1 sec	1 sec	10 sec	100 sec
50 μm	2.5 sec	25 sec	4 min	42 min
100 μm	10 sec	100 sec	17 min	3 hrs
250 μm	63 sec	10 min	2 hrs	17 hrs
500 μm	4 min	42 min	7 hrs	3 days
750 μm	9 min	94 min	16 hrs	7 days
1 mm	17 min	3 hrs	28 hrs	12 days

Nucleation of Cells

During the injection phase, the shot is injected under pressure into the cavity. The suddenly induced thermodynamic instability (which can be obtained either by the rapid decrease in pressure or the rapid increase in temperature) decreases the gas solubility in the polymer so that the gas starts emerging from the solution via nucleation. Depending on the thermodynamic state, the gas nucleates at different points in the matrix. The number of sites at which the gas nucleates is governed by various factors [6, 39] such as the amount of thermodynamic instability induced by the sudden pressure drop, the decrease in the interfacial tension between the polymer and the gas, and the presence of high-energy sites like impurities, crystals, fillers, etc., that facilitate the nucleation process.

Growth and Coalescence of Microcells to Form the Final Foam Structure

The growth of microcells and the final microstructure depend on the number of nucleating sites and the time at which the microcells nucleate. The microcells that nucleate earlier have a tendency to grow larger [23]. They have a lower energy level than the microcells nucleating at a later time. These smaller microcells coalesce into larger cells to achieve a lower energy level, thus making the larger bubbles grow even larger. The difference between the internal pressures of the gas and the surface tensions produced due to the interfacial forces produced between the gas–polymer interfaces and the strength of the solidifying polymer melt determine the growth of the cells.

1.5 Development of Microcellular Injection Molding

Microcellular injection molding enables molders to reduce material consumption while producing strong, lightweight products. Microcellular technology was developed by Professor Nam. P. Suh and his graduate student, Jane Martini, at Massachusetts Institute of Technology (MIT) in response to a problem posed by Mr. Gordon Brown of the Eastman Kodak Company. Eastman Kodak aimed to reduce the plastic consumption in their products without compromising their toughness [37]. The idea was to replace the volume occupied by plastic material with tiny bubbles having sizes less than the size of naturally occurring flaws in the polymer. This was accomplished by saturating the polymer with supercritical fluid (SCF) (e.g., nitrogen or carbon dioxide) and later inducing a thermodynamic instability to reduce the dissolubility of the gas in the polymer. The reduced solubility resulted in nucleation of the gas at numerous sites in the polymer, thus forming microcellular structures. Since its inception, a lot of work has been done with microcellular plastics (MCPs) to advance it from a laboratory concept to a technology worthy of worldwide commercialization. Figure 1.1 shows an early design of equipment that was used to produce microcellular plastics. The equipment consisted of a pressure vessel capable of holding highly pressurized atmospheric gases such as nitrogen or carbon dioxide in a super-critical state. Inside the pressure vessel, a plastic sheet or a batch of plastic sheets would be mounted.

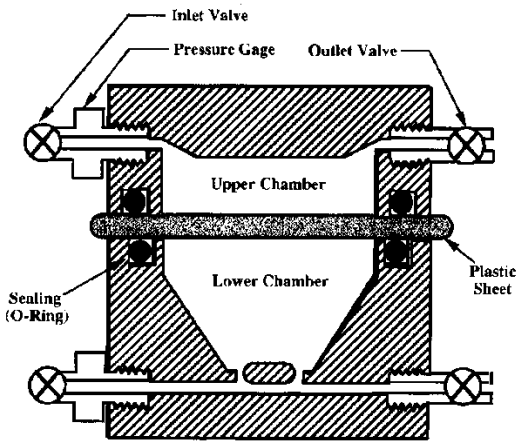

Figure 1.1. Batch processing equipment for manufacturing microcellular plastics.

The polymer sheets could be heated and melted by electric heaters. Since only a batch of plastics could be foamed at a time, this process was known as the batch process of manufacturing microcellular polymers. The batch process consisted of supersaturating the heated polymer in a pressure chamber filled with gas under pressure, and later reducing the pressure drop in the chamber. The process of supersaturation was entirely diffusion driven and would take several hours, if not days, to complete. When a homogenous polymer–gas phase mixture was formed, nucleation was induced by a sudden thermodynamic instability (a significant pressure drop or rapid increase in temperature). This process was successful in producing lightweight parts with various thermoplastics such as polystyrene (PS), polypropylene (PP), polycarbonate (PC), polymethylmethacrylate (PMMA), polyethylene (PE), and some thermosets. Recently a two-step batch foaming process was used to foam various polymers using CO_2 as the physical blowing agent. In the first step, a thin polymer sheet was saturated with supercritical CO_2 (sc-CO_2) at 13.6 MPa at 40 °C for a certain amount of time, followed by the sudden release of pressure. In the

second step, the sheets were immersed in a hot batch for 5–20 sec for foaming and then the cell structure was frozen by immersing it immediately in an ice bath [40]. Figure 1.2 shows micrographs of microcellular plastics foamed by batch foaming.

Although MCPs offered several advantages, one of the major shortcomings of the batch process was the slow production rate. The creation of a saturated polymer–gas mixture within short cycle times and inducing nucleation by creating a sudden pressure drop posed some problems to manufacturing MCPs in a continuous fashion. The work done by Vipin Kumar, Chul Park, Dan Baldwin, and S. W. Cha led to the graduation of the batch process into semi-continuous and continuous applications such as injection molding, thermoforming, and extrusion commercialized with the trade name MuCell. Injection molding with MCPs blends atmospheric gas (usually nitrogen or carbon dioxide) at a high-pressure, high-temperature "supercritical" state with the polymer melt in the screw barrel to create a single-phase polymer–gas solution. To facilitate the fast and homogeneous mixing of the gas and polymer, and to maintain a single-phase solution prior to injection, the melt-pressurization pressure (MPP) inside the screw barrel is typically kept between 12 and 20 MPa. Such a pressure level is approximately one order of magnitude higher than the typical back pressure (generally between 0.3 to 3 MPa) employed in the conventional injection molding process. During injection molding, the sudden pressure drop in the material as it flows through the nozzle triggers the thermodynamic instability of the polymer–gas solution. As a result, the gas starts emerging from the polymer–gas solution and forms numerous microscale cells. Figure 1.3 shows a schematic of injection molding with MCPs and the main components of the MIM system.

Figure 1.4 shows the characteristic microstructures observed in a MIM molded part, including a polymer-rich skin layer. Due to the high cooling rates of injection-molded parts, the rapidly increasing strength of the surrounding matrix ensures minimum nucleation and growth of cells. This ensures that most MIM parts have polymer-rich regions. The size and thickness of this region usually depends on various processing factors such as the mold temperature, gas levels, etc. In general, the size of the cells observed in the part is inversely proportional to the cell density, both of which are determined by cell nucleation and growth, the amount of gas dissolved in the polymer, and other process conditions that affect the state and strength of the melt. As shown in Fig. 1.4, the typical cell diameter in microcellular injection molded parts is on the order of 10–100 microns (as opposed to 250 microns or more with the conventional structural foam molding process).

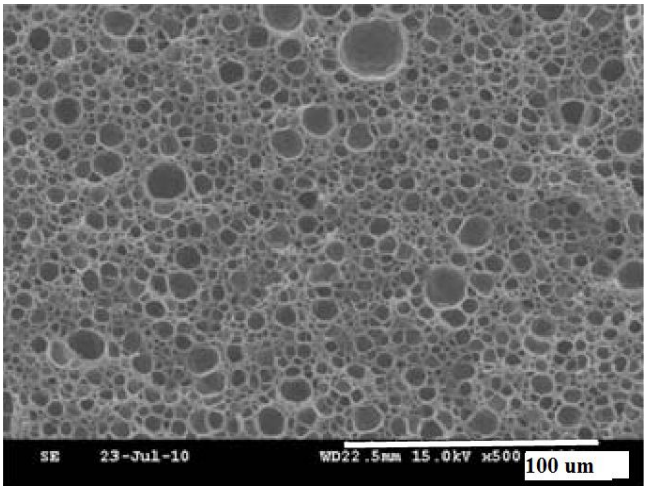

(a) Amorphous PET [40]

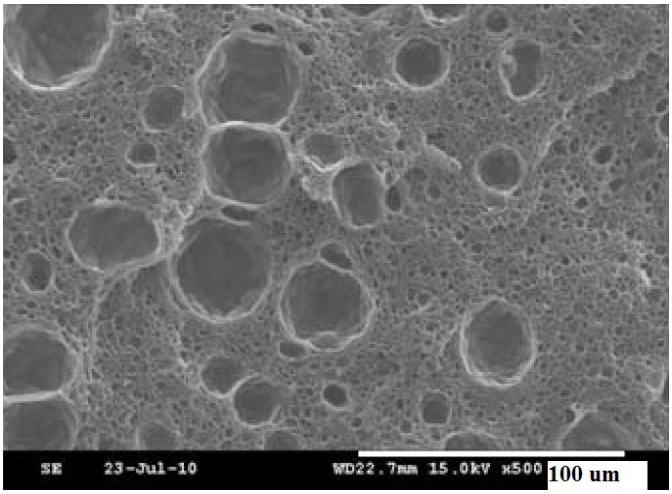

(b) Thermoplastic polyether ester elastomer [40]

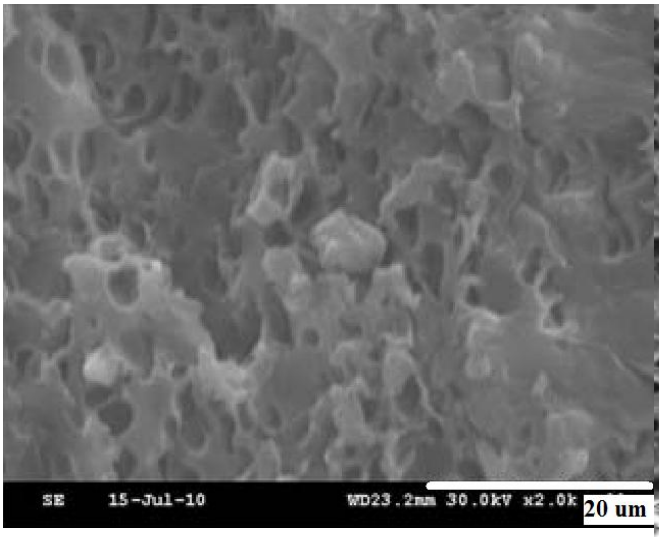

(c) TPU [40]

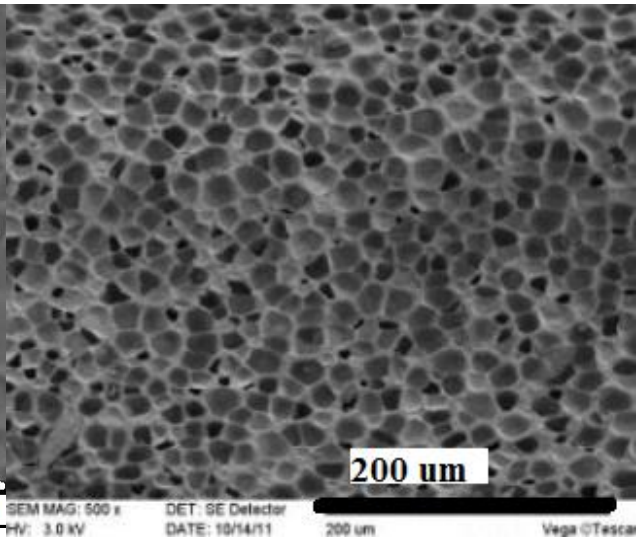

(d) TPU [41]

Figure 1.2. SEM images of various foamed polymers foamed by the batch foaming process.

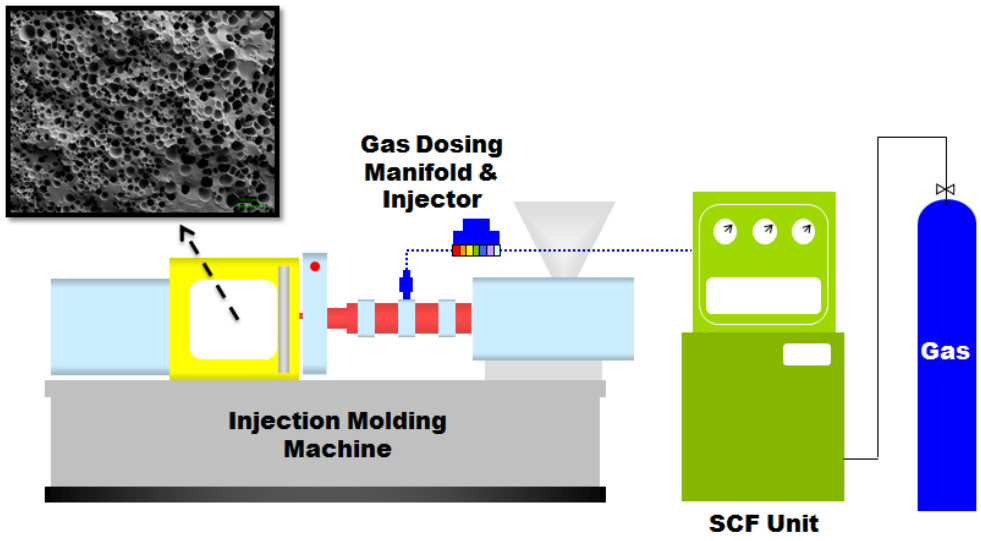

Figure 1.3. Microcellular injection molding system.

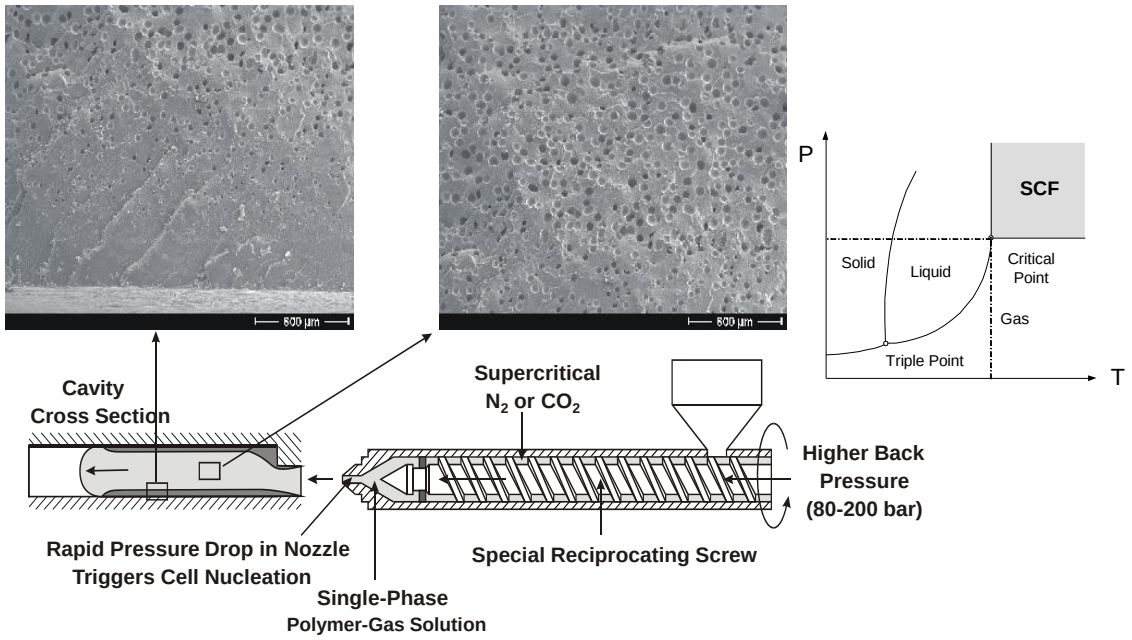

Figure 1.4. Schematic of injection molding of microcellular plastics with characteristic micro-structures.

Despite the considerable advantages offered by this process, microcellular injection molding is by no means a panacea for all molding problems or superior to its conventional counterpart in all aspects. Three of the major problems with microcellular injection molding are (1) the control of the state of thermodynamic instability (via temperature and pressure variation) to create fine and uniform microcells throughout the part, (2) maintenance of critical mechanical properties while realizing material savings, and (3) inferior surface quality of MIM parts. For example, experimental studies indicate that microcellular injection molded parts tend to exhibit a non-uniform distribution of cell size and cell density with certain materials, with inadequate process set-up, or at high levels of SCF content or weight reduction. The continuous and efficient generation of a single-phase polymer–gas solution with proper gas content also poses a challenge during processing. Although microcellular injection molding offers a plausible means to improve the impact strength and bending stiffness-to-weight ratio, the inherent reduction in such mechanical properties as tensile strength, tensile modulus [42], and weld-line strength [43] could hamper the broader industrial implementation of this process in areas of structural components and critical applications. In addition, the frequently occurring swirling pattern on part surfaces could potentially affect cosmetic appearance requirements [44, 45]. Furthermore, as with other emerging processes, the processing know-how for microcellular injection molding has yet to be developed to enable the molding industry to fully realize the process benefits. At present, the process requires changes in machinery components, such as the screw barrel design, and licensing fees. Furthermore, additional machinery is required for each machine to compress, meter, and dose the SCF into the barrel, which is costly and takes up a lot of shop-floor space. The amount of investment in additional machinery, the purchase of costly licenses, and the

changes in basic injection machine components has hindered the ubiquitous use of SCF foaming technology in the field of injection molding.

1.6 Supercritical Gas-Laden Pellets Injection Molding Foaming Technology (SIFT)

Recently, a novel method to produce microcellular injection molded parts was proposed by Lee et al, known as supercritical fluid-laden pellets injection molding foaming technology (SIFT). This method enables the injection molder to achieve foaming with a physical blowing agent without changes to machinery or investment in extra machinery. This is realized in a two-step manner. First, the PBA is injected and mixed into the polymer during an extrusion process. The extruded material is then cooled down very quickly to prevent the gas from foaming in the polymer. The polymer strands, containing the dissolved and trapped SCF gas, are then pelletized. These gas-laden pellets can be prepared either on the manufacturing premises or logistics and distribution can be setup so that they can be distributed as foamable polymer raw materials. The next step is to use these gas-laden pellets in one or multiple conventional injection molding machines for injection molding. Since these pellets still contain gas inside, once melted and blended in the barrel under high temperature and pressure, a single-phase gas–polymer solution can be achieved. As soon as this solution is injected into the mold cavity, it will create foamed injection molded parts due to the cell nucleation induced by the sudden pressure drop and sharp decrease of gas solubility in the polymer, which is a mechanism similar to microcellular injection molding. A schematic of this method is shown in Figure 1.5. The experimental details will be discussed in the next chapter.

Using this method, gas-laden pellets can be produced by an extruder equipped with a gas injection device. Modification and device additions are only needed for one extruder, and the gas-laden pellets produced can be used by multiple conventional injection molding machines to produce lightweight, foamed parts without any modification or additional equipment for the injection molding machines. In this way, the equipment costs, as well as the amount of work to modify the machines, can be significantly reduced. Since extrusion is a continuous process, production efficiency can be ensured. This process employs commonly used physical blowing agents like N_2 or CO_2, and thus general concerns surrounding chemical blowing agents are no longer an issue. A lower degree of saturation can also help reduce the swirling patterns associated with foam molding and yield better quality surfaces [45]. Further studies conducted to validate this technology have shown that weight reductions of up to 10% have been achieved with a good microstructure. Use of fillers, such as nanoclay and talc, can be used effectively to increase nucleation and attain a better and more consistent microstructure [46]. In addition, the lower degree of supersaturation, which is inherent to this process, can delay the nucleation of the cells to help avoid straition and stretch marks, which are seen consistently in the MuCell process [47]. Since extrusion is not an on-line process with injection molding, pellets can be made using different blowing agents, such as N_2 and CO_2, and then mixed in the injection molding process in adequate proportions to achieve the synergistic effects of both blowing agents [48]. It is known that N_2 can achieve a higher degree of supersaturation with limited gas dosage, while CO_2 can assist with cell growth by acting as a plasticiser. Recent usage of this technology with MuCell was tried to achieve low density foams of TPU, and it was seen that the co-blowing agents helped achieve better foaming with TPU [49].

Although this novel technology has the potential to be an ideal and cost effective solution for foaming thermoplastics, there are certain improvements that need to be made before it can be enthusiastically accepted by the plastics industry. The gas trapped in the gas-laden pellets slowly diffuses out, thus reducing the degree of super-saturation. The gas remaining inside of the pellets depends on many factors, such as the starting concentration of the gas in the pellets, the storage conditions, and the time elapsed since the pellets were extruded [33]. The starting concentration of the gas within the pellets is defined as the percentage of gas in the pellets at the end of the extrusion process. This initial concentration depends on a lot of factors such as the amount of gas added during the SIFT process, the throughput of the extruder, and the rate of diffusion after exit from the extruder die and during the cooling of the pellets. Along with this, there is a general lack of process and operating knowledge that needs to be generated to support the commercialization of this technology.

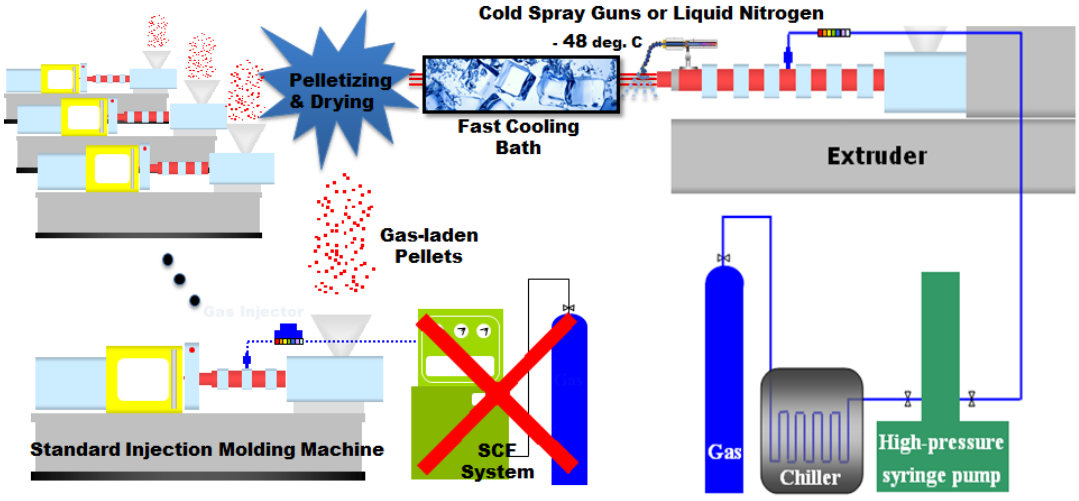

Figure 1.5. Schematic diagram of the SIFT process.

1.7 Thermoplastic Polyurethane

TPU (thermoplastic polyurethane) is becoming a very popular thermoplastic because of its versatility in configuration. The first commercial thermoplastic polyurethanes were established in Germany by Bayer–Fabenfabriken and in the United States by B.F. Goodrich in the 1950's. TPU belongs to a group of thermoplastic elastomers (TPEs) that combine the mechanical properties of vulcanized rubber with the processability of thermoplastics. Unlike rubbers, they can be repeatedly melted and processed due to the absence of strong chemical networks and covalent cross-linking. The most important feature of TPU is that it exhibits the superior properties of an elastomer, while still allowing it to be reprocessed and recycled like a thermoplastic. This property gives it a vast advantage over thermoset polyurethane (PU) and other thermoset elastomers, which cannot be reprocessed and recycled. TPUs are sold as a fully reacted product that can be reshaped into its final form by conventional thermoplastic processing methods such as injection molding, extrusion, and compression molding, or by solvent processing to form coatings, adhesives, and films. The resin consists of linear polymer chains in block structures that are made of alternating soft segments (SS) and hard segments (HS). The HS are made from diisocyanate (e.g., diphenylmethane-4,4-diisocyanate (MDI) by the addition of a chain extender diol (e.g., butanediol)), while the SS consist of long flexible polyether or polyester chains which interconnect the hard segment blocks, thus giving the resultant material the elasticity associated with the elastic soft segment and the strength associated with the hard segment [50]. Varying the structures and molecular weights within its ingredients allows urethane manufacturers to manufacture custom TPUs as per the properties desired. Using a polyol with a polyester chain typically gives rise to a stronger TPU with more interconnections among

the molecules, but at the same time, it makes the TPU prone to microbial attacks and reduces the temperature stability, especially at lower temperatures. A polyether-based TPU, although with weaker mechanical properties, is more prevalent in applications where TPU is chosen for its tactile properties. Figure 1.6 shows the typical structure of thermoplastic polyurethane.

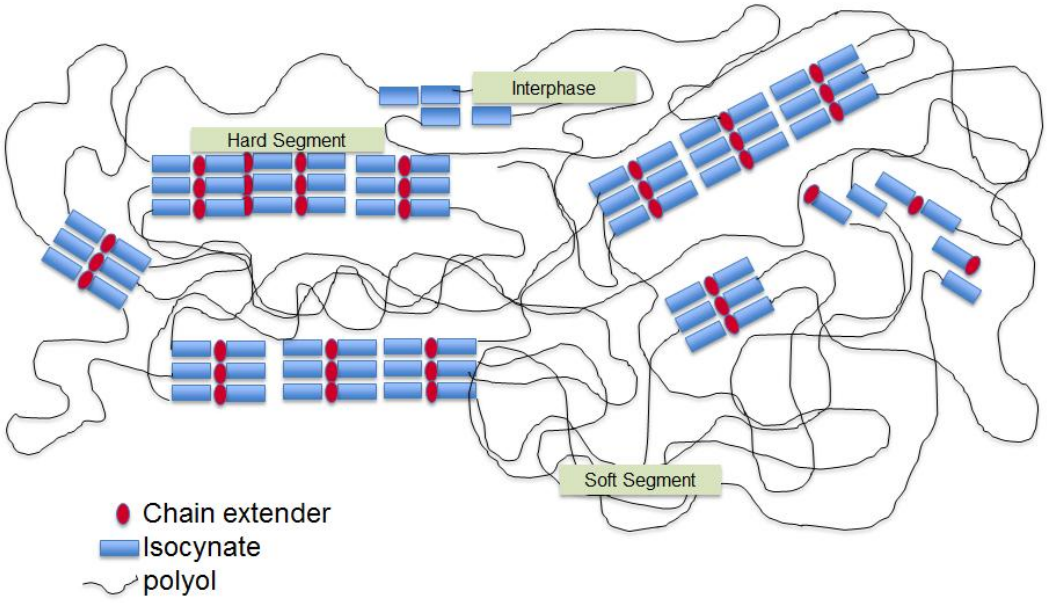

Figure 1.6. Typical structure of thermoplastic polyurethane.

Typically, TPU exhibits excellent mechanical properties in combination with elasticity, high flexibility, and shear strength at low temperatures, as well as high abrasion, wear, and age resistance. While exhibiting high resistance against chemicals, water, fat, oil, and microbes, it is biodegradable and, in most cases, biocompatible [51]. TPU has good coloring properties, and coupled with a soft rubbery feel, it makes an ideal material for applications which come into contact with the human body. It is no wonder that TPU is finding applications in automobile,

construction, footwear, electronics, appliances, and many other industry segments. Figure 1.7 shows some applications of TPU currently in the industry.

Figure 1.7. Some applications of polyurethane in industry [52].

1.8 TPU Foams

Due to the rising cost of fossil-based polymers and the increasing demand for lightweight, shock absorbing materials, polymeric foam has become a very important area of interest in the polymer processing field. Polyurethanes are the only class of polymers that display thermo-

plastic, elastomeric, and thermoset behaviors depending on their chemical and morphological makeup. Around 66% of all polyurethanes are used in the production of foams. Previously, polyurethane foams used physical blowing agents such as CFCs and HCFCs. As in all industrial processes, a focus on cost, yield, effective waste management, and legislative changes has prompted leaps in innovation. Raw material manufacturers have responded to these market trends and to regulatory changes by improving PU raw materials and advancing foam technology in partnership with machine manufacturers. TPU is one such success story, where by reducing the strength of the cross-linking bonds, a recyclable grade of PU was formed, which could be processed using the regular methods of processing thermoplastics.

The foaming of TPU was particularly studied because it resolved issues of the high cost of TPU and also its medium to high hardness. TPU is also the material of choice to obtain low density foams because of its suitable mechanical properties. Low-density TPU foam shows various benefits such as being lightweight, highly flexible, having a great cushioning effect, and fast energy restoration in compression. It is widely used in furniture, automotive, sportswear, and packaging applications [6]. Furthermore, TPU foams can be easily manufactured in a variety of densities and properties, ranging from highly resilient to highly compressible, with different processing methods, such as injection molding, casting, and extrusion. The use of PU and TPU foams in energy management solutions and applications has been well known and well-studied. Low thermal conductivity, stability over a wide range of temperatures, and good acoustic damping properties make it an ideal material in the heat and noise insulation industry. The thermal and noise insulating properties of PU depend on its cell size and number of layers. In general, the smaller the cells, the lower the thermal and noise conductivity, and the better the

insulating properties [52]. TPU foams are durable, flexible, and wear-resistant over a wide range of temperatures, while providing traction, a consistent cushioning effect, and resistance to oils, water, and chemicals. In terms of physical properties, they have excellent abrasion, splinter, cut, and scratch resistance, high strength, excellent flex properties, good low temperature performance, resistance to sea-water and microbial attack, good coloring capabilities, and excellent bond capabilities with other parts due to the reactive nature of their urethane linkages. Certain formulations of PU have better coefficients of dynamic friction than most other competing materials [53]. These properties make it extremely popular for furniture, automobile interiors, and sporting applications including athletic shoes, sport shoes, ski shoes, and in-line skates [54].

Recently, because of its superior properties, TPU is fast gaining market share over traditional materials such as leather, crepe rubber, cork, vulcanized rubber, flexible PVC, thermoplastic rubber, polyurethanes, and ethyl vinyl acetate (EVA) in cushioning and shoe-sole applications. A large percentage of the total TPU produced is used by the shoe industry because of its good properties. Mid-soles are a low density part made of microcellular foam, which forms a part of the shoe-sole. Its function is to create a shock-absorbing unit in the cross-section of the shoe, to absorb energy upon impact, and to provide the comfort and cushioning effect when under loading. The sole, because of its functionality, is also the heaviest part of the shoe, and there is a continuous drive towards decreasing the overall weight of the shoe without compromising its properties. Generally, the outsoles are denser (0.60 to 1.2 g/cm^3) than the midsoles (0.30 to 0.60 g/cm^3).

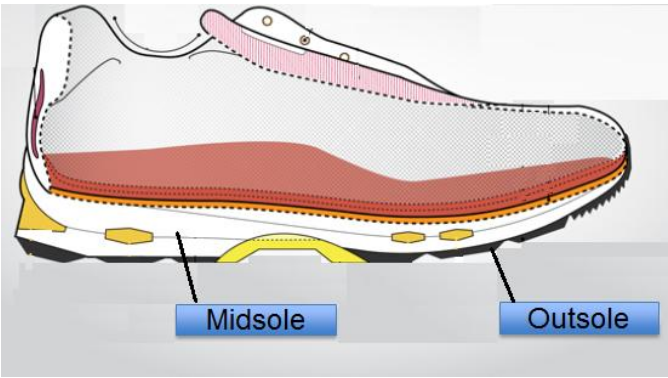

Figure 1.8. Anatomy of a running shoe [55].

Other than the anticipated customer expectations from shoes (i.e., of being attractive, comfortable, trendy, long-lasting, and with good traction properties), being lightweight is one of the most important buying criteria for a lot of customers in all types of shoes. Customers in many countries have been known to weigh shoes in order to buy the lightest pair. Studies have also indicated the ability of foamed insoles to significantly reduce the peak impact loading during running and thereby reduce the number of running-related injuries [56]. Loads equaling 1.5 to 5 times body weight are repeatedly absorbed through each leg and it is suggested that this repeated loading and the associated impact shocks cause microtrauma to the underlying tissues and may eventually cause enough damage to impair function through stress fractures, shin splints, and other related injuries [57]. It is therefore important that the sole, with all of its components, be as light and shock absorbing as possible, while increasing customer experience regarding performance.

To date, there have been studies conducted on producing TPU foams using various processing techniques. Ito et al. [58] and Lin et al. [41] produced TPU foam using a batch

foaming process with autoclaves and CO_2 as the blowing agent. Hossieny et al. [59] also used batch foaming with butane to produce expanded TPU foams. Li et al. [60] and Prasad et al. [61] utilized a solid state microcellular foaming (SSMF) process to produce a porous pad using TPU. Michaeli et al. [62] produced low density TPU foams using foam extrusion with CO_2. Dai et al. [63] fabricated microcellular TPU fibers using a foam extrusion filament spinning process.

Most of the studies of TPU foams were done using a batch process or an extrusion foaming process. While batch foaming suffers from the inherent problem of low production rates, extrusion is limited by the degree of flexibility in part geometries. An effective solution to both of these issues is to obtain TPU foaming with the versatile injection molding process. Earlier studies have shown that TPU can be foamed well using chemical blowing agents [11, 64] and physical blowing agents [33, 65] such as N_2 and CO_2, which can be used in conjunction with the injection molding process. With foaming by either physical or chemical blowing agents, material consumption can be reduced by volume expansion, and the hardness can also be effectively reduced without the addition of any plasticizers [66]. Microcellular injection molding (MIM) and SIFT uses environmentally benign physical blowing agents such as N_2 and CO_2 and can be used to effectively achieve low density TPU foams.

Although a lot of research has been focused on foaming TPU with chemical blowing agents and generic physical blowing agents, very little or no work has been done with physical blowing agents such as N_2 and CO_2 with processes such as microcellular injection molding and SIFT. Preliminary studies on highly expanded TPU foams with microcellular injection molding and SIFT have been reported by Sun et al.

1.9 Research Motivation

Research and innovation in polymer foaming is driven by the huge cost savings in raw materials, increased processing windows of the injection molding process, and certain niche advantages that foaming processes offer. Recent changes mandated by the Montreal Protocol to phase out the use of widely used CFC and HCFC blowing and foaming agents have shifted the focus to environmental friendly methods of foaming plastics and elastomers. Microcellular injection molding (MIM) and SIFT are relatively new environmentally friendly processes with zero ozone layer depletion and extremely insignificant global warming potential, thus showing a lot of promise in being the method of choice for the effective foaming of plastics. However, they have their own challenges. The relative lack of process knowledge, and challenges with obtaining a consistent microstructure and a good surface finish, are still an issue for MIM. TPU is the material of choice in the manufacturing of extremely low density foams with customizable properties of resilience and cushioning, while maintaining important properties of elasticity, microbial and hydrolysis resistance, and flexibility at low temperatures. Foamed TPU is finding increasing applications in the apparel and sports industry where the reduction in density of the foam provides necessary comfort for the user, whereas good rebound resilience properties of the foam will provide the springiness required from the specific application. The industry currently uses parts with densities ranging from 0.40 to 0.60 g/cm^3 and rebound resilience values measuring around 30–40%. In general, rebound resilience reduces with the density of foamed TPU. One of the aims of this research is to stretch these boundaries for density reduction, while achieving good loss of hysteresis and rebound resilience values. Not much work has been done with TPU and SIFT, so it was set as one of the research goals to study if SIFT alone or SIFT in

combination with different foaming technologies could be used to achieve a bulk density of 0.25 g/cm^3 without compromising rebound resilience. At the same time, it has been recognized that different local mechanical properties are preferred in a single foamed part. For example, in a running shoe, a high energy absorbing heel region and a highly resilient toe region can improve the performance of athletes while absorbing shock. For this purpose, a novel processes is proposed and investigated in this study.

1.10 Objectives of Research

It has been shown that the shoe industry needs unique properties from the mid-sole and outsole of the shoes and there is a push in the research toward making the mid-sole lighter but more rebound resilient. TPU is one material that has been gaining market share in this application because of its high toughness, good mechanical properties, and excellent ability to foam. Earlier technologies, which were prevalently used for foaming TPU, used physical blowing agents such as CFCs and HCFCs. These have been phased out of use slowly due to their high ozone depletion potential. Chemical blowing agents have also been used with TPU because of their ease of use, but some of their harmful effects are less than desirable. Use of environmentally benign physical blowing agents, such as CO_2 and N_2, have been tried recently in the process of injection molding of TPU and they have shown a lot of promise for this specific application. Currently, the industry uses bulk densities of 0.40 to 0.60 g/cm^3 for shoe soles because of process limitations. This research aims at expanding these boundaries by achieving highly expanded low-density TPU foams with desirable properties via testing the following hypotheses.

Hypothesis 1: Bulk densities of less than 0.25 g/cm^3 can be achieved with TPU with the process of microcellular injection molding by the optimization of process parameters.

Hypothesis 2: Bulk densities can be further reduced in microcellular injection molding by the synergistic effect of co-blowing agents using gas-laden pellets manufactured by SIFT as an input to the microcellular injection molding process.

Hypothesis 3: The use of physical cross-linking agents, nucleating agents, and special processes in injection molding, such as retractable core technology, can be used to further reduce the bulk density of TPU and control the microstructure.

Hypothesis 4: Core-retraction technology, if used in conjunction with MIM, can provide additional tools to control the timing of cell nucleation and growth.

Hypothesis 5: Development of a three-stage foaming process can be used to manufacture foamed injection molded TPU parts with extremely low and customized localized densities, thereby producing parts with customizable microstructures and mechanical properties.

1.11 Organization of Thesis

This thesis is organized in chapters to make readability easier. They are mentioned below.

Chapter 1 – Introduction

Chapter 2 – Comparative Study of Different Foaming Agents for TPU

Chapter 3 – Highly Expanded TPU Foams Using Cross-Linking Agents

Chapter 4 – Low-Density TPU Foams Using Nanoclay as a Nucleating Agent

2 COMPARATIVE STUDY OF DIFFERENT FOAMING AGENTS FOR THERMOPLASTIC POLYURETHANE

2.1 Introduction

Previously, volatile chemicals with low boiling points, such as chlorofluorocarbons (CFCs) and hydrochlorofluorocarbons (HCFCs), were used for foaming PU because of their low cost, high solubility, and ease of processability. However, with the ever-growing environmental concerns of these chemicals' harmful effects on the ozone layer, the use of these compounds has been eliminated from practice by the Montreal Protocol.[15] This has sparked an interest in the polymer processing field to develop additional methods for foaming TPU with environmentally sustainable foaming agents using continuous processes such as injection molding. Chemical blowing agents (CBAs) are often used for foaming thermoplastics because of their stability during transportation and storage, in addition to their ease of dispensing and use. During the injection molding process, when heated above a critical temperature, CBAs decompose and generate gases such as carbon dioxide (CO_2), carbon monoxide (CO), and nitrogen (N_2). Once the polymer is injected into the mold cavity, the sudden pressure drop causes the gas to expand and form microscale voids throughout the part. Though easy to use, CBAs do not allow precise control over the foaming process or the microstructure.[13] Furthermore, residual CBA carriers and byproducts, such as water, tend to be left behind, which can lead to additional degradation of the polymer matrix, a reduction in mechanical properties, and contamination of the mold surface.[67]

The use of environmentally benign physical blowing agents (PBAs) for foaming polymers such as TPU can help to mitigate the concerns of using CBAs. On numerous occasions, TPU has been shown to foam well with PBAs using batch foaming processes,[40, 50, 68, 69] extrusion,[62] and, in injection molding[49, 70, 71] specifically, the microcellular injection molding process (MIM)[30, 49], or the supercritical gas-laden pellets injection molding foaming technology (SIFT) process.[49, 72] Figure 2.1 below illustrates both the MIM and SIFT processes. In these techniques, a polymer melt mixed with a gas pressurized into a supercritical fluid (SCF) state forms a single-phase polymer–gas solution in the injection unit barrel that is subsequently injected into the mold cavity. As the polymer–gas solution passes through the gate and into the mold cavity, the sudden pressure drop causes thermodynamic instability. As a result, dissolved gas begins emerging from the solution and generating microscale bubbles inside of the molded part. Being that these processes employ commonly used PBAs such as N_2 and CO_2, concerns surrounding the use of CBAs are not an issue with these techniques. By foaming with either PBAs or CBAs, material consumption can be dramatically reduced by volume expansion while improving processability. The material hardness can also be effectively reduced without the addition of any plasticizers. In addition, it has been found that the microcellular structure can be further refined if co-blowing agents (e.g., N_2 and CO_2) are employed through the blending of gas-laden pellets loaded with different gases or by combining MIM with SIFT. Although there have been previous studies that discuss TPU foaming with CBAs and PBAs separately, no studies have been conducted that directly compare foaming techniques such as SIFT and MIM with CBA foaming. In this study, popular methods used to foam TPU were tested and evaluated with the intention of providing industry with a comparative discussion regarding PBAs, CBAs,

and foaming of this versatile material. Parameters such as bulk density, microstructure size, and compressive strength have also been assessed and compared.

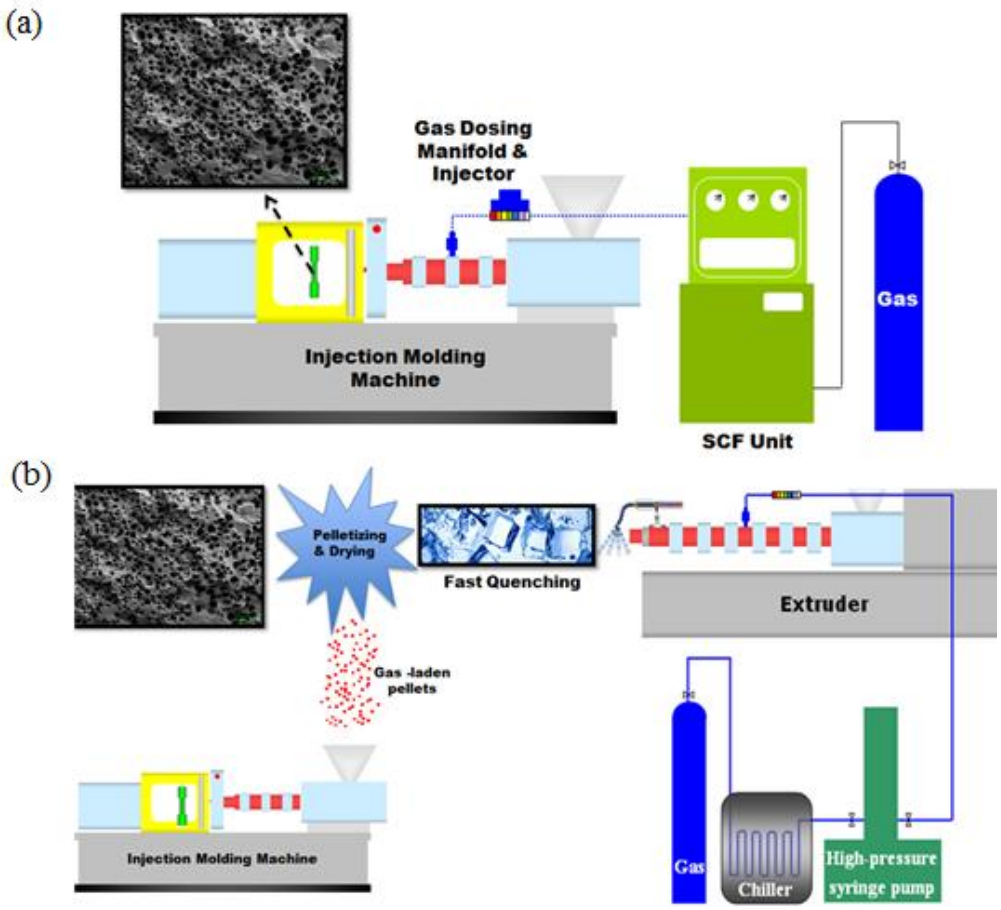

Figure 2.1. An illustration of the (a) MIM and (b) SIFT processes.

2.2 Experimental Methods and Materials

2.2.1 Materials

TPU 1180A (BASF Corporation), which is a polyether-based polyol in its configuration, was foamed using three different processes; namely, CBA foaming, MIM using N_2 as a PBA, and a sequential process of SIFT+MIM using CO_2 and N_2 as co-blowing agents in the SIFT and MIM processes, respectively. The CBA used in this study was Endo Foam 70 Microcell (iD Additives, Inc.), which is an endothermic CBA that gives a yield of 70 cc of CO_2 gas/gram of CBA and decomposes at 162.8 °C. One of the byproducts of CBA decomposition is water. Commercial grades of CO_2 and N_2 were purchased from Airgas and used as received.

2.2.2 Equipment

An 18 mm co-rotating twin screw extruder, model LZE-18 (Leistritz), was fitted with a high pressure syringe pump (ISCO 260D, Teledyne) and used to manufacture the gas laden pellets via the SIFT process. An injection molding machine (Arburg ALLROUNDER 320S) equipped with a MuCell gas injection system (Trexel Inc.) was used for sample fabrication. A custom injection mold was designed and fabricated from 6061 aluminum. Specifically, Figure 2.2 depicts the resultant component with a center sprue gate.

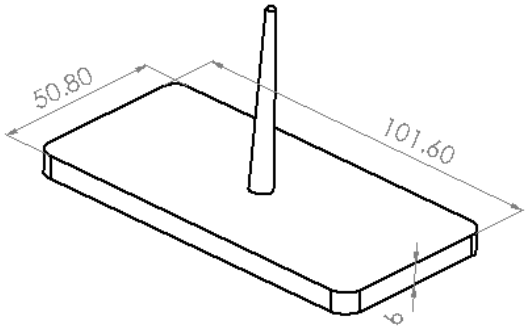

Figure 2.2. Custom injection molded component with central sprue gate (50.8 × 101.6 × 6 mm).

Density measurements were recorded following ASTM D792 and the Archimedes buoyancy principles. The microstructures of the foamed samples were observed using a scanning electron microscope (SEM) (JCM-5000, NeoScope). A CO_2 laser cutter (PLS6.75, Universal Laser Systems) was used to cut ASTM D638 Type V tensile specimens and 28 × 28 mm compression samples, which were then evaluated with a universal testing machine (5967, Instron). Thermal gravimetric analysis (TGA) (Q50, TA Instruments) and differential scanning calorimetry (DSC) (Q20, TA Instruments) were performed on the samples.

2.2.3 Experimental Conditions

The CBA was dry blended with TPU at 1%, 3%, and 5% by weight to increase its weight reduction capability. The weight reduction was achieved by lowering the shot size and increasing the gas dosage. The gas dosage levels were calculated for the three loading levels according to the gas yield of the CBA. CBA loading levels of 1%, 3%, and 5% by weight yielded a saturation level of 0.10%, 0.25%, and 0.43% in the polymer, respectively. The dosage level was calculated

by dividing the total weight of gas as calculated from the gas yield by the shot weight of plastic (density of TPU times the shot size shown in Table 2.1). A nomenclature of 1%, 3%, and 5% of BA levels corresponding to the loading of CBA has been maintained in this publication for ease of reading. The yield of gas was calculated from the CBA loading level and the same amount of gas was dosed by injecting supercritical fluid into the MIM and SIFT+MIM processes. Specifically, CO_2 was used as the PBA in the SIFT process, and N_2 in the MIM process. TPU 1180A pellets were directly used in the MIM process with N_2 as the blowing agent. The amount of 0.2% CO_2 by weight was added to the TPU 1180A pellets in the SIFT process. After 30 minutes of drying at 60 °C to remove the surface moisture, the gas remaining in the pellets was measured and found to be 0.08% CO_2. These gas laden pellets were sequentially fed into the MIM process to obtain the final foamed samples in the SIFT+MIM process. The process parameters are reported in Table 2.2.

Table 2.1. Nomenclature of trials and experimental design.

Technique	BA	Content (%)	Shot Size (cm^3)	Density (g/cm^3)	Cell Size (μm)	Cell Density ($\times 10^6$ cells/cm^3)
Injection Molding	CBA	1	37.0	1.05	N/A	0
		3	23.5	0.55	238	0.56
		5	21.0	0.57	258	0.70
MIM	PBA	1	37.0	1.16	N/A	0
		3	23.5	0.47	192	0.79
		5	21.0	0.38	153	1.72
SIFT (CO_2) + MIM (N_2)	PBA	1	37.0	0.83	321	0.03
		3	23.5	0.54	46	14.41
		5	21.0	0.49	146	3.6

Table 2.2. Processing parameters for injection molding and twin screw extrusion processes.

Injection Molding		
Parameter	Unit	Value
Back pressure	bar	80
Injection pressure	bar	2500
Injection speed	cm^3/s	60
Screw rotation speed	rpm	190
Mold temperature	°C	45
Barrel temperature	°C	195–210

Twin Screw Extrusion		
Parameter	Unit	Value
Screw rotation speed	rpm	90
Barrel temperatures	°C	155–170

2.3 Results and Discussion

2.3.1 Thermal Analysis

Weight loss analysis was performed by heating a known mass of CBA to 220 °C under vacuum for 30 minutes in an oven. The remaining mass was measured with an analytical balance and the difference was attributed to gas release from decomposition. A 17% loss of weight was recorded during the heating process, indicating that 83% of the CBA remained in the form of residue consisting of the CBA's carrier polymer and the blowing agent's decomposition byproducts.[73] Thermogravimetric analysis (TGA) was carried out on the foamed injection molded samples with a 3% BA loading level by heating to 600 °C at a rate of 10 °C/minute. Figure 2.3 (a) displays the change in mass with respect to temperature. It can be observed that

the TPU+CBA sample had a lower degradation temperature when compared to neat and PBA foamed samples. Furthermore, from the derivative weight loss curve (Figure 2.3 (b)), it can be noted that the degradation rates were dissimilar between TPUs foamed with CBAs vs. PBAs. The chemical reaction of the CBA decomposition and the by-products, such as water, affected the TPU matrix and caused it to degrade. This prompted the onset of degradation at a lower temperature for the samples foamed with CBAs. The delayed second peak in the derivative weight loss curve was more difficult to attribute to a specific cause, but was most likely related to the transport of the volatile compounds of TPU decomposition being impeded by the early onset degradation products of the CBA. The propensity of TPU to degrade with shear and moisture was shown earlier to be high. PBAs did not increase the tendency of TPU to weaken or degrade, as the degradation profiles were very similar to that of the pure TPU. The presence of PBAs like CO_2 have been known to help reduce the viscosity of the polymer during injection molding, which further reduces the degradation due to shear.[34]

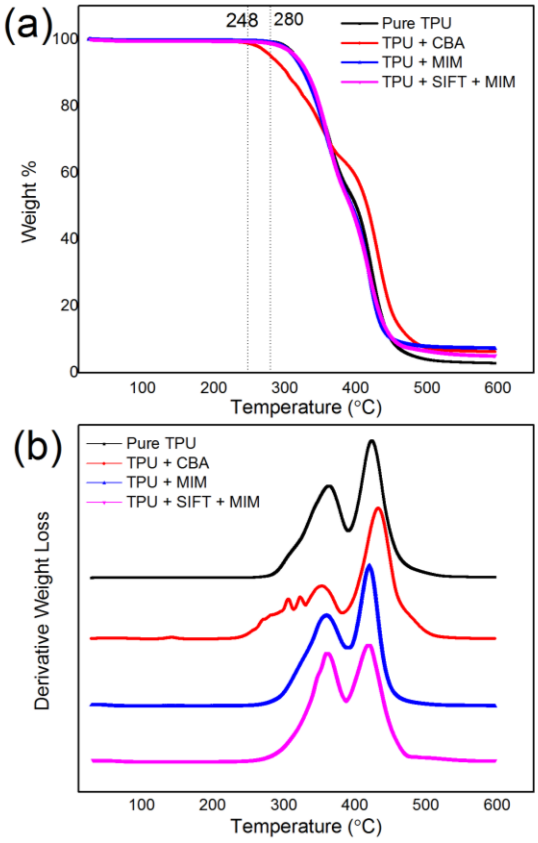

Figure 2.3. TGA results indicating (a) weight loss (%) and (b) decomposition rate vs. temperature of 3% BA samples.

2.3.2 Differential Scanning Calorimetry

Differential scanning calorimetry (DSC) was performed to measure the energy input required to exert constant temperature changes within the various samples. The tests were conducted at a constant temperature change of 10 °C per minute during heating and cooling. Three samples were tested from each batch with the most representative curves presented in Figure 2.4. It was observed from the DSC data collected in Figure 2.4 that the samples foamed with PBAs had the

same gentle curvature that can be seen with solid, neat TPU, indicating that the polymer's structure and morphology were unchanged.[74, 75] The samples molded with CBA, however, displayed additional and sharper peaks, thus indicating a change in the molecular structure, crystal morphology, or the presence of an additional material. The third case most likely as the CBA's carrier polymer will have its own exo- and endothermic peaks which may overlap with those of the TPU. There are usually three distinctive regions in TPU formations; namely, the hard segment region, the soft segment region, and an interphase region where the hard segments are not completely aligned. It has been shown that additional thermal processing cycles, such as extrusion, can create a more dispersed hard segment phase.[76] With respect to the first cooling curve, a broader peak is indicative of a more dispersed intermediate region while a narrow peak is suggestive of more aligned hard segments. At processing temperatures, the hard segments can act as immiscible particles in the soft polyol matrix, thereby introducing nanoscale heterogeneity, which can act as heterogeneous nucleation sites to initiate cell nucleation. Furthermore, previous research has shown that the presence of immiscible and well-dispersed sites can act as low energy nucleation sites resulting in a more uniform microstructure.[50, 77] Therefore, from the first cooling curve, it can be expected that the SIFT+MIM, with its more gentle curve, would have more distributed hard segments and would display a better foamed morphology.

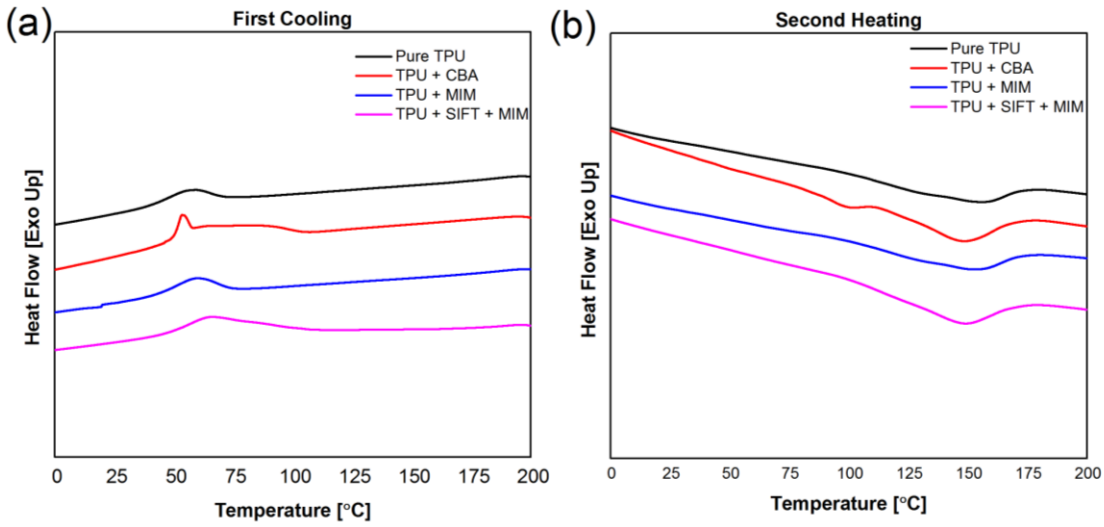

Figure 2.4. DSC results from the (a) first cooling and (b) second heating scans.

2.3.3 Scanning Electron Microscopy

The foamed internal structures of the TPU samples were imaged via scanning electron microscopy (SEM) after being cryogenically fractured using liquid nitrogen at the location shown in Figure 2.5. The SEM images are shown in Figure 2.6 for comparison.

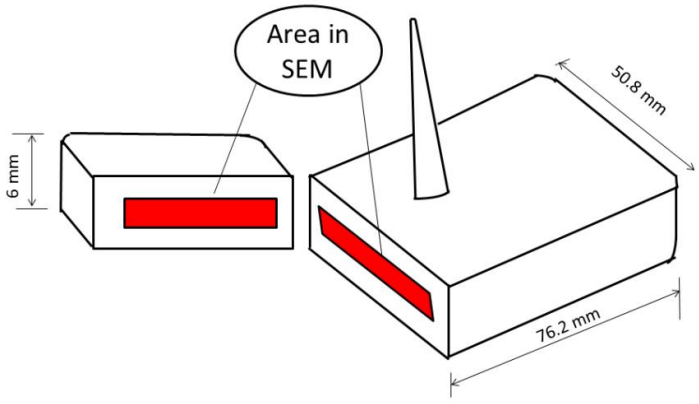

Figure 2.5. Schematic illustration identifying the region of interest for SEM imaging. All dimensions are in mm.

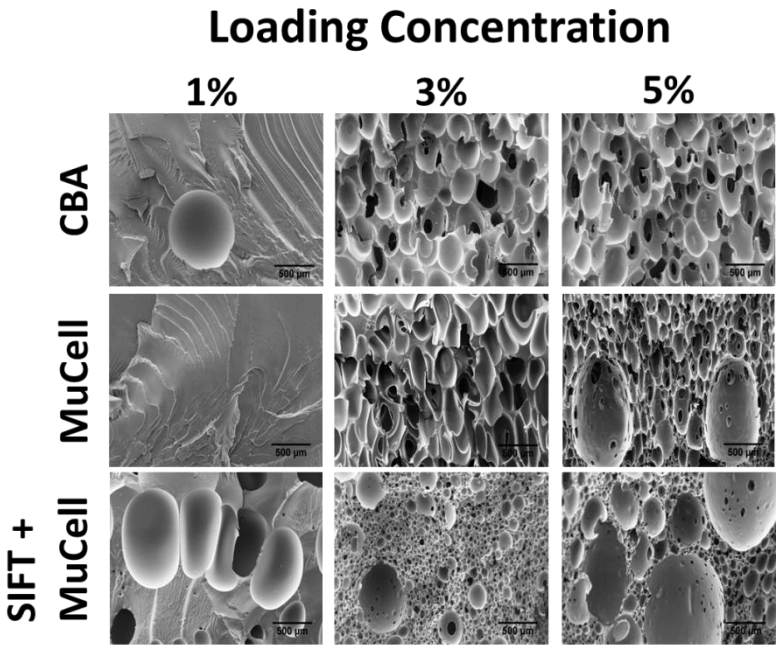

Figure 2.6. Representative SEM images comparing various loading levels and processes for foamed TPU. Scale bar denotes 500 μm.

It can be observed that samples foamed with SIFT+MIM had the lowest cell size and highest cell density among all of the samples, especially at medium gas saturation levels. As the gas saturation further increased, cells coalesced and increased in size. Next, the SEM images were used to analyze the cells size formed within each of the TPU specimens, and the number of cells within each image was computed using the ImageJ software. Within the defined region of interest (ROI), the cell density was calculated using the formula in Equation (2.1) and reported previously in Table 2.2. Figures 2.7 (a), (b), and (c) are a graphical representation of the bulk density, cell size, and cell density, respectively.

It can also be observed from Figure 2.7 (a) that there was negligible foaming in samples with 1% BA, which required the maximum injection volume. Typical cell sizes were measured with image analysis tools in ImageJ software after calibration. The average cell sizes of samples with different (physical or chemical) levels of blowing agent (BA) were calculated and are shown in Figure 2.7 (b). Furthermore, it could be argued that 1% BA by weight did not release enough gas to saturate the polymer matrix enough to initiate and sustain nucleation. The cell density of different methods of foaming at increasing blowing agent concentrations is plotted in Figure 2.7 (a),

$$\text{Cell density} = \left(\frac{\text{N}}{\text{A}}\right)^{\frac{3}{2}} X \frac{\rho_{solid}}{\rho_{foam}} \tag{2.1}$$

where N is the number of cells within the ROI, A is the area of the ROI (mm^2), and ρ_{solid} and ρ_{foam} are the densities of the solid and foamed parts, respectively.

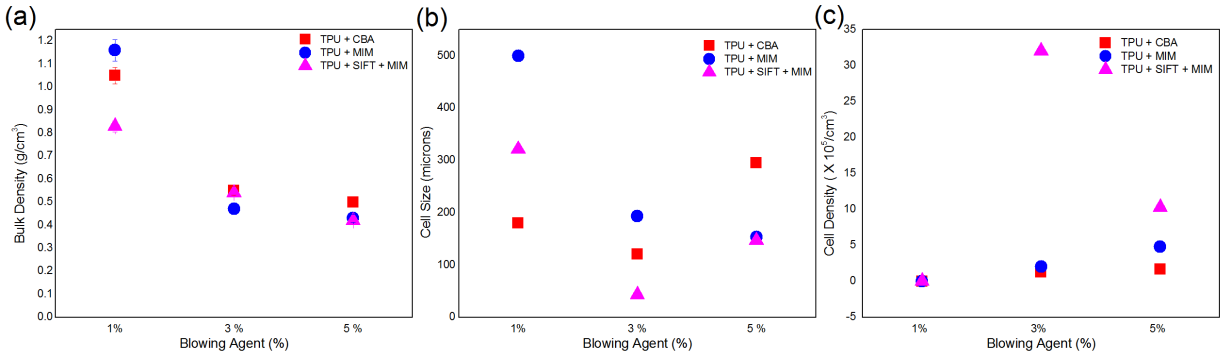

Figure 2.7. Graphical representation of typical (a) bulk densities, (b) cell sizes, and (c) cell densities of foamed TPU samples.

A separate trial was conducted with extruded TPU pellets (without any blowing agent added in the SIFT process) in the MIM process, to ensure that the extra thermal cycle was not the reason for the better microstructure seen in the SIFT + MIM process. The microstructure observed in this trial was similar to MIM process. Previous studies have shown that CO_2 can act as a plasticizer for the polymer matrix, thereby decreasing viscosity.[34] CO_2 has also shown the ability to reduce the surface tension of the polymer matrix, which also increases foaming capabilities.[78] Nucleation was further enhanced by the synergistic effects of the co-blowing agents, where small amounts of N_2 increased the degree of supersaturation in the polymer due to its inherent low solubility and the CO_2 reduced the surface tension and viscosity of the polymer.[77, 79] This phenomenon explains why the samples foamed with SIFT+MIM had the lowest cell size and highest cell density among all of the samples. In general, foaming with PBAs when compared with CBAs was more aggressive, and with a BA loading over 3%, there were diminishing returns which suggested that the 3% loading was the recommended CBA–polymer combination. On the other hand, a higher loading of PBA could also lead to undesirable cell coalescence, thereby increasing the cell size and decreasing the cell density.

2.3.4 Mechanical Strength – Hysteresis

Uniaxial hysteresis compression tests of 100 cyclic loadings and unloadings were conducted on all of the samples. The resultant stresses were measured against the defined strain and strain rates during the procedure; Figure 2.8 displays a typical outcome. As shown in the plot, the loading and unloading curves of the foams during a cyclic compression test followed two separate and distinct paths. Due to the viscoelastic nature of the foam, the samples were capable

of absorbing kinetic energy during the loading cycle and dissipating it as heat. Energy lost during deformation was measured as the difference between the energy required to load the sample (Area A+B) and the energy required to unload the sample (Area B). The area between the curves (Area A) was the energy lost during deformation. This ratio A:(A+B) provided a simple measure of the foam elasticity and resilience of the foamed material. The lower the ratio, the better the foam performed with respect to returning the energy absorbed during deformation. Higher hysteresis ratios indicated that the foams were more energy absorbent and dissipating, which is more ideal for applications where shock absorbing properties are of paramount importance.

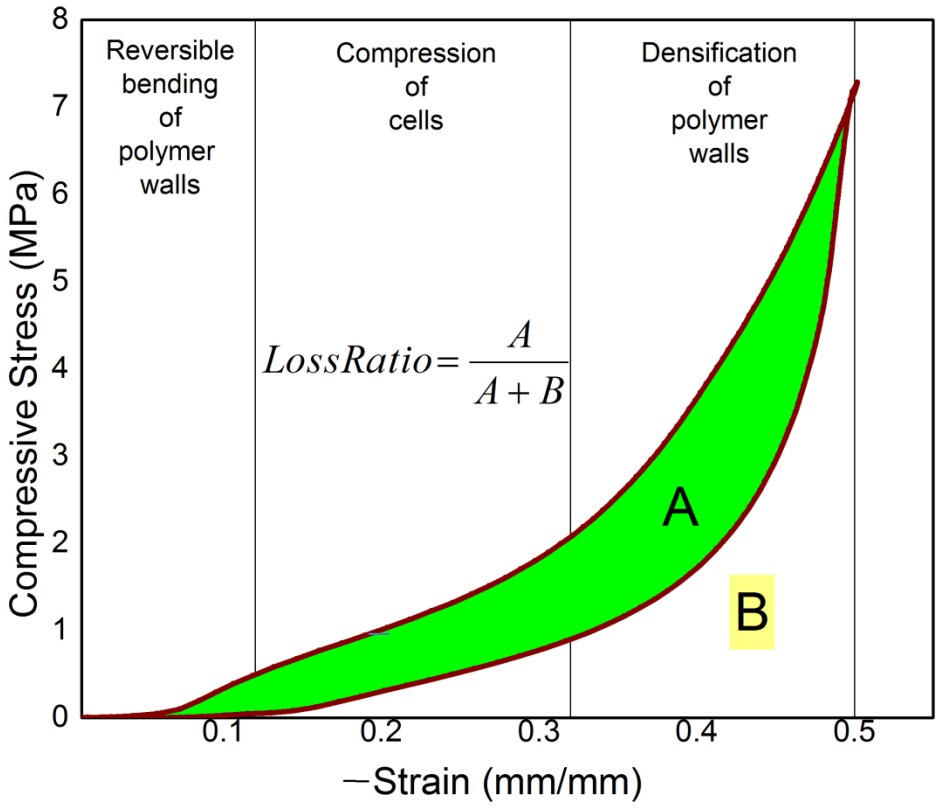

Figure 2.8. Typical hysteresis loop of foamed TPU samples and the three distinct regions during compression.

A typical hysteresis loop of TPU foam has three distinct regions (cf. Figure 2.8). The first and initial small elastic region relates to the energy required for bending the polymer walls between the microcells. As the foam becomes highly expanded, the material (wall) regions become thinner and the elastic regions get smaller. The second stage is described as the polymer walls buckling and the microcells compressing. In this region, the stress does not increase at the same rate as the strain. In the last stage, at high strain, the walls of the polymer start compressing against neighboring walls; this is referred to as the densification region. In this region, the stress rises rapidly with increased strain. The stress–strain behavior of TPU typically demonstrates strong hysteresis, time dependence, and cyclic softening. It is generally observed that the stress–strain curve gets more compliant with numerous loadings as compared to the first cycle. Most of the softening occurs in the first cycle.

Figure 2.9 shows hysteresis loops for the 1^{st}, 50^{th}, and 100^{th} cycles for samples foamed with the three BA loading levels produced in this study. It can be seen that the hysteresis area in all cases for the first cycle is significantly larger than the rest of the cycles. The softening behavior stabilizes after the initial 3 to 4 cycles. The softening behavior occurs because of the bending/breakage of bonds within the hard segments and also as absorbed energy gets dissipated as heat, thus raising the temperature of the samples. The unloading paths all follow similar curves, irrespective of the number of loadings, and there is a small amount of residual strain in the sample immediately after the first cycle, which recovers slowly after the test is finished; this is an indication of its viscoelastic behavior.[80] The hysteresis curves for the samples made with CBA show a higher modulus at the start of the test, as compared to foaming with PBA, as seen in Figure 2.9. CBAs tend to increase the modulus and reduce the softness of TPU. Also, it can be

observed in Figure 2.9 that MIM at a 1% loading level had the least density reduction due to poor foaming, and showed the highest recorded stress at 50% strain. Manufacturing foams with co-blowing agents, with a combination of the SIFT and MIM processes, yielded the softest foams, which had the least amount of compressive stress recorded at 50% strain.

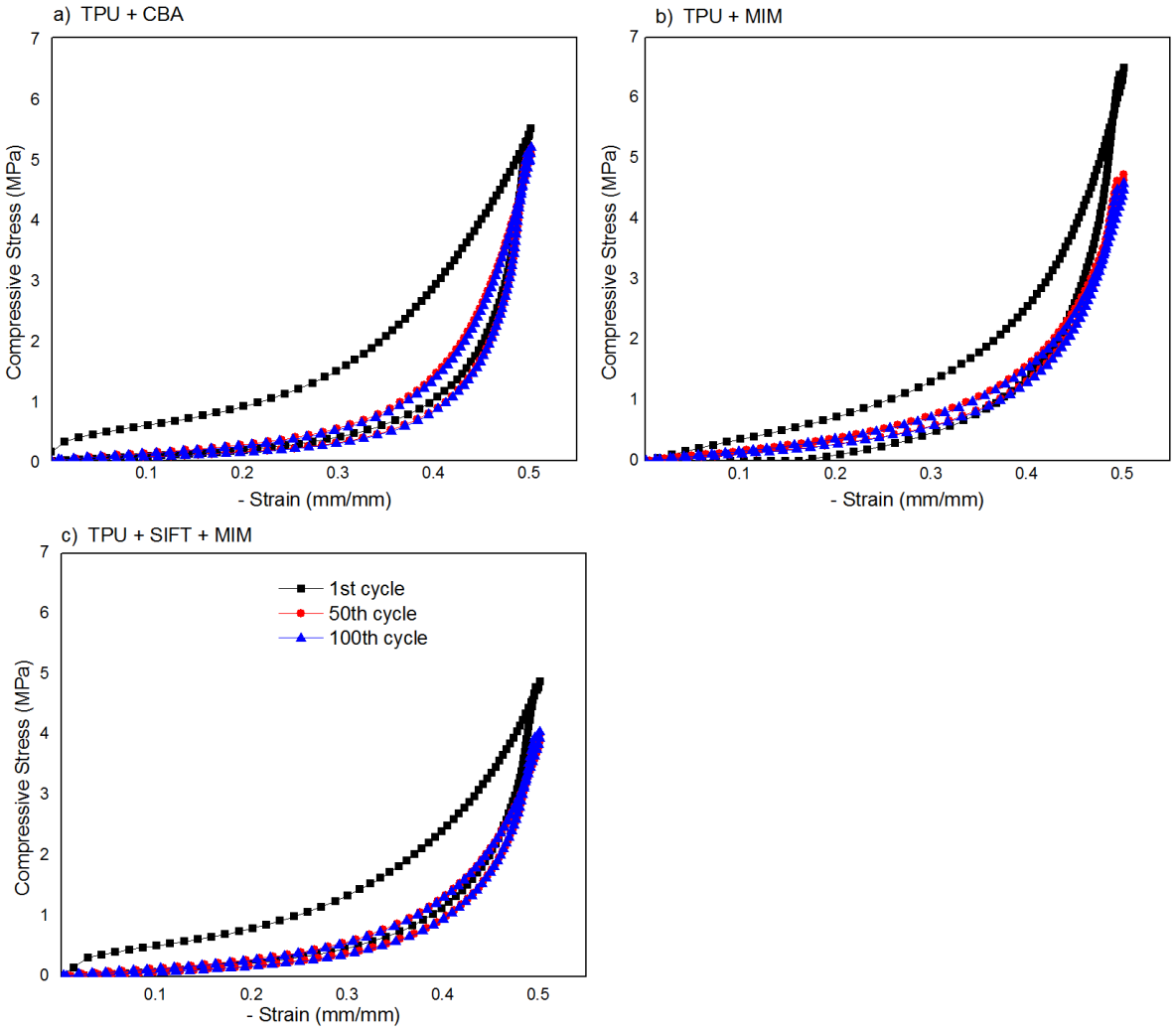

Figure 2.9. The 1st , 50th, and 100th compressive hysteresis cycles for TPU foamed samples with 3% loading for (a) CBA, (b) MIM, and (c) SIFT+MIM.

To more readily compare the softening effects of the various samples due to cyclic compression, hysteresis ratios were calculated and plotted for the 100th cycle and reported in Figure 2.10. It can be observed that, in general, as the content of the BA increased, the bulk density and the hysteresis loss ratio decreased. Despite having the lowest bulk density, PBAs showed lower values of hysteresis ratios, thus yielding more resilient foams. One explanation for this observation could be the finer microstructure and lower degree of degradation due to thermal processing. The 3% loading content appeared to be the optimum loading concentration for the various BAs.

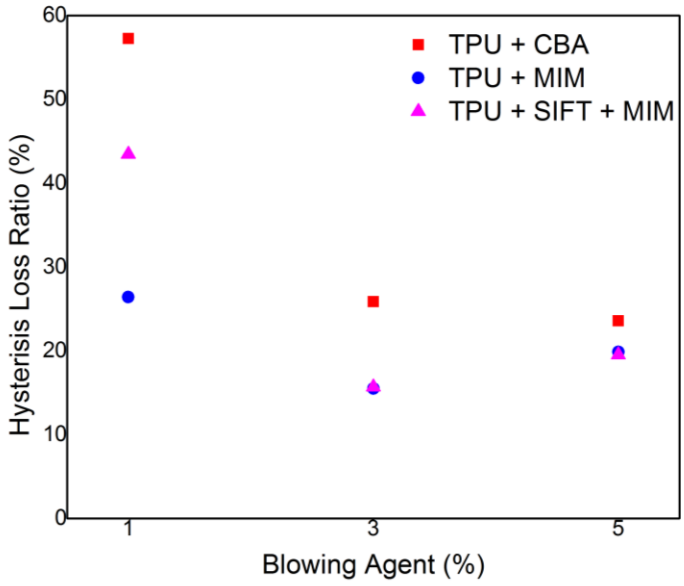

Figure 2.10. Hysteresis loss (%) of various foaming methods for the 100th cycle.

2.4 Conclusions

In this study, injection molded foamed TPU was produced using CBAs and PBAs. TPU was foamed with PBAs, such as N_2, in the MIM process, and a combination of CO_2 and N_2 as co-blowing agents in the SIFT+MIM process. Weight loss analyses and TGA results showed that CBA left a heterogeneous residual material in the TPU polymer matrix of more than 80 percent of its initial loading weight, thus resulting in decreased thermal stability, whereas the PBA samples did not cause any significant changes in the polymer matrix. Among the samples, specimens molded with a combination of PBAs yielded the smallest cell size and the maximum cell density. The use of PBAs was more suitable for achieving low density foams with TPU as PBA provided additional blowing capability while retaining the elasticity of the material. Among the two processes of foaming TPU, the use of co-blowing agents yielded the lowest cell size and the highest cell density, and also yielded the softest foams. Hysteresis loss had a strong inverse relationship with bulk density, although this effect was not consistent and depended on many other factors such as the microstructure. The stress–strain behavior of TPU demonstrated hysteresis and cyclic softening. The hysteresis loss ratios of the samples blown with PBAs were lower than those observed with CBAs. By using CO_2 and N_2 as co-blowing agents in the SIFT+MIM combined process, the lowest hysteresis loss ratios indicative of highly resilient foams were achieved at the lowest bulk densities. This process shows a lot of promise for certain applications of TPU foams that require higher resilience foams at very low bulk densities.

3. EFFECT OF CROSS-LINKING AGENT ON THE FOAMABILITY OF MICROCELLULAR INJECTION MOLDED TPU

3.1 Introduction

Thermoplastic polyurethanes (TPUs) belong to a group of thermoplastic elastomers consisting of linear segmented block copolymers of hard and soft segments.[52, 81, 82] By merely changing the ratios of its constituents, the properties of TPU can be modified, enabling the production of custom-made TPUs as per application requirements.[52, 83, 84] This versatility of TPU, coupled with the fact that it can be reground, reshaped, and recycled, has led to an increase in market share for high performance elastomers. TPU has been shown to foam well with the use of chemical blowing agents[64, 85] and blowing agents[62, 86], and exceptionally well in batch foaming processes.[40, 86] While achieving cell sizes on the submicron scale, cell densities as high as 10^{14} per cubic centimeter have been achieved by solid state batch foaming.[40] Because batch processes do not involve the flow of material, they can be carried out at sub-processing temperatures, where the melt strength counteracting the bubble pressure is very high, which subsequently limits and controls cell growth. Nevertheless, batch processes have the inherent disadvantages of cost, limited geometries, and restricted applications, and thus are not feasible for all industrial sectors. In semi-continuous and continuous processes such as injection molding or extrusion, TPU has to be processed at higher temperatures, around 170 °C to 210 °C. At that temperature range, the melt strength of TPU is much weaker as compared to that of batch foaming, thus posing challenges in controlling the microstructure and mechanical properties of the semi-continuously or continuously foamed TPU, especially at

higher foaming ratios or density reductions. Melt strength is related to the molecular chain entanglements of a polymer and its resistance to untangling under strain. While extensional viscosity is usually a good measure of melt strength, it can be defined as the resistance of the polymer melt to stretching. As extensional viscosity is linearly related to shear viscosity by the Trouton's ratio, melt strength is described by relating it to shear viscosity in this manuscript.[87]

In the MIM process, the strength of the polymer melt inside of the mold cavity rapidly increases as the part cools down. The increasing viscosity and melt strength of the polymer inhibits further cell growth.[88] Microstructure deterioration at high foaming ratios is thus more likely at the center of the cross-section in a thick MIM part, which usually is the last to cool down. Since both the phenomena of cell growth and increasing melt strength occur simultaneously, precise cell size control is very difficult. This phenomenon of cell nucleation and growth, which dictates the final microstructure, results from a simultaneous transient process that depends on several factors such as the number of nucleating sites, strength of the polymer matrix at the time of bubble growth, and supersaturation level of the blowing agent.

TPU foams are manufactured in a variety of densities, typically ranging from 0.4 to 0.8 g/cm^3, with properties ranging from highly compressible to highly resilient. A lower bulk density of foam typically yields softer foams, with lower TPU usages, thus addressing the cost and part weight issues with TPU.[80] These properties make it extremely popular for furniture, automobile interiors, and sporting applications, including athletic shoes, sport shoes, ski shoes, and in-line skates.[54] In this study, highly expanded homogenous TPU foams with densities less than 0.20 g/cm^3 were manufactured by microcellular injection molding with nitrogen (N_2) as the

blowing agent. To achieve aggressive density reductions, it is important that cell growth occurs at a higher mold temperature before the material hardens and loses it foamability due to cooling. However, an increased melt strength that inhibits cell coalescence is also required to achieve a homogenous microcellular structure. In light of this dilemma, it is hypothesized that with a cross-linking agent, the strength of the melt can be improved during processing even at high temperatures, which will help achieve better control of the foamed structure. The presence of a cross-linking agent, which acts as a source of impurities, can also help create more nucleating sites and further improve the microstructure, even at high density reductions.

3.2 Experiments

3.2.1 Materials

TPU (Elastollan® 1180A10, BASF), a flexible polyether-based elastomer, was used as the polymer matrix in this study. It had a density of 1.11 g/cm3. Its glass transition temperature (T_g) was –50°C (based on DSC tests), and it had a melt flow index of 3.06 g/10 min (190 °C/2.16 Kg). Joncryl (supplied by BASF), in a form of powder, is a cross-linking agent that increases the melt strength of the TPU by providing better cross-linking between the hard and soft segments while maintaining the polymer as a thermoplastic material. Commercial grade N_2 as the blowing agent in the super-critical fluid (SCF) state was purchased from Airgas and used as received in the microcellular injection molding process.

3.2.2 Equipment

An 18 mm, co-rotating, twin-screw extruder (LZE-18, Leistritz) was used to compound the cross-linking agent with the TPU for rheological and thermal testing. A 56T Arburg ALLROUNDER (320S) injection molding machine equipped with a microcellular injection molding (MIM) gas injection system (aka MuCell system) was used for molding the samples. To avoid subjecting TPU to multiple thermal cycles, the cross-linking agent was directly introduced in the injection molding process by a dry mixing method to produce highly foamed ASTM 638 Type I tensile test bar samples. Density was measured using ASTM D792, which is based on the Archimedes buoyancy principles. The microstructure of the foamed samples was observed using a scanning electron microscope (SEM) (JCM-5000, NeoScope). Thermogravimetric analysis (TGA) (Q50, TA Instruments) and differential scanning calorimetry (DSC) (Q20, TA Instruments) were performed on the samples using heating rates of 10˚C/min for TGA and 20˚C/min for DSC with a cooling rate of 10˚C/min for DSC. Viscosity measurements were made on a TA Instruments AR 2000ex stress-controlled rheometer with 25 mm parallel plates at 210˚C. Oscillatory tests with shear rates from 0.1 rad/s to 100 rad/s were used to record the viscosity as a function of the shear rate. A gel permeation chromatography (Viscotek GPCMax) machine was used to measure the molecular weight averages and distribution of the samples based on the column separation method.

3.2.3 Experimental Conditions

The purpose of this experiment was to achieve the lowest possible bulk density with TPU while maintaining a good microstructure. Three weight percent cross-linking agent was used in the MIM process with N_2 as the blowing agent to form extremely low density TPU foams as compared to pure TPU foams made via the same process. Earlier studies have shown that processing parameters such as the mold temperature, gas dosage level, and shot size have a significant influence on the bulk density and microstructure.[49] To achieve the lowest bulk density, these factors were varied in a systematic fashion, and the optimized processes that achieved the lowest possible density with a consistent and homogenous microstructure with the two material combinations are tabulated in Table 3.1. It can be seen that the presence of the cross-linking agent enabled lower densities while achieving consistent microstructures at higher mold temperatures and higher levels of gas saturation. At the same process settings, pure TPU foams displayed coalescence and degradation of the microstructure. To achieve optimal process settings with pure TPU, which yielded maximum density reductions while maintaining an acceptable microstructure, both the gas content and the mold temperature had to be reduced. Thus, the optimal processing conditions required to achieve the lowest density for pure TPU and TPU with the 3% cross-linking agent were different, as shown in Table 3.1.

Table 3.1. Optimized processing conditions.

	Units	TPU	TPU + 3% Joncryl®
Mold temperature	°C	45	52
Percentage of blowing agent	%	0.48	0.96
Cooling time	s	34	34
Mold intermittent opening	mm	0.5	0.5
Back pressure	MPa	11	11
Injection pressure	MPa	250	250
Pre-drying	°C/hrs	100/4	100/4
Barrel temperature	°C	210/210/210/195/190	210/210/210/195/190
Injection speed	cm^3/s	70	70
Screw rotation speed	rpm	100	100
Bulk density measured	g/cm^3	0.193	0.159

3.3 Analysis and Results

3.3.1 Bulk Density

The bulk density was measured as per ASTM D792 using the buoyancy method and the results of the optimized trials are tabulated in Table 3.1. It can be observed that the presence of the cross-linking agent enabled more aggressive foaming of the TPU with increased mold temperatures and higher gas content. With the cross-linking agent, a minimum bulk density of 0.159 g/cm^3 was achieved with a consistent microstructure, as compared to a minimum density of 0.193 g/cm^3 for pure TPU foams.

3.3.2 Rheological Results

A rheological study was conducted to understand the effects of the 3% cross-linking agent on the viscosity of TPU. An initial stress sweep was performed at 210 ˚C and a frequency of 1 Hz to determine a suitable strain percent at which to run oscillatory tests. Figure 3.1 shows the results of the strain sweep as the storage modulus with respect to the strain percent. A strain of 2.5% was found to be in the linear viscoelastic region and thus used in subsequent tests. Figure 3.2 shows the viscosity with respect to the shear rates of the two materials in the frequency sweep. The tests were done at 210 ˚C with a 500 micron gap under oscillatory shear. TPU compounded with the cross-linking agent showed a higher viscosity as compared to pure TPU. At low frequencies, the pure TPU had an initial drop in viscosity that the TPU with cross-linking agent did not show. This indicated a change in the microstructure of the molten TPU due to cross-linking. Figure 3.3 shows the loss tangent Tan δ as a function of frequency. It can be seen that both samples had a broad peak in Tan δ, where the pure TPU peak occurred at a higher frequency and higher value of Tan δ than the TPU with cross-linking agent. This was due to the cross-linked polymer's more networked microstructure which decreased damping in the material.[89] It can also be observed from Figure 3.1 that material compounded with the cross-linking agent displayed a higher storage modulus which indicates that the cross-linking agent helped increase the melt strength of the polymer. These details can be used to design processing parameters and guide material applications.

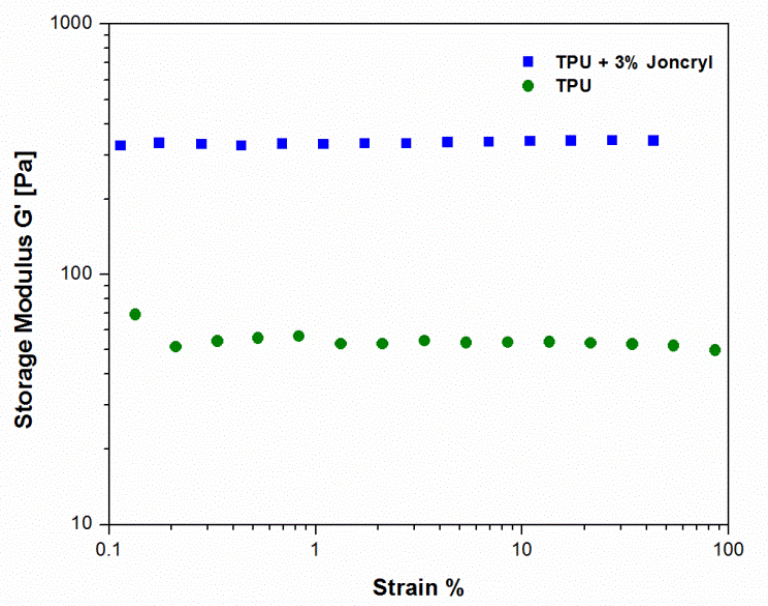

Figure 3.1. Storage modulus as a function of strain % for TPU and TPU + 3% Joncryl.

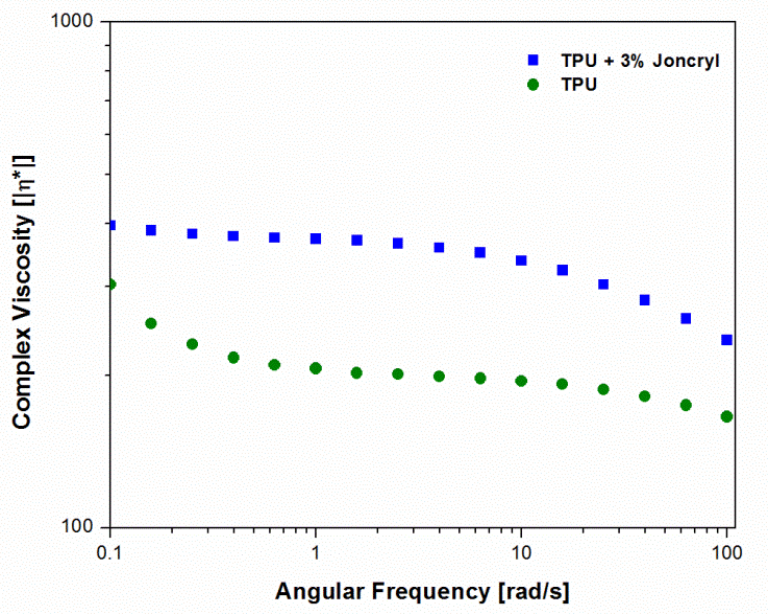

Figure 3.2. Complex viscosity as a function of angular frequency for TPU and TPU + 3% Joncryl.

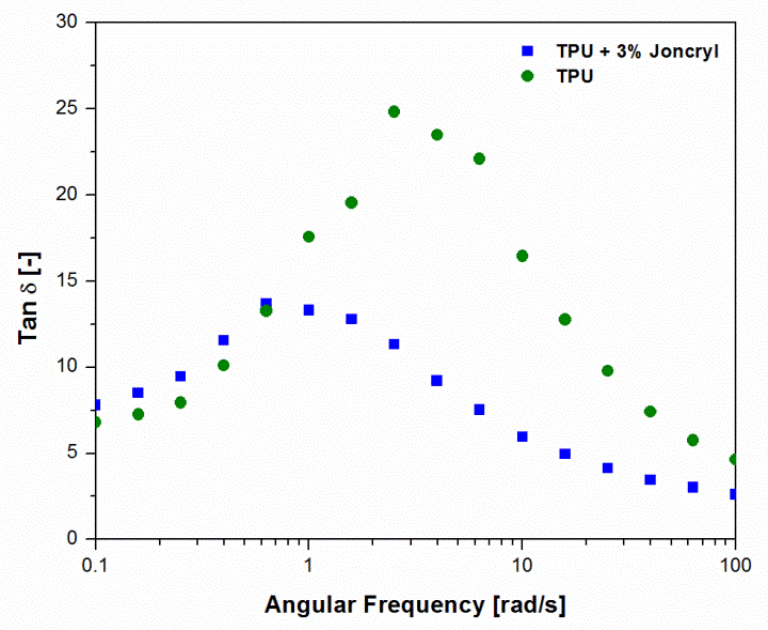

Figure 3.3. Tan δ as a function of angular frequency for TPU and TPU + 3% Joncryl.

Gel permeation chromatography (GPC) was conducted on both samples dissolved in tetrahydrofuran (THF) at a 0.25 mg/ml concentration. Results showed an increase in the weight average molecular weight (M_w) by 5.0% from a base molecular weight of 202000 g/mol for TPU, which can explain the increase in shear viscosity and storage modulus as seen in the rheological tests. Polystyrene was the standard used in the GPC test.

3.3.3 Thermogravimetric Analysis (TGA)

Thermogravimetric analysis (TGA) was performed on a TA Instruments Q50 with a heating rate of 10 °C/min and sample weights in the range of 25 to 30 mg. Figures 3.4 (a) and (b) show the weight loss and derivative weight loss, respectively, as a function of temperature for the two compositions of TPU. Pure TPU showed an early onset of degradation as compared to TPU

compounded with the cross-linking agent, suggesting that the cross-linking agent also helped to improve the thermal stability of TPU.

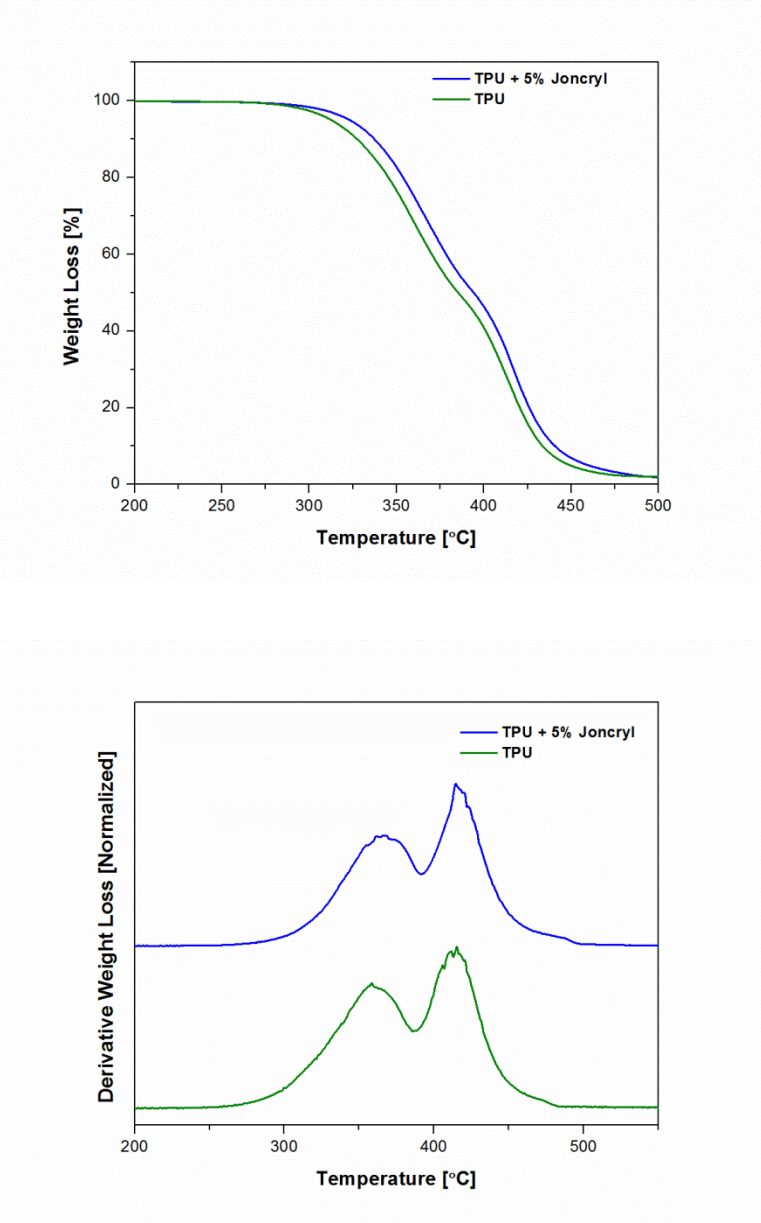

Figure 3.4. Thermo-gravimetric analysis (TGA): (a) weight loss as a function of temperature, and (b) derivative weight loss as a function of temperature.

3.3.4 Differential Scanning Calorimetry (DSC) Analysis

Differential scanning calorimetry (DSC) was conducted on three compositions of TPU (TPU, TPU + 3% Joncryl, and TPU + 5% Joncryl) to emphasize the effect the cross-linking agent has on the crystallinity of TPU. DSC was performed on a TA Instruments Q20 with a heating rate of 20°C/min and a cooling rate of 10˚C/min. The 10˚C/min cooling rate was the maximum rate the DSC equipment could reliably attain. Sample weights were in the range of 6 to 10 mg. Figures 3.5 (a) and (b) show the first cooling and second heating curves of TPU, TPU + 3% Joncryl, and TPU + 5% Joncryl, respectively. During cooling, the TPU specimen has 3 distinct exothermic peaks that arise from the short and long range orders and the crystallization of the hard segments in TPU. When the cross-linking agent Joncryl is added, the ability of the crystals to form as in pure TPU is impeded. Furthermore, increased viscosity with the addition of cross-linking agent as confirmed by the rheology tests can impede the formation of crystalline hard segments. The effect can be seen as a decrease of intensity as in the peak at 118˚C, a decrease of intensity and a shift to lower temperature as observed in the peak at 54˚C, or an elimination of a peak entirely exhibited in the peak at 107˚C for the 5% Joncryl case. In the second heating curves one major peak at 134˚C and an extended shoulder of that peak are visible in all three samples, but the peak's intensity diminishes as the percent loading of the cross-linking agent increases. A smaller peak in either cooling or heating indicates less crystallinity, again due to the cross-linking agent's interference with crystallization.[90]

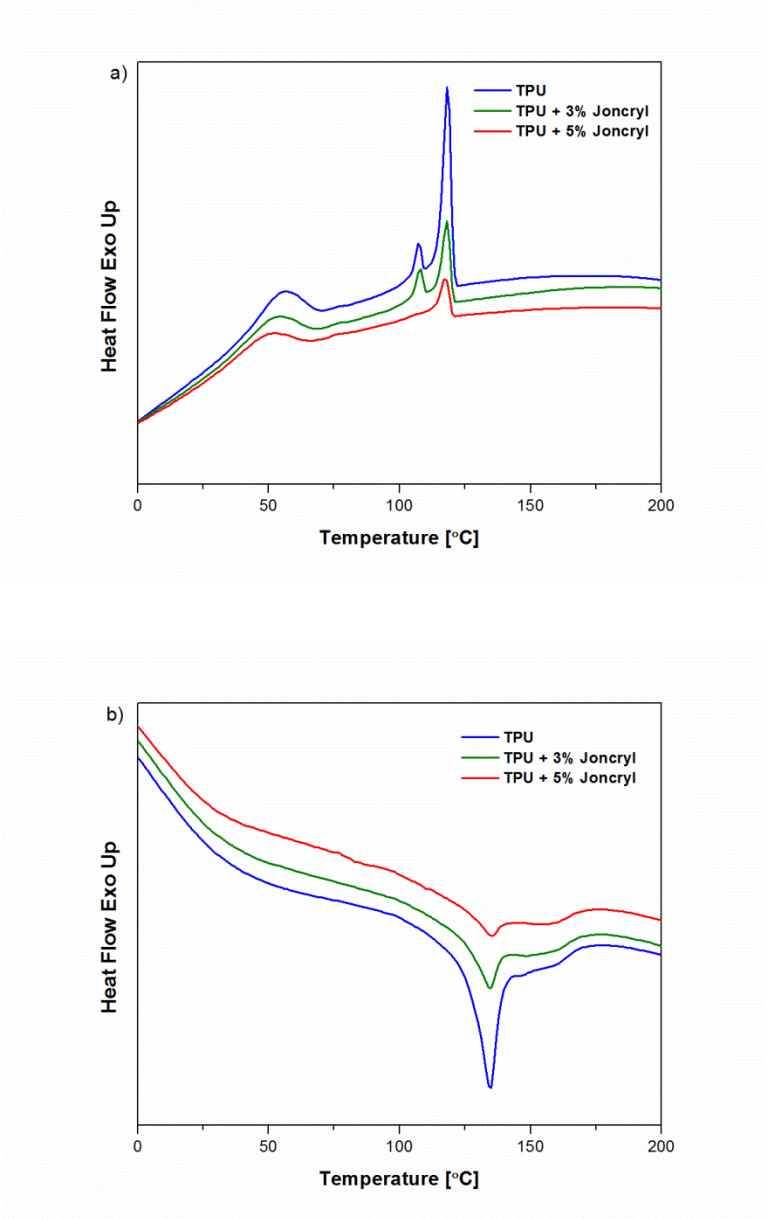

Figure 3.5. Differential scanning calorimetric analysis for TPU: (a) 1st cooling curve and (b) 2nd heating curve.

3.3.5 Mechanical Testing

Solid ASTM D638 Type I tensile bars were injection molded with TPU and TPU com-

pounded with 3 % and 5 % cross-linking agents to study the effects of cross-linking agents on the tensile strength of TPU. The processing parameters used in injection molding are tabulated in Table 3.2. Tensile testing was performed on the foamed and unfoamed specimens on a mechanical tensile testing machine (Instron 5967) according to ASTM D638. The specimens were held between static and movable clamps and stretched with a cross-head speed of 500 mm/min to a 400 % strain. Figure 3.6 shows the tensile stress as a function of strain obtained during the tensile testing of the pure and foamed specimens. Figure 3.7 shows a comparison of the tensile modulus normalized by foam density of the pure and foamed tensile bars with and without cross-linking agents. It can be seen that both the tensile modulus and the tensile strength increased in the unfoamed specimens with the addition of the cross-linking agent. Foamed specimens compounded with a cross-linking agent displayed higher values of tensile strength and tensile modulus as compared to those without the cross-linking agent, in spite of having a lower density. The tensile modulus normalized with density (cf. Figure 3.7) showed that foamed samples displayed higher specific moduli as compared to their solid counterparts.

Table 3.2. Processing conditions for injection molding solid samples.

Parameter	Units	Value
Mold temperature	°C	25
Cooling time	s	75
Injection pressure	MPa	250
Pre-drying	°C/hr	80/4
Barrel temperature	°C	215/210/200/195/190
Injection speed	cm^3/s	25
Screw rotation speed	rpm	100

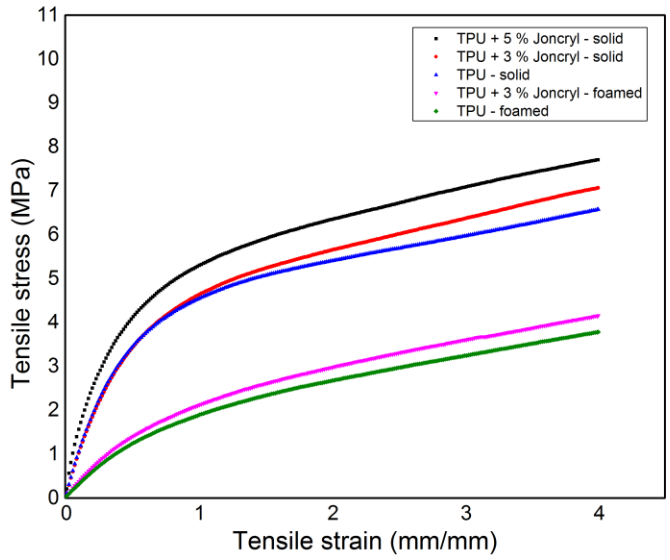

Figure 3.6. Tensile testing of the TPU parts molded with and without a cross-linking agent.

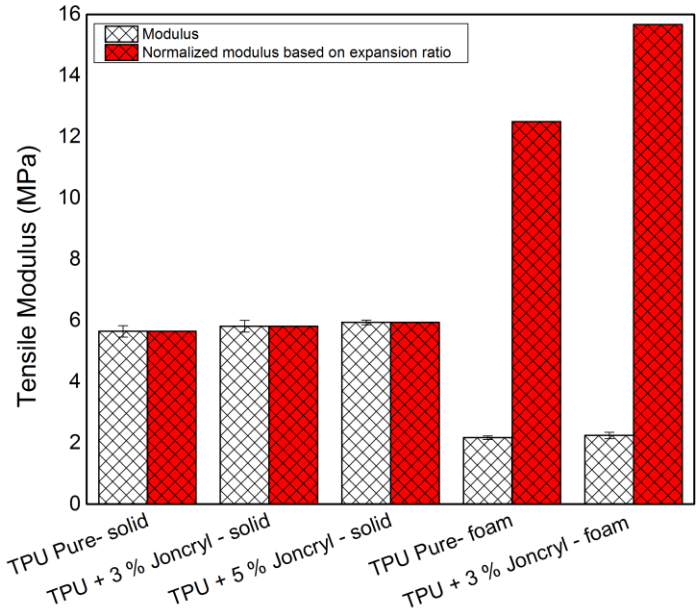

Figure 3.7. Tensile moduli for solid and foamed TPU parts molded with and without a cross-linking agent.

3.3.6 Microstructures

The microstructures of the foamed samples were observed by cutting the tensile bar samples across the flow direction. Both materials showed good microstructures with the absence of any large voids as can be seen in Figure 3.8. The density reduction was achieved by bulk expansion of the parts. The mold was opened prematurely according to the parameters listed in Table 3.1 to allow the part to expand, thus changing its cross-sectional area.

Figure 3.8. Images of the foamed cross-sections of microcellular injection molded TPU parts with a cross-linking agent.

3.3.7 Scanning Electron Microscope (SEM) Analysis

The foamed TPU specimens were cryogenically fractured using liquid nitrogen at approximately half the tensile test bar flow length. SEM specimens were prepared by coating them with a thin layer of gold. Figure 3.9 shows the SEM images of the TPU specimens molded with and without the cross-linking agent at the edge and the center of the cross-section, across the flow

direction. As can be seen in Figure 3.9, foaming with the cross-linking agent yielded a cell structure that was distinctly different from that of the pure TPU. First, at the center of the part (cf. Figure 3.9), the TPU compounded with the cross-linking agent showed a more closed-cell microstructure, even when molded at lower bulk densities, whereas pure TPU showed a deterioration of its microstructure via cell coalesce, even at higher densities.

The final microstructure of an injection molded part is a result of the competing transient processes of cell nucleation/growth and strengthening of the polymer around the growing bubbles. The center region of the injection molded part, being the last to cool, usually shows the coarsest microstructure across the cross-section of a foamed part. The increased melt strength achieved by the addition of the cross-linking agent helped to reduce the cell size and cell coalescence. The cell size distribution in the TPU specimens with the cross-linking agent was more uniform than that in the pure TPU specimens, except in regions near the part's edge. Recall that the cross-linking agent enabled TPU to expand to a very low foam density of 0.159 g/cm^3 at a higher gas content and mold temperature. As for the pure TPU, which didn't have the cross-linking agent, similar processing parameters yielded parts with huge voids in the central region. For pure TPU, both gas content and mold temperature had to be reduced to mold parts of acceptable quality, and those parts could only be expanded to 0.193 g/cm^3 at the best. However, open cell formation and cell coalescence can be seen in the center region, which negatively affected the mechanical properties of the microcellular pure TPU parts.

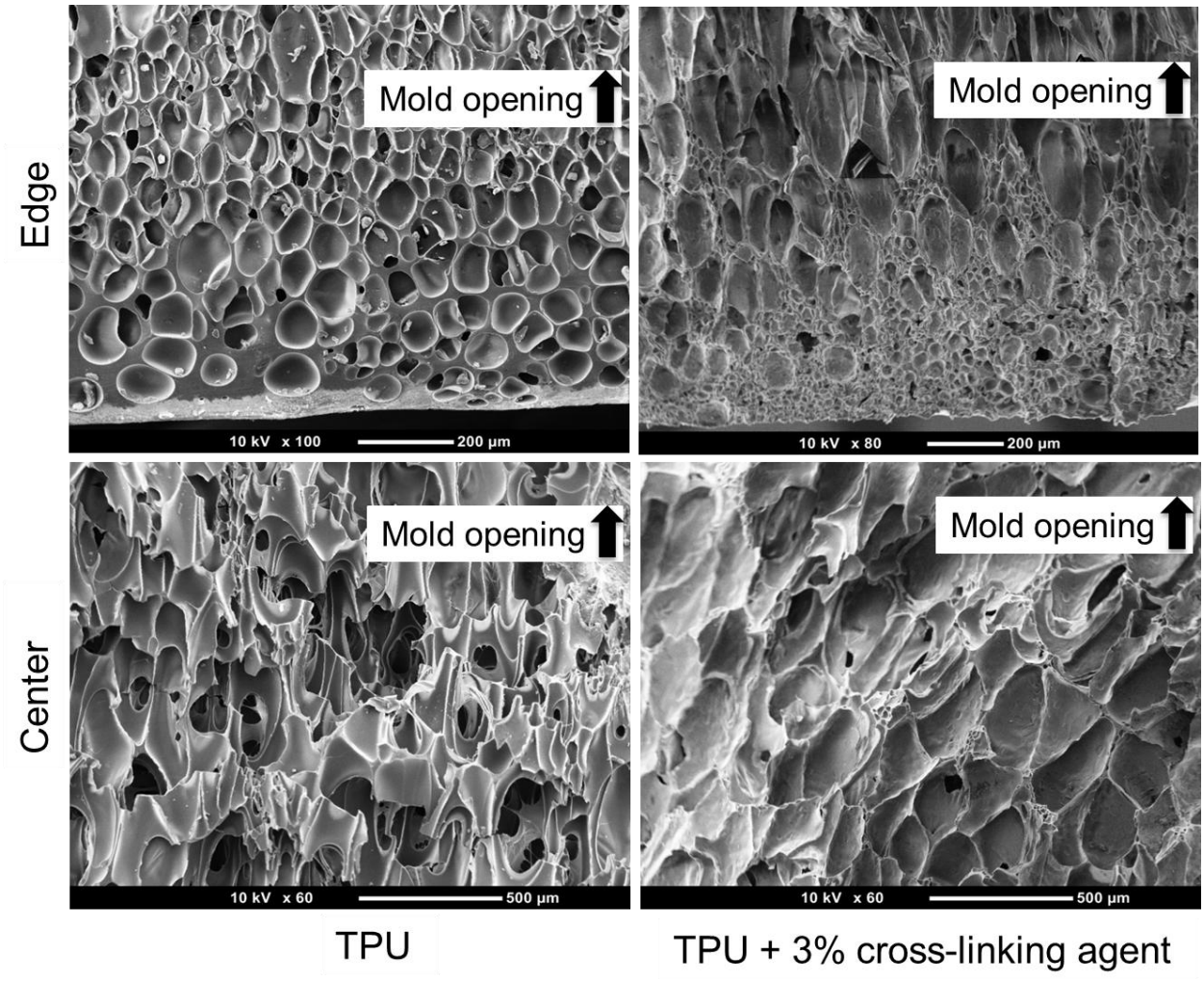

Figure 3.9. SEM images of TPU parts molded with and without a cross-linking agent across the thickness direction.

Second, it can be seen that a large number of smaller cells could be observed at the edge of the part (cf. Figure 3.9) without the polymer rich skin. In addition, a bimodal cell structure was observed in the TPU with the cross-linking agent. Figure 3.10 shows a histogram of cell sizes observed at the edge of the part. Two distinct peaks were seen in the material compounded with the cross-linking agent, which is indicative of a bimodal structure. It has been shown earlier that

increased tensile stresses in the polymer matrix, caused by stretching of the polymer during cell growth, can facilitate the nucleation of secondary cells.[91, 92] The growth of the secondary nucleated cells was inhibited by the increasing melt strength due to part cooling and the depletion of gas around the cells. The secondary nucleated cells were thus smaller in size, which can be observed as the bimodal structure seen in the SEM images. Recall that the addition of the cross-linking agent resulted in an increased storage modulus and viscosity (cf. Figures 3.1 and 3.2). Therefore, at a similar strain, it can be assumed that the TPU compounded with the cross-linking agent experienced larger tensile stress around a growing cell, which would further facilitate secondary nucleation by reducing the critical bubble radius for nucleation.[92] Furthermore, it should be noted that addition of cross-linking agent enabled the use of aggressive molding conditions such as higher mold temperature and gas saturation levels to achieve even lower bulk densities. Higher degree of supersaturation facilitates the nucleation of cells and a higher mold temperature can facilitate the growth of cells near the edges of the part, as seen near the edges of specimens molded with cross-linking agent (cf. Figure 3.9). On the other hand, a lower degree of supersaturation in the case of pure TPU would result in a smaller nucleation rate. The dissolved gas diffused over smaller number of cells thus resulting in larger cells, as observed at the edge of pure TPU foamed specimens in Figure 3.9.

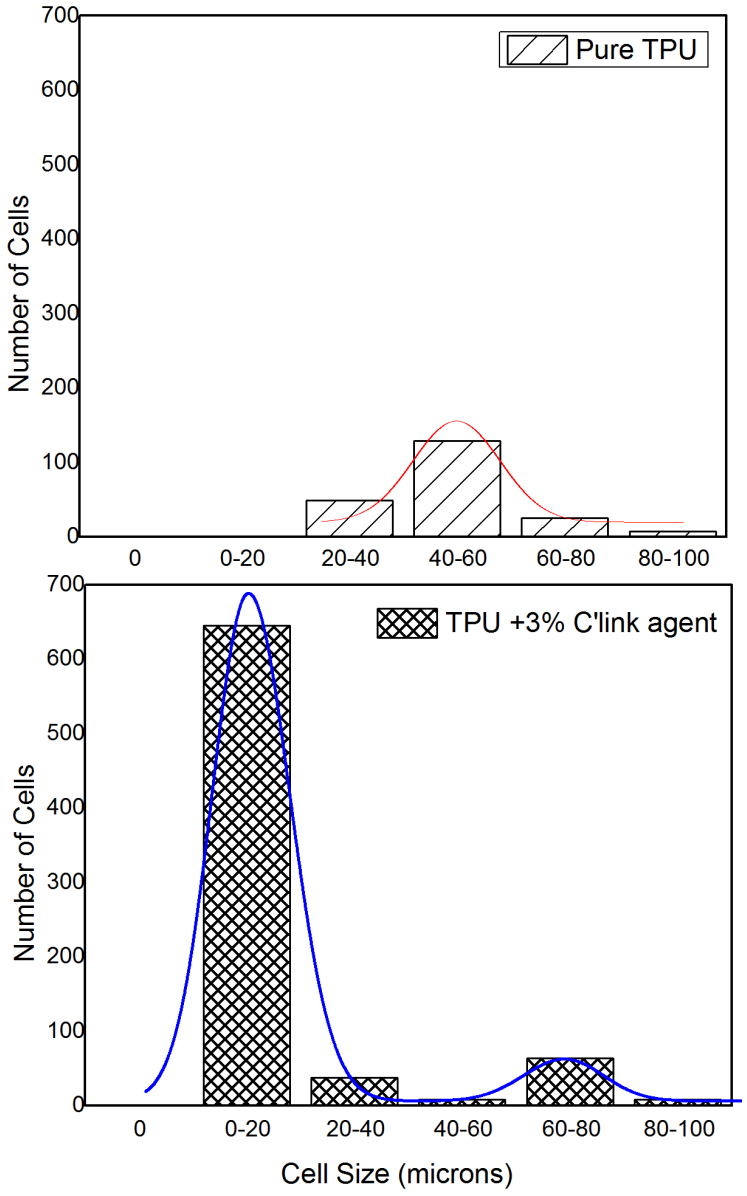

Figure 3.10. Histogram of cell sizes for TPU foamed parts molded with and without a cross-linking agent.

3.4 Conclusions

The addition of a cross-linking agent to TPU increased the molecular weight, storage modulus, and viscosity of the TPU while reducing the tan delta values. These changes were indicative of increased melt strength with compounded TPU compared to pure TPU during foaming. When foaming TPU with a cross-linking agent, higher melt strength allowed us to reach a lower density by foaming more aggressively via increasing the mold temperature and gas dosage levels. TPU with the cross-linking agent could be foamed to a minimum density of 0.159 g/cm^3 at the higher end of the processing window as compared to a minimum density of 0.193 g/cm^3 for pure TPU foams. SEM analyses of the foamed parts showed a more intact foamed structure for TPU with the cross-linking agent, with less cell coalescence in the center of the molded part even at higher density reductions. The skin layer analyses showed that extremely small cells nucleated and grew near the skin layer, as compared to pure TPU foams. To achieve extremely low bulk densities in the microcellular injection molding of TPU while maintaining a good consistent microstructure throughout the thickness of the part, it is essential that bulk expansion through cell growth occurs at higher melt strength.

4 EFFECT OF NUCLEATING AGENT AND TWO-STAGE EXPANSION ON THE MORPHOLOGY AND MECHANICAL PROPERTIES OF MICROCELLULAR INJECTION MOLDED THERMOPLASTIC POLYURETHANE

4.1 Introduction

In the microcellular injection molding (MIM) cycle, a homogenous polymer–gas solution is created by mixing a physical blowing agent (such as CO_2 or N_2) with the molten polymer during the screw reciprocation process. As the polymer–gas solution experiences a thermodynamic instability during injection, cell nucleation occurs. With cell nucleation, the gas surrounding the nucleation sites starts diffusing toward the gas-depleted regions, and hence bubble growth occurs. The growth of the cell depends on the pressure of the gas inside the cell and the strength of the polymer matrix surrounding it. The strength of the polymer inside the mold cavity rapidly increases as the part cools down during the cooling cycle of the process. This phenomenon of cell nucleation and growth, which leads to the final microstructure, is therefore of a transient nature. The final microstructure of an MIM part depends on a lot of factors such as the number of nucleating sites, the supersaturation level of the blowing agent, the strength of the polymer matrix at the time of growth, and the processing parameters of the MIM process. Achieving a fine, cellular, closed-cell structure is especially challenging due to the thermodynamically unstable cells and the short time span and rapid temperature change between cell nucleation and growth. Furthermore, as the desired density reduction increases beyond the recommended 8–10 wt%, getting a fine and uniform microstructure becomes particularly challenging because the

polymer wall thickness between adjacent cells is inversely proportional to the weight reduction. [18] Cell growth also depends on the number of nucleating sites and the stiffness of the polymer material. The final cell size and density are further affected by the degree of cell coalescence, which leads to a deterioration of cell density and a bigger cell size. Cell coalescence is more severe in a system with non-uniform cell size due to the rupture of cell membranes caused by the differential pressure between cells of different sizes.

With TPU specifically, it can be seen that the strength of the melt at higher temperatures is low and, coupled with the elastic nature of the soft segments, allows TPU to foam to greater weight reductions as compared to regular thermoplastics.[49] Although lower densities are possible, achieving a homogenous microstructure throughout the cross-section is challenging. It is imperative to have a high density of cell nucleating sites, which can help to lower the pressure inside each individual cell and thus deter cell coalescence. It is well-known that the addition of suitable microscale and nanoscale nucleating agents in foaming polymers leads to low energy barrier sites at the interface between the polymer and the additives thereby improving cell nucleation.[32, 42, 92] In a two-step batch foaming process, where foaming was carried out at or below the glass transition temperature, sub-micron size cellular foams have been shown to be possible with and without the presence of nanoclay.[29, 68, 76, 93-95] To achieve a well dispersed microcellular structure, it is important that there be a large number of nucleating sites, and the growth of cells be inhibited by strengthening the melt of the surrounding matrix by either rapidly cooling the melt, or by the addition of agents that can augment melt strength. It has been shown that the complex viscosity and the dynamic storage modulus of TPU can be increased significantly by the incorporation of organoclay, which aids the formation of an interphase

between the soft and hard segments of the TPU matrix.[96] In this study, highly expanded TPU foams were manufactured via microcellular injection molding with nitrogen (N_2) as the physical blowing agent. In addition, cavity expansion at a preset time during cooling (when the melt strength of TPU became higher due to cooling) was employed to further reduce the foam density. It is generally seen that rebound resilience deteriorates with bulk density of the foam, as the foam becomes more compressible and shock absorbing. It is imperative for certain applications in the sport-wear industry to have improved rebound resilience properties while achieving lower densities. It is envisioned that the presence of well dispersed nanoclay in the TPU matrix, which can act as a nucleating agent while strengthening the matrix, coupled with the promotion of cell growth at a lower melt temperature by delayed cavity expansion, would help create very low density TPU foams with a good microstructure. Furthermore, improved rebound resilience properties for the foam can be achieved by increasing alignment of polymer and microcells in the testing direction coupled with a better control on microstructure in the process of microcellular injection molding.

4.2 Experimental Methods and Materials

4.2.1 Materials

TPU (Elastollan® 1180A10, BASF), a flexible polyether-based elastomer, was used as the polymer matrix in this study. The layered nanoclays used were an organically modified mont-morillonite, Cloisite® 30B (C30B), from Southern Clay Products, Inc. C30B is a natural clay modified with a functional group (methyl bis-2-hydroxyethythyl ammonium quaternary salt). It has a cation exchange capacity of 90 meq/100 g. Organically modified layered clays have the

potential of strong interactions with polymer molecules due to their functional group polarity. Typically, a modified nanoclay has a density of 1.98 g/cm^3 and uses MT_2EtO as a modifier at a concentration of 90 meq/100 g of clay. It should be noted that MT_2EtOH consists of methyl, tallow, bis-2-hydroxyethyl, and quaternary ammonium. Nitrogen gas was purchased from Airgas and used as received as a physical blowing agent in the MIM process.

4.2.2 Equipment

An 18 mm co-rotating twin screw extruder, model LZE-18 (Leistritz), was used to compound nanoclay with TPU. An injection molding machine (Arburg ALLROUNDER 320S) was used for sample fabrication. The injection molding machine was equipped with microcellular injection molding capability (MuCell® Trexel, Inc.) that enabled precise control of the gas injection dosage by adjusting the pressure drop between the gas delivery and the exit, the gas flow rate, and the valve open time. A custom injection mold was designed and fabricated from 6061 aluminum. Figure 4.1 depicts the resultant component with a center sprue gate. The densities of the foamed samples were measured using ASTM D792 with Archimedes buoyancy principles. The microstructures of the foamed samples were observed using a scanning electron microscope (SEM) (JCM-5000, NeoScope). Cyclic compressive strengths were studied using a universal testing machine (5967, Instron). Viscosity measurements were made on a TA Instruments AR 2000ex stress controlled rheometer. Rebound resilience was tested as per ASTM D 3574-11H. Image analysis was conducted using ImageJ software.

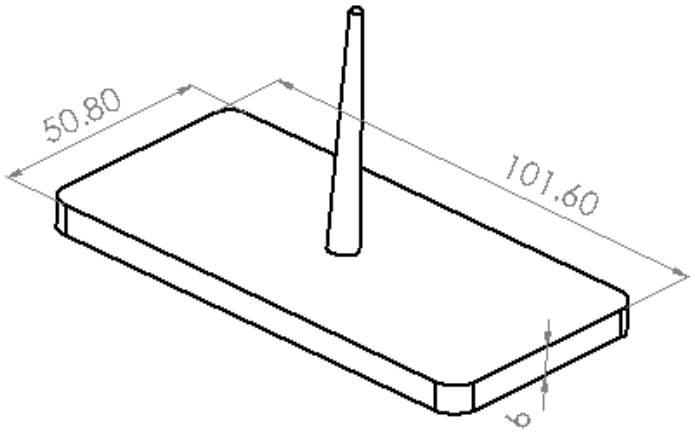

Figure 4.1. Schematic of an injection molded component. The original cavity thickness without mold cavity expansion is 6 mm. (Unit: mm)

4.2.3 Experimental Conditions

Five percent nanoclay by weight was compounded using a twin-screw extruder, as that composition of nanoclay had shown earlier to be capable of achieving the highest density reductions.[97] The material preparation and processing parameters used prior to and in the extrusion process are tabulated in Table 4.1. To maintain a similar thermal and shear history, unfilled TPU was also extruded with the same processing conditions to be later used in the MIM process and rheological tests for comparison. After compounding, the extrudate strand was pelletized into pellets. Extruded pellets were dried to remove any moisture before being used for microcellular injection molding. Foamed samples, with nitrogen as the physical blowing agent, were injection molded with TPU and TPU + 5% nanoclay, as per the parameters shown in Table

4.1. Density reduction was obtained by injecting a 24 cm^3 polymer–gas mixture into a larger cavity. The melt was allowed to foam and cool for 160 s in the mold (hereafter referred to as non-expanded samples). A second set of samples with even lower bulk densities (hereafter referred to as expanded samples) were produced by injecting the same shot volume into the mold cavity followed by rapidly expanding the cavity volume. The volume expansion was achieved by pre-maturely opening the mold cavity to an intermittent distance of 3 mm after undergoing 60 s of cooling. The expanded part was further allowed to cool for 100 s before ejection from the mold. . As the mold cavity was expanded, the internal pressures of nucleated cells enabled the stretching of the fast cooling elastic TPU to expand in the direction of mold opening. Although slight post-molding expansion was observed for the expanded samples, the overall flatness of the samples were maintained.

Table 4.1. General material preparation and processing parameters for twin screw extrusion and injection molding processes.

Twin Screw Extrusion		
Parameter	Unit	Value
Drying temperature	°C	100
Drying time	hours	2
Screw rotation speed	rpm	150
Barrel temperatures	°C	180/180/180//190/190/200/200
Injection Molding		
Parameter	Unit	Value
Drying temperature	°C	100
Drying time	hours	2
Back pressure	MPa	15
Melt temperatures	°C	185/190/200/210/210
Injection pressure	MPa	250
Injection speed	cm^3/s	70
Screw rotation speed	rpm	190
Mold temperature	°C	40
Gas dosage	%	0.5
Shot weight	cm^3	24
Mold opening speed	cm/s	5

4.3 Results and Discussion

4.3.1 Density Measurements

The mass densities in g/cm^3 of both non-expanded and expanded samples were determined using the buoyancy method as per ASTM D792. The average density measured of the expanded and non-expanded samples is tabulated in Table 4.2. It can be noted that although the same shot size was injected into the cavity, the density of the samples with nanoclay was slightly higher because nanoclay has an inherently high density as compared to TPU.

Table 4.2. Results of SEM analysis and mechanical tests.

Measured Variables	Units	TPU		TPU + 5 % Nanoclay	
		Non-expanded	Expanded	Non-expanded	Expanded
Bulk density	g/cm^3	0.68	0.42	0.70	0.43
Average cell size ± std dev	microns	27.5 ± 9.5	69.8 ± 17.8	19.3 ± 7.64	26.4 ± 8.1
Cell density	x10^7 cells/cm^3	2.65	2.05	3.17	3.05
Rebound resilience	%	38.0	44.7	36.0	41.0
Hysterisis loss ratio	%	32.6	22.3	40.75	37.3

4.3.2 SEM Analysis

The microstructures of TPU and TPU/nanoclay composite foams were investigated using a Neoscope SEM (JEOL-5000). The injection molded parts were cryogenically fractured using liquid nitrogen at locations shown in Figure 4.2. The exposed cross-sections were sputter-coated

with gold before SEM imaging. Figure 4.3 shows the SEM images of the samples with TPU and TPU compounded with 5% nanoclay, with and without mold expansion. It can be seen from the SEM images (cf. Figure 4.3 (a) and (c)) that in non-expanded samples, both materials showed a uniform closed-cell microstructure. There seems to be equilibrium between the internal pressures of the nucleated bubbles and the melt strength/local pressure exerted by the polymer walls around the cells. However, as the samples underwent the mold expansion stage, the micro-structure exhibited a significant change (cf. Figures 4.3 (b) and (d)). Using SEM images and the Image Pro-Plus software package, the cell diameter (d) in μm was measured to study the cell size distribution in a region of interest. The histogram of the number of cells within specific cell diameter ranges was curve-fitted using the Gaussian method and is shown in Figure 4.4. It should be noted that a narrower fitted curve signifies more uniform cell size distributions, and that a curve shifted to the left signifies a smaller average cell size. The cell density (N_f) in cell/cm^3 was calculated using Equation 4.1 and reported in Table 4.2.

$$N_f = \text{Cell density} = \left(\frac{N}{A}\right)^{\frac{3}{2}} \times \frac{\rho_{solid}}{\rho_{foam}} \tag{4.1}$$

Without mold expansion, the average cell diameter decreased from 27.5 μm to 19.3 μm (cf. Table 4.2) when nanoclay was added. The cell density increased with the incorporation of nanoclay. Nanoclay has been extensively used in earlier studies as a nucleating agent for foaming applications.[42] The decreased activation energy at the polymer–nanoclay interface provides a way to generate foams with significantly increased cell densities. With the mold expansion, the cavity volume suddenly increased, reducing the local pressure around the growing

cells. This thermodynamic instability and the internal pressures of the bubbles enabled the cells to further expand, seeking a new equilibrium between the internal pressure of the evolving cells and the strength of the melt around it. It is important to note that this secondary expansion occurs at much lower melt temperatures. At lower temperatures, the lower kinetic energy associated with the gas molecules, as well as the lower diffusion rates coupled with the higher melt strengths of the polymer, can help to achieve expansion without severely affecting the desired microstructures.

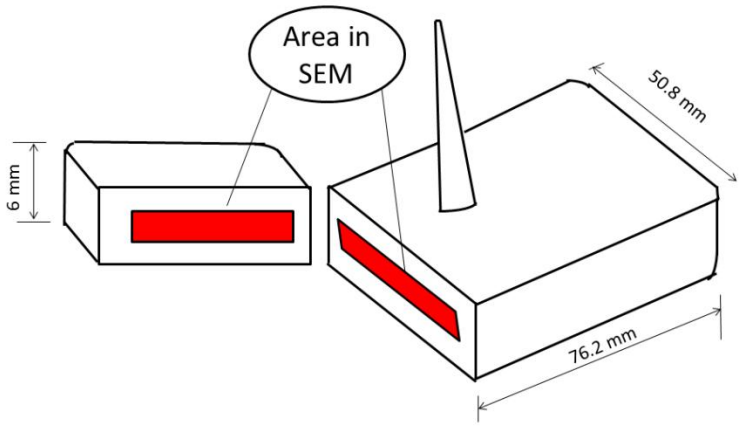

Figure 4.2. Cavity dimensions and location of SEM samples. Cavity thickness is enlarged to show the SEM imaging area.

The expanded TPU samples displayed more cell coalescence than those compounded with nanoclay. The polymer walls of the expanded TPU samples were aligned in the direction of mold opening (cf. Figure 4.3 (b)). With higher expansion ratios, the expanding gas could rupture the TPU skin and form aligned open-cell structures in the foam matrix. The expanded samples with the nanoclay showed a more controlled expansion of cells, while avoiding breaching of cell

walls. It can be argued that due to the higher cell density of samples with nanoclay, at a given gas dosage level, the internal pressures inside the nucleated cells will be lower, as the blowing agent will be distributed over a larger number of cells. This coupled with the rheological changes—specifically higher viscosity with the incorporation of nanoclay in the TPU matrix—helped to prevent the rapid degradation of the microstructure during expansion (cf. Figure 4.3 (d)). The effect of incorporating nanoclay into the TPU matrix on the rheological properties is discussed in detail in the next section. The cell size of the expanded TPU/nanoclay samples increased slightly to 26.4 μm to accommodate the expanding gas, but because of the higher viscosity of the matrix and the greater nucleation density, the cell structure did not deteriorate. Significant alignment and rupturing of cell walls as seen with TPU was not observed with the expanded TPU/nanoclay samples.

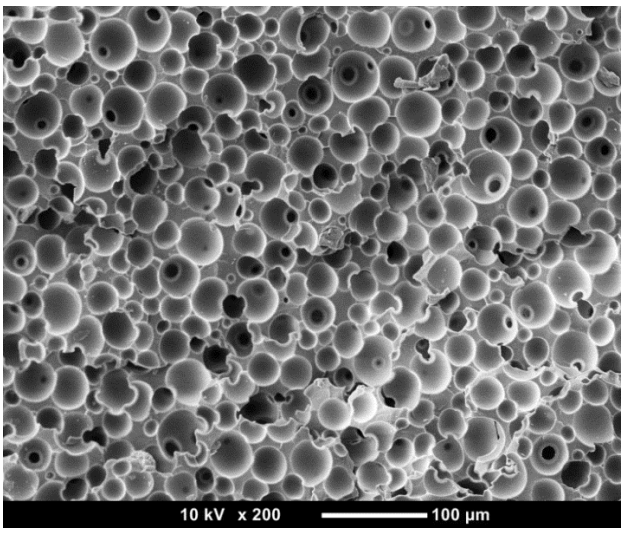

(a) TPU without mold expansion.

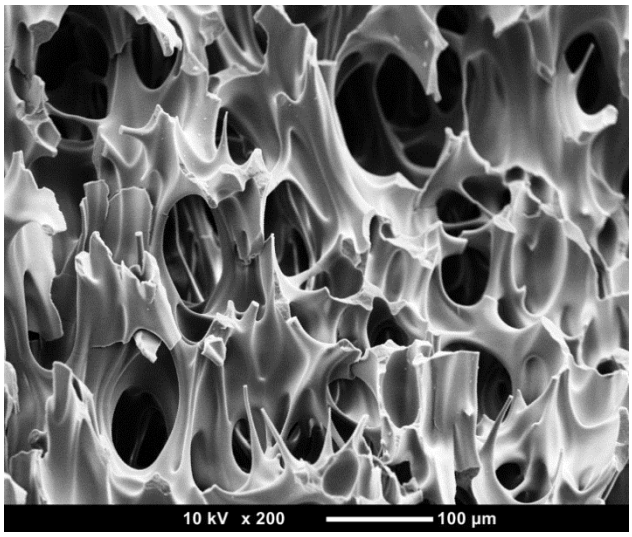

(b) TPU with mold expansion.

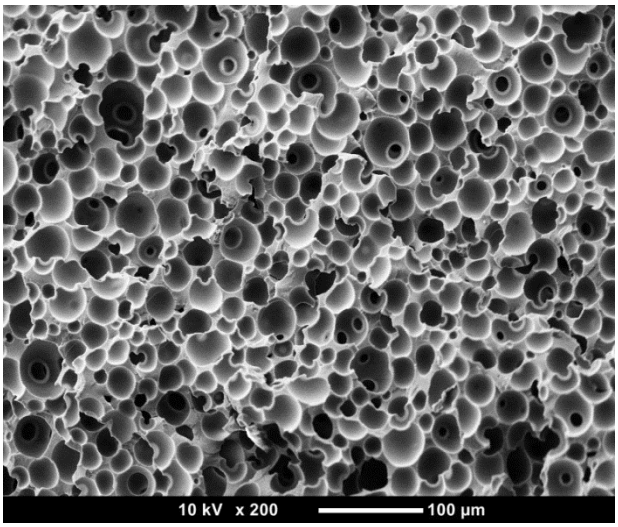

(c) TPU + 5% nanoclay without mold expansion.

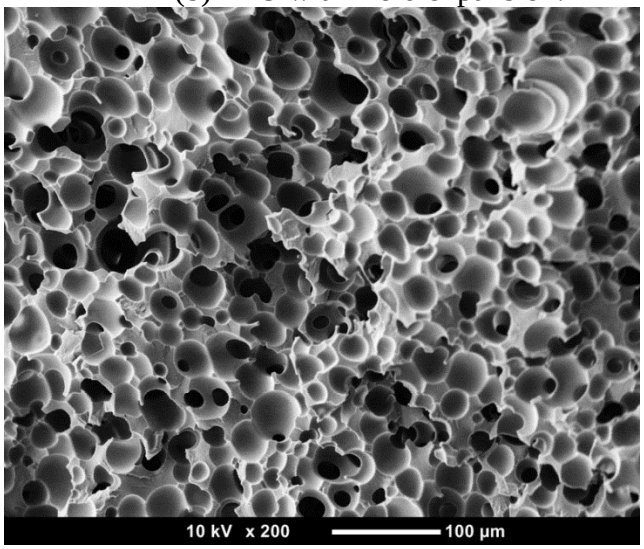

(d) TPU + 5% nanoclay with mold expansion.

Figure 4.3. SEM microstructures of parts with TPU and TPU clay composites, with and without mold expansion.

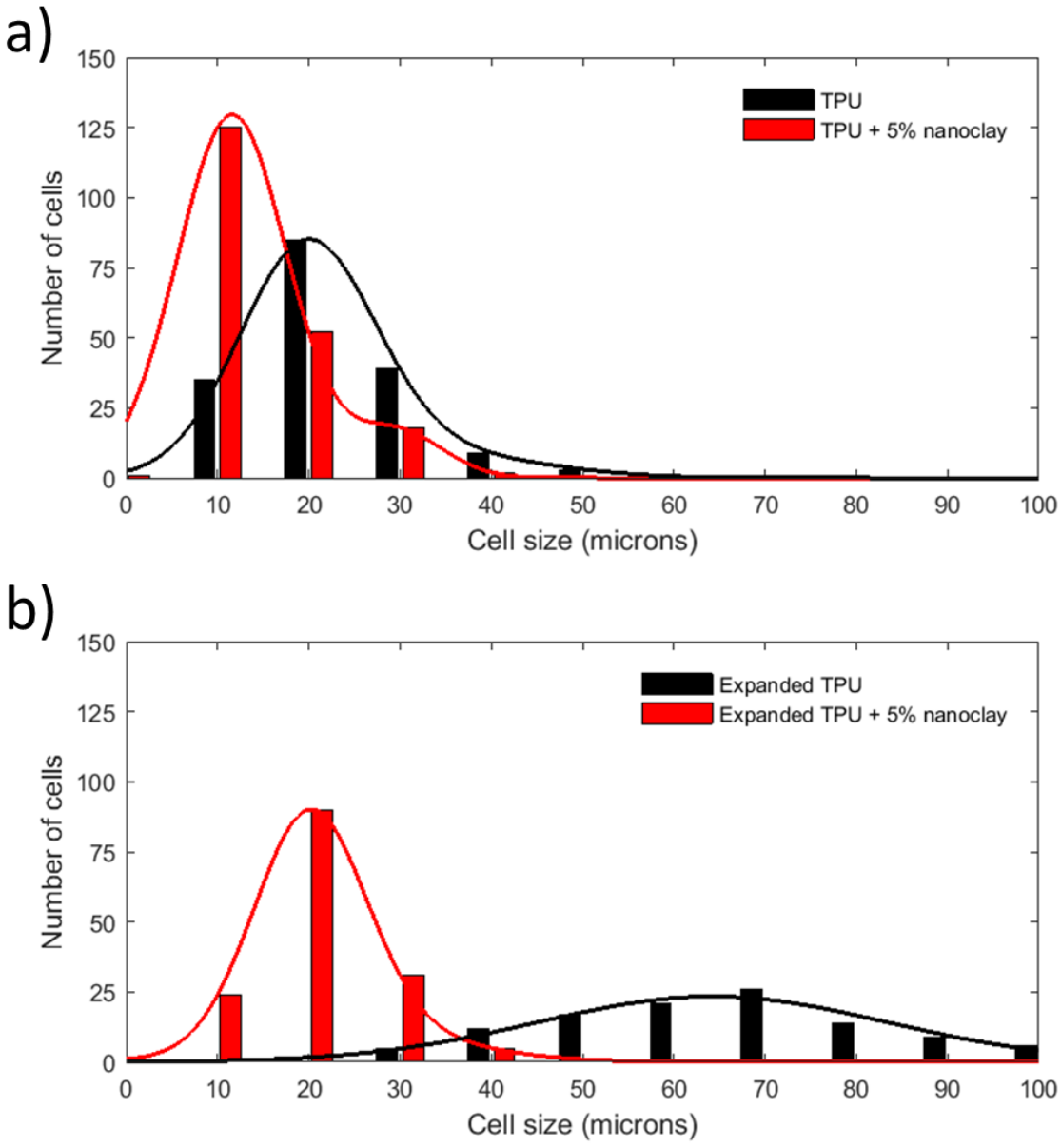

Figure 4.4. Effect of nanoclay addition on the microstructure of (a) non-expanded and (b) expanded TPU.

4.3.3 Rheological Analysis of Materials

Frequency sweeps, which ranged from 0.01 s^{-1} to 100 s^{-1}, were conducted on both TPU and TPU/nanoclay and were used to record the complex viscosity as a function of angular frequency. A 25 mm parallel plate oscillatory rheometer at 200˚C was used with a gap of 500 microns. The results of the tests are shown in Figure 4.5. As seen in Figure 4.5, TPU compounded with nanoclay displayed a higher complex viscosity at lower shear rates. Material compounded with nanoclay showed more shear thinning phenomenon at higher shear rates, which can be due to directional orientation of polymer chains and silicate layers along the flow direction dominated by nanoclay filled TPU. Nucleation and cell growth are both governed by the rheology of the melt, the gas diffusivity, and the solubility/dosage level of the gas. Melt strength, defined as the resistance to extensional flow in polymers and also referred to as their ability to withstand extension without breaking, is relevant to cell expansion because cell or bubble growth is purely extensional; specifically, equibiaxial extensional flow.[98, 99] Equation 4.2 describes the relationship between equibiaxial extensional viscosity (η_b) and shear viscosity (η) at small strains for Newtonian fluids.[87] Equation 4.3 relates the shear viscosity (η) to the complex viscosity (η*) via the Cox–Merz Rule over a large range of shear rates, where $\dot{\gamma}$ is the shear rate and ω is the angular frequency.[100]

$$\eta_b = 6\eta \tag{4.2}$$

$$\eta(\dot{\gamma}) = \eta^*(\omega) \tag{4.3}$$

One can easily relate the equibiaxial extensional viscosity with the complex viscosity; at least in theory and recognizing the non-Newtonian, shear-thinning behavior of the polymer melt that

$$\eta_b(\dot{\varepsilon}) = 6\eta^*(\omega) \tag{4.4}$$

where $\dot{\varepsilon}$ is the extensional strain rate. With increasing nanoclay content, higher viscosities and higher melt strengths can be expected. This increase in melt strength during foaming prevents the cells from growing too large, coalescing, and forming an open cellular structure.

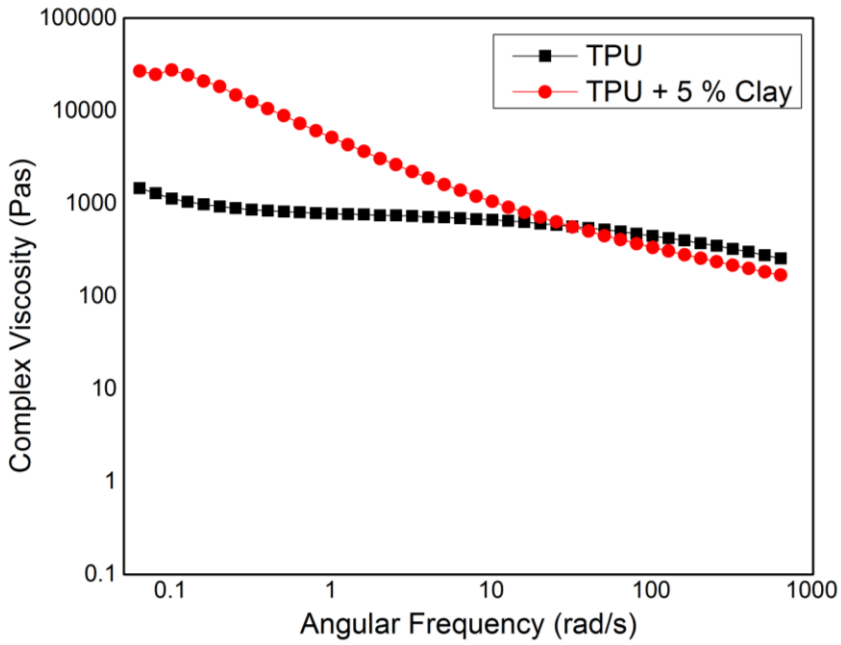

Figure 4.5. Complex viscosity as a function of shear rate for TPU and TPU + 5% nanoclay.

4.3.4 Mechanical Testing

Compressive Hysteresis Tests

Uniaxial cyclic compression hysteresis tests were conducted on microcellular injection molded foamed samples using an Instron 5967 testing machine at a rate of 50 mm/min. Samples were compressed to half of their original thickness for 100 cycles and the stresses observed were recorded. Figure 4.6 displays a typical outcome for a TPU foamed sample. As shown in the plot, the loading and unloading curves of the foamed sample during a cyclic compression test followed two separate and distinct paths. Due to the viscoelastic nature of the foam, the samples were capable of absorbing kinetic energy during the loading cycle and dissipating it as heat. Energy lost during deformation was measured as the difference between the energy required to load the sample (Area A+B) and the energy required to unload the sample (Area B). The area between the curves (Area A) was the energy lost during deformation. This ratio A/(A+B), known as the hysteresis loss ratio, provides a simple measure of the foam elasticity and resilience of the foamed material. The lower the ratio, the better the foam performed with respect to returning the energy absorbed during deformation. Higher hysteresis ratios indicate that foams are more energy absorbent and dissipating, which is more ideal for applications where shock absorbing properties are of paramount importance.

A typical hysteresis loop of TPU foam has three distinct regions (cf. Figure 4.6). The first and initial small elastic region relates to the energy required for bending the polymer walls between the microcells. As the foam becomes highly expanded, the material (wall) regions become thinner and the elastic regions get smaller. The second stage is described as the polymer

walls buckling and the microcells compressing. In this region, the stress does not increase at the same rate as the strain. In the last stage, at high strain, the walls of the polymer start compressing against neighboring walls; this is referred to as the densification region. In this region, the stress rises rapidly with increased strain. The stress–strain behavior of TPU typically demonstrates strong hysteresis, time dependence, and cyclic softening. It is generally observed that the stress–strain curve gets more compliant with numerous loadings as compared to the first cycle. Most of the softening occurs in the first cycle. The softening is usually linked to the permanent breakage of bonds and the irreversible destruction of some hard segment formations.[80]

Hysteresis curves for the first cycles of the samples are shown in Figure 4.7. It can be observed that with mold expansion, the foams immediately get softer, requiring less energy to achieve 50% compression. The non-expanded foams require more stress to achieve the same strain, which means that they would support more weight in load bearing applications. The weight/stress a foam can support before its densification occurs is a major input in the selection of foam for a specific application. It can be observed that the compressive moduli displayed by non-expanded foams in the early stages of compression are significantly higher than those of expanded foams. Furthermore, the loading and unloading curves of the non-expanded samples are significantly different as the foams are denser. A change in moduli can be observed around a strain of 40%, which signifies the start of the densification of the foam and the collapsing of the polymer walls. Unexpanded TPU shows a slightly higher level of stress at 50 % strain (cf. Figure 4.7) as compared to those with clay as foam densification, which is represented by a sharp increase in slope of the stress-strain curve starts early in the pure non-expanded TPU foams. Expanded foams, on the other hand, show flatter profiles during the loading and unloading

cycles, and do not reach the densification stage even at 50% strain. The addition of nanoclay did not have a significant effect on the hysteresis profile of the foams. The expanded and non-expanded foams with nanoclay had a slightly higher modulus as compared to those without nanoclay. The loss of energy as a percentage was calculated and is reported in Figure 4.8. Due to the viscoelastic nature of the foam, the foam is capable of absorbing some kinetic energy during the loading cycle and dissipating it as heat, and is thus a measure of the energy lost in the mechanical cyclic compression test. It can be observed from Figure 4.8 that the mold expansion process reduces the hysteresis loss ratio. The samples with nanoclay have higher hysteresis loss ratios signifying that the energy absorbing characteristics of the foams increased with the incorporation of nanoclay. The increased energy losses could be a result of internal friction and straining or breaking of bonds between the nanoclay and the TPU, which were absent in pure TPU. In both materials (the TPU and the TPU/nanoclay composite), the mold expansion process reduced the hysteresis loss, which correlates well with the increased values of rebound resilience observed with the same samples.

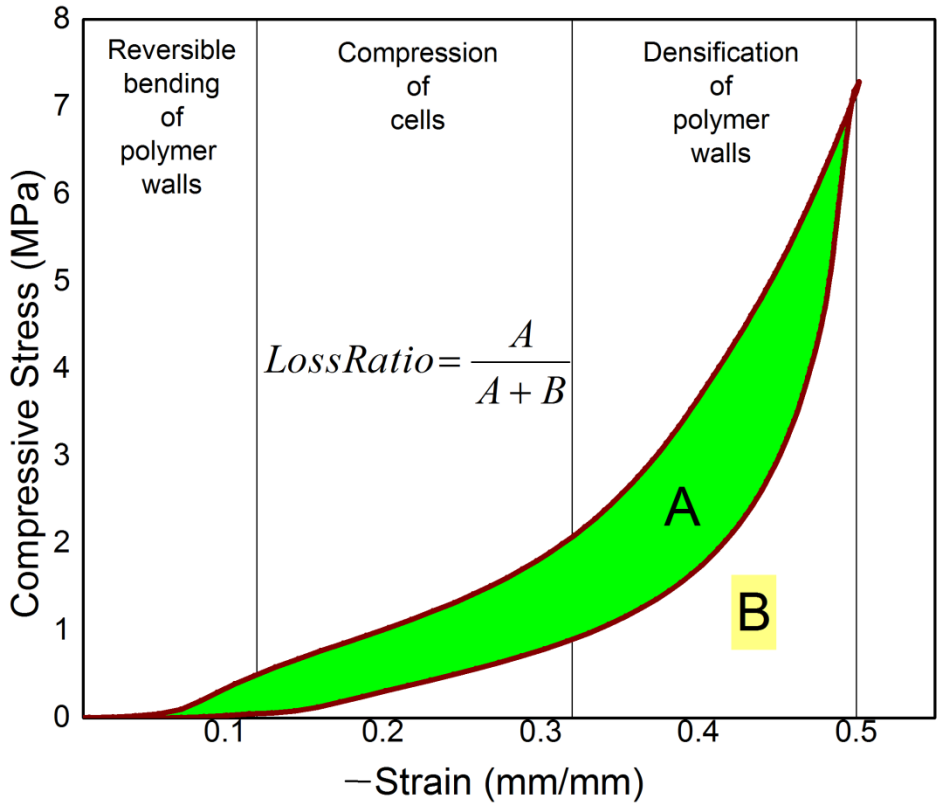

Figure 4.6: Typical hysteresis loop of foamed TPU.

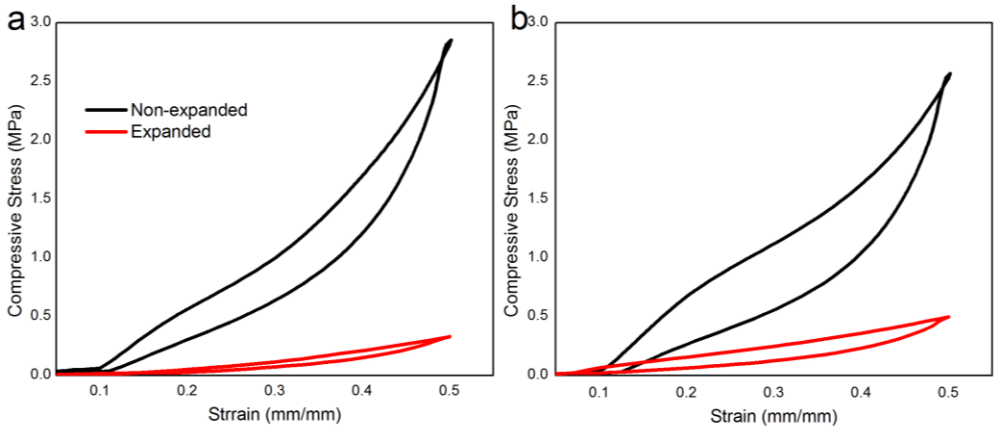

Figure 4.7. First cycle hysteresis loops for the foamed samples of (a) TPU and (b) TPU + 5% nanoclay.

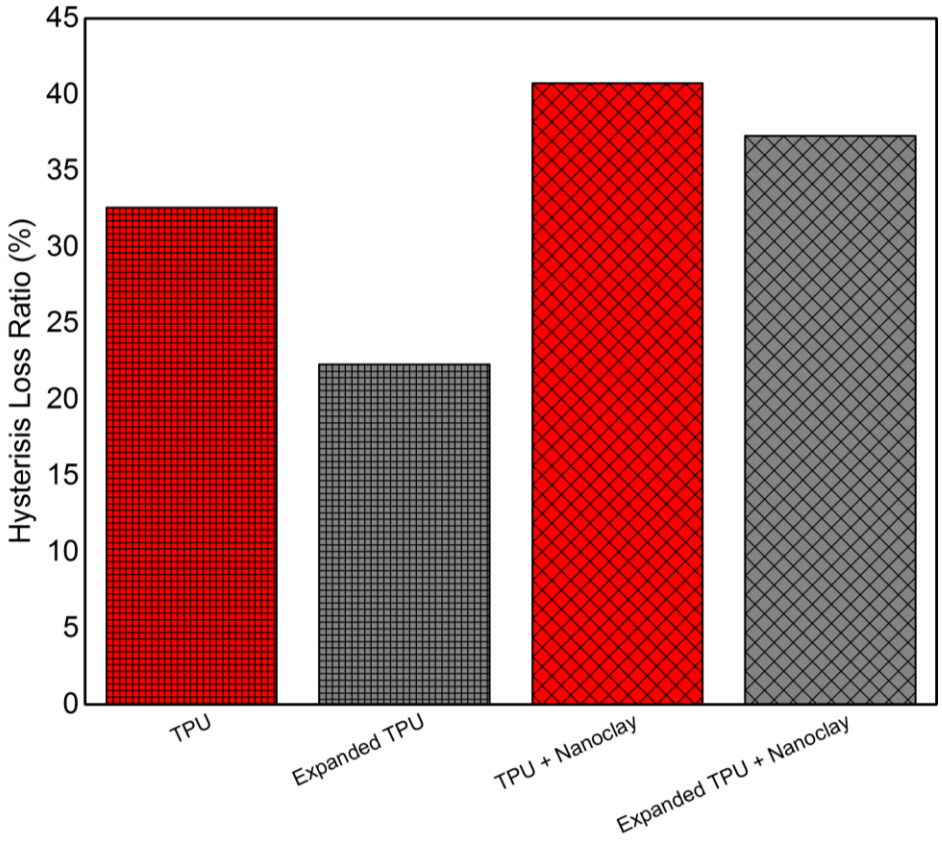

Figure 4.8. Hysteresis loss percentages.

Rebound Resilience

Rebound resilience tests were carried out on the samples according to ASTM D 3574-11H. Rebound resilience is an indicator of springiness of the foam and is typically measured by dropping a 16 mm diameter steel ball from a height of 500 mm. Unlike the hysteresis compression tests, which measure energy absorption characteristics of foams at higher strain percentages and compression ratios, rebound resilience testing is usually differentiated by its higher strain rates and lower values of strain. Foam properties like the solid layer thickness, microstructure, alignment of polymer walls and microcells seems to have a more accentuated

effect on the rebound resilience. In certain applications like the midsoles of sports shoes, low density foam with high rebound resilience is desired. Rebound resilience usually shows a decreasing correlation with the bulk density of foam, and the desirable property is higher resilience while achieving the lowest density; resilience values normalized with density are reported in Figure 4.9. It can be observed that the addition of nanoclay did not have any consistent or significant effect on the rebound resilience values. The mold expansion process definitely had a strong positive effect on the normalized rebound resilience values in both material combinations. Non-normalized rebound resilience values also increased significantly as observed in Table 4.2. Resilience values of neat TPU increased by a higher percentage, 35%, for expanded TPU, as compared to a 29% increase for nanoclay-filled TPU. It can be seen that the resilience values or springiness of the foam can be increased even while achieving lower densities. Since the TPU was expanded in the mold opening stage after 60 seconds of cooling, the expansion occurred at much lower melt temperatures and was possible because of the elastic nature of TPU. This caused the elastic TPU to be stretched as it was cooling down, creating polymer and micro-cell alignment in the direction of mold opening and also causing the TPU to be pre-stressed. In this study, the direction of mold opening is also the direction of resilience testing. It has been demonstrated earlier that the nonlinearity in the compressive response of foams at low strain percentages is governed by cell ligament buckling [101] or the quasi-reversible bending of cell ligaments. Foams with anisotropic cells have an increased alignment of polymer ligaments, and furthermore, display increased compressive moduli in the direction in which the cells are elongated. This alignment of polymer walls, molecules, and microcells in the loading direction can help to achieve higher resilience values while decreasing the bulk density

of the foam. The increase in rebound resilience was higher in the case of TPU, where the cells and molecules were more aligned in the direction of mold expansion. The tests were repeated after 30 days to observe if relaxation changed the rebound resilience values. The rebound resilience values tested after 1 month showed no degradation in rebound properties.

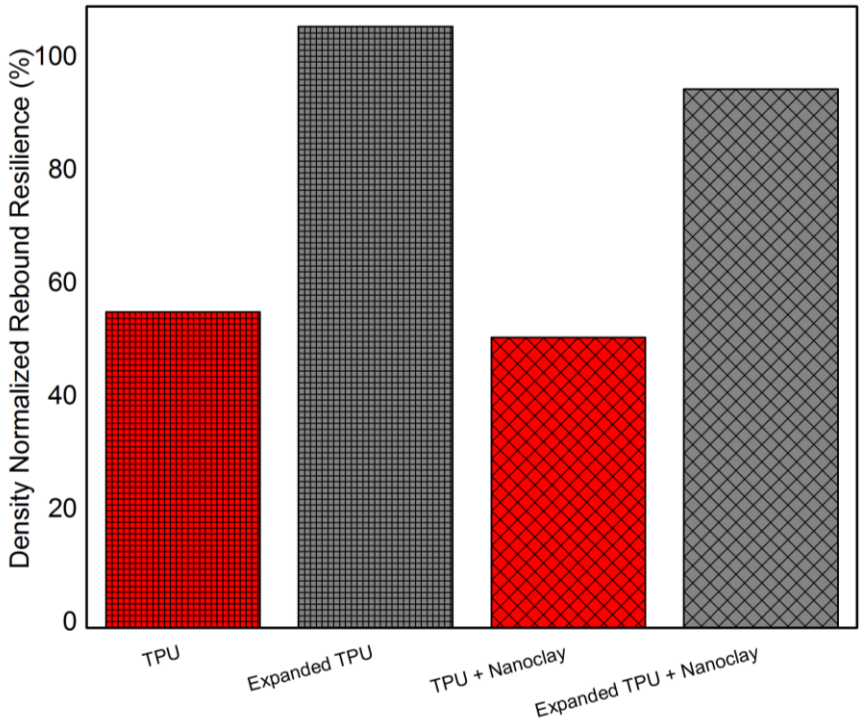

Figure 4.9. Density normalized rebound resilience test results.

4.4 Conclusions

Thermoplastic polyurethane (TPU)/clay nanocomposite foams were prepared using twin-screw extrusion blending and microcellular injection molding. Samples were created with two densities by using early cavity expansion. The microstructure of the TPU/nanoclay foams,

investigated by scanning electron microscopy (SEM), showed that the presence of nanoclay led to higher cell densities and smaller cell sizes in the non-expanded samples. The microstructures of the expanded samples with nanoclay were found to be significantly different than those without nanoclay. Rheology tests showed that TPU compounded with nanoclay displayed a higher complex viscosity than the neat TPU, especially at low shear rates. The presence of nanoclay helped control the microstructure of the foam, even at a high foaming ratio, by increasing the melt strength and nucleation density. The cell structure of the expanded TPU/nanocomposite foam has less deterioration that expanded pure TPU. The process of bulk expansion significantly increased the resilience and springiness of the foam, while reducing the density and hysteresis loss ratio. Foams with bulk expansion were significantly softer than those without bulk expansion.

5 APPLICATIONS OF CORE RETRACTION IN MANUFACTURING LOW-DENSITY POLYPROPYLENE FOAMS IN MICROCELLULAR INJECTION MOLDING

5.1 Introduction

Special injection molding processes that reduce material consumption are highly desirable from the viewpoint of not only reducing production costs and making products more energy efficient, but also in the sustainability of natural resources. Microcellular foaming employs supercritical fluid (SCF) as a physical blowing agent and is capable of producing lightweight plastic foams with an average cell size of 100 μm or less.[18] The idea of microcellular foaming was combined with injection molding to develop the microcellular injection molding process (MIM), which is commercially known as the MuCell process. This process continues to attract attention because it saves on material and energy costs while improving dimensional stability [31, 102], allowing extra part design freedom, increasing production efficiency, and reducing residual stresses. MIM facilitates the molding of thin and thick walled products while reducing cavity pressure [103], thus increasing tool life and enabling the use of extremely delicate and complex inserts for plastic products, especially in the electronics [104] and medical industries [65]. Although this technology enables the plastic part designer to overcome some processing limitations of conventional injection molding, such as large flow length-to-thickness ratios, warpage, and uneven shrinkage [18], it creates other challenges. Microcellular injection molded parts rarely exhibit mechanical properties that are better than those of solid injection molded parts. The strength of the plastic part is dependent on the microstructure of the foam [42], which

in turn depends on factors such as material and processing parameters, density reduction, and part thickness. Density reduction is one of the primary mechanisms targeted by various industries to reduce energy and fuel requirements, while encouraging environmentally friendly product development. For MIM, weight reductions limited to between 5 and 10%, and wall thicknesses less than 3 mm, are recommended to avoid significant deterioration of microstructure and thus decreases in mechanical properties.[18] Thicker foamed parts and parts molded with higher density reductions usually show degradation in the microstructure, and thereby display inferior mechanical properties. The inability to target higher density reductions in the MIM process without compromising on properties prolongs the return on investment period in this capital-intensive technology.

The microstructure of a MIM part is the result of transient processes of cell nucleation and growth battling with material cooling.[105] In particular, internal pressures of the evolving gas compete with the increasing melt strength of the rapidly cooling polymer matrix to determine the final cell size and whether cell coalescence will occur. The pressure profile in the cavity during injection usually has the least pressure at the end of the fill and the highest pressure at the gate, which is reflected in the microstructure of the foam. Typically, the cells are finer near the gate region and grow larger at the end of the fill region. However, this trend can be reversed under certain unusual circumstances as will be discussed later. Furthermore, as the plastic is quickly cooling, there exists a gradient in the melt temperature and the melt strength between the walls and the center of the part. The center of the part will have a higher temperature, and therefore a lesser melt strength and a longer cooling time, during the process of cell nucleation and growth. This results in larger cells at the center of the part and smaller cells near the skin. Although MIM

parts have a polymer-rich skin layer, at high weight reductions the skin layer can become very thin or sometimes compromised. This can become a challenge in the conventional MIM process.

Polypropylene is a commodity plastic that is used extensively in the automobile and appliance industries because of its outstanding functional characteristics, low material cost, improved abrasion and chemical resistance, and high rigidity as compared to other members of the polyolefin family. Foamability of polypropylene in injection molding is challenging as the weak melt strength, low solubility, and high diffusivity of typical blowing agents can result in the degradation of microstructures and inconsistent properties. Several studies using polymer blends [46, 106, 107], fillers [105, 108], or blends of co-blowing agents [48], as well as changing the material's molecular weight and chemical structure [109, 110], have been performed with polypropylene to improve its foamability. Core retraction is a process of physically moving a part of the mold cavity by mechanical, pneumatic, or hydraulic means during the molding cycle. It has been used extensively in injection molding to enable the molding of undercuts and side features. In order to target higher density reductions while achieving good microstructures, a uniform pressure drop across the cavity and the ability to tune the melt strength is desirable to control cell coalescence. Core retraction-aided microcellular injection molding (CR-MIM) is a process that employs the motion of a retracting core with the purpose of achieving a fine microstructure at high expansion ratios. Once the polymer–gas solution is injected into the mold cavity, a part of the cavity is retracted to create a sudden pressure drop and space for the material to expand.[111, 112] Furthermore, nucleation and cell growth can be delayed by starting with a thinner cavity thickness (and thus a higher cavity pressure that hampers cell nucleation) and by controlling the timing of the core retraction after injection. In this study, applications of core

retraction are evaluated in the molding of thick polypropylene parts with the aim of achieving better microstructures and controllable skin regions at high density reductions.

5.2 Materials and Equipment

Pro-fax SR256M, a clarified polypropylene (PP) random copolymer resin from LyondellBassel with a melting point of 140 °C and a melt flow index of 2.0 g/10 min (2.16 kg and 230 °C) was used in this study. Nitrogen (N_2) was used as received from Airgas as the physical blowing agent in the MIM process.

A custom injection mold was manufactured to mold a rectangular cavity with a core that retracts in the thickness direction as shown in Figure 5.1. The retraction of the core was achieved by attaching the moving core to a hydraulic cylinder. The cylinder was activated through the core-pulling function of the injection molding machine. The maximum allowable hydraulic pressure for the cylinder was 20 MPa, which ensured that the cavity created a cavity pressure higher than the critical pressure of the dissolved gas. In this study, the core was retracted to 5.1 and 7.6 mm, from an initial thickness of 3 mm, which yielded a density reduction of 30% and 55%, respectively. Injection molding was performed on a 56T Arburg machine with a 25 mm injection screw. The microstructures of the foamed samples were observed using a scanning electron microscope (SEM) (JCM-5000, NeoScope). A CO_2 laser cutter (PLS6.75, Universal Laser Systems) was used to cut tensile bars at various distances from the gate to examine the microstructure. Tensile strengths were studied using an Instron 5967 tensile testing machine at a strain rate of 5 mm/min until fracture.

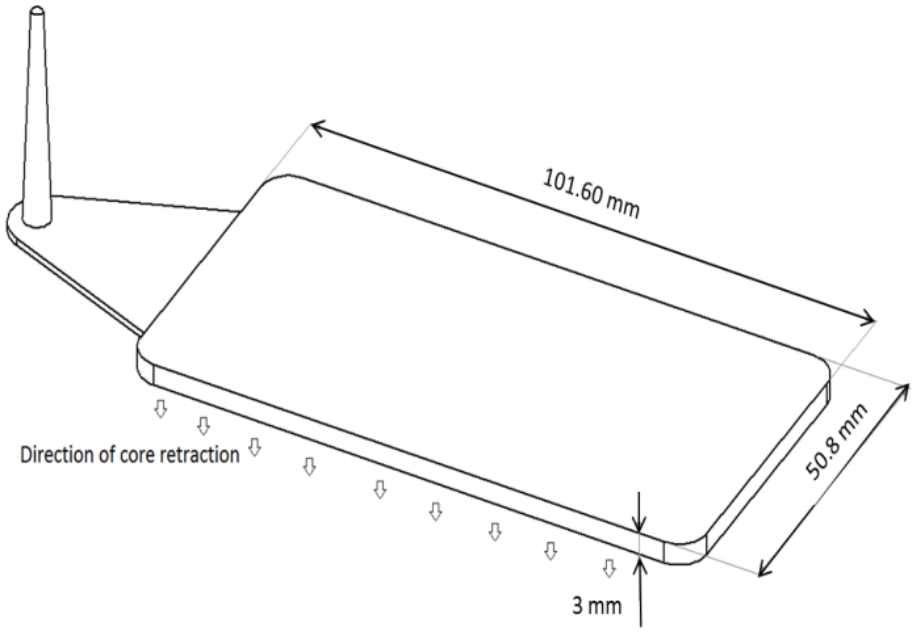

Figure 5.1. Schematic of the injection molded part showing the direction of core retraction.

5.3 Experimental Conditions

In this study, the density reduction and time delay before core retraction were varied as per Table 5.1. For comparison, parts were also molded at a 55% weight reduction with the MIM process. This was done by injecting a polymer–gas solution into an already retracted cavity of 7.6 mm thickness and is denoted as Trial 5 (cf. Table 5.1). The processing parameters used for the molding process are tabulated in Table 5.2. It was experimentally confirmed in a separate trial that the bubbles disappeared when the cavity was fully packed and not allowed to retract. This means that the pressure exerted by the hydraulic cylinder was sufficient to maintain the melt under pressure to thwart cell nucleation and growth. The slow depressurization rate and a packed shot volume ensured that no cell nucleation occurred prior to core retraction.

Table 5.1. Experimental design for CR-MIM (Trials 1–4) and conventional MIM without core retraction (Trial 5).

Trial No.	Density Reduction	Delay Time	Core Retraction
1	30	2	5.1
2	55	2	7.6
3	30	3.5	5.1
4	55	3.5	7.6
5	55	0	0

Table 5.2. Processing conditions for the molding processes.

Processing Parameters	Units	Value
Processing temperature	°C	190/190/200/210
Loading of SCF	%	0.62
Cooling time	s	120
Injection pressure	MPa	150
Injection speed	cm^3/s	70
Packing pressure	MPa	150
Back pressure	MPa	8
Mold temperature	°C	25
Shot weight	cm^3	24

5.4 Results and Discussion

5.4.1 Scanning Electron Microscopy

The parts were fractured using liquid nitrogen 50 mm from the gate (around mid-point in the part shown in Figure 5.1). After coating with a thin layer of gold using a sputter coater, the microstructures were studied at the edge and the center of the part in the thickness direction. Figures 5.2 (a) and (b) show SEM images at the edges of the parts with a 30% density reduction at two delay times. As can be seen, the polymer-rich skin increased with the time delays. Equations 5.1 and 5.2 denote the Gibbs energy (ΔG^{**}) (energy barrier to nucleate) and the critical radius of nucleation (R_{cr}) for homogenous nucleation, respectively. The parameter ΔP is the instantaneous pressure drop.

$$\Delta G^{**} = \frac{16\pi\gamma^3}{3(\Delta P)^2} \tag{5.1}$$

$$R_{cr} = \frac{2\gamma}{\Delta P} \tag{5.2}$$

The critical radius of nucleation depends of the surface energy and the pressure difference between the nucleating gas and the polymer matrix and will affect the nucleation density. As the injected material cooled down, the viscosity—and therefore the surface energy (γ)—increased.[6] The critical radius and energy barrier for nucleation increased by a power of 1 and 3, respectively, as the surface energy increased, thereby hampering nucleation in those regions. The polymer-rich region devoid of cells can thus be controlled by the delay time. It has been

observed in this study that the surface finish of the parts improved with some delay time compared to typical MIM parts, although class A surfaces could not be achieved.

The polymer-rich skin thickness depends on the delay time, cooling rate, and temperature-dependent material properties like viscosity and melt strength. A line of small nucleated cells can be observed at a distance of approximately 220 μm from the edge in both samples. These cells were the cells that had nucleated during the injection of the material, and remained small in size as the material around them became more viscous. It is likely those cells were formed by gas coming out from the shear-induced, crystallizing PP during filling. When the second nucleation occurred due to core retraction, these pre-nucleated cells started to grow. Growth was evident at the increased expansion ratios. Figures 5.2 (c) and (d) show the SEM images at the center of the parts. It can be observed that a smaller delay time caused the cell density to increase and the cell size to decrease. As the polymer-rich skin region increased in the case of larger delay times, the nucleated cells needed to expand further to fill the cavity. It can also be seen from Equations 5.1 and 2 that with increased delay times, the energy barrier for nucleation and the critical radius of bubbles rapidly increased along with an increase in material viscosity. This led to a lower degree of nucleation, which negatively affected the cell density and the cell size. Nonetheless, even at a 35% density reduction, the microstructure was stable, and cell coalescence was avoided with the CR-MIM process.

Figure 5.3 shows SEM images at the edge and center of the part with a density reduction of 55% at delay times of 2 and 3.5 seconds. As the density reduction increased from 30% to 55% by increasing the core retraction distance and keeping the shot size same, the cell size increased, and

the nucleated cells got a chance to grow more to fill the expanded mold cavity. When the line of pre-nucleated cells underwent a sudden pressure drop due to core retraction, they started growing. The pressure drop was higher in the case of the 55% density reduction as compared to the 30% density reduction because the core was being retracted a longer distance. The viscosity was higher in the transition region between the solid skin and the hotter central region, while the cells expanded in the direction of the core retraction. The growing cells were frozen in an elongated shape as the melt had cooled sufficiently to prevent the cells from reorganizing into a more energy efficient spherical shape. The alignment of the cells in this region in the direction of the core pull was also evident. Figures 5.3 (c) and (d) show the cell structure in the center of the part. It can be seen that the cell size distribution became different than their 30% density reduction counterparts. In particular, the cells were smaller for parts molded with a 3.5 s retraction delay, as compared to a 2 s delay, which displayed coalesced cells. It can also be observed that at a 55% density reduction, less coalescence was observed at higher delay times as the temperature of the melt was lower when nucleation and growth occurred.

The regular MIM foaming method was not able to completely fill the cavity at the desired 55% density reduction (Trial 5) whereas, with the application of core retraction, the 55% density reduction could easily be achieved and the mold was completely filled. The surface finish of the parts molded with core retraction was also visibly better. A foaming method with retraction can be used to obtain higher density reductions with an integral and customizable skin layer, while also obtaining a better surface finish. The SEM images of foamed parts produced by the CR-MIM process versus the regular MIM process are compared in Figure 5.4. It can be observed that a thicker polymer-rich skin was achieved with the CR-MIM process by delaying nucleation. The

alignment of cells in the transition zone is possible, if desired, with proper settings of the delay time and cooling rates. The microstructure at the center of the parts showed less coalescence in the case of the CR-MIM process, whereas inconsistent cell structure and the presence of large coalesced cells could be observed in the case of MIM at a 55% density reduction.

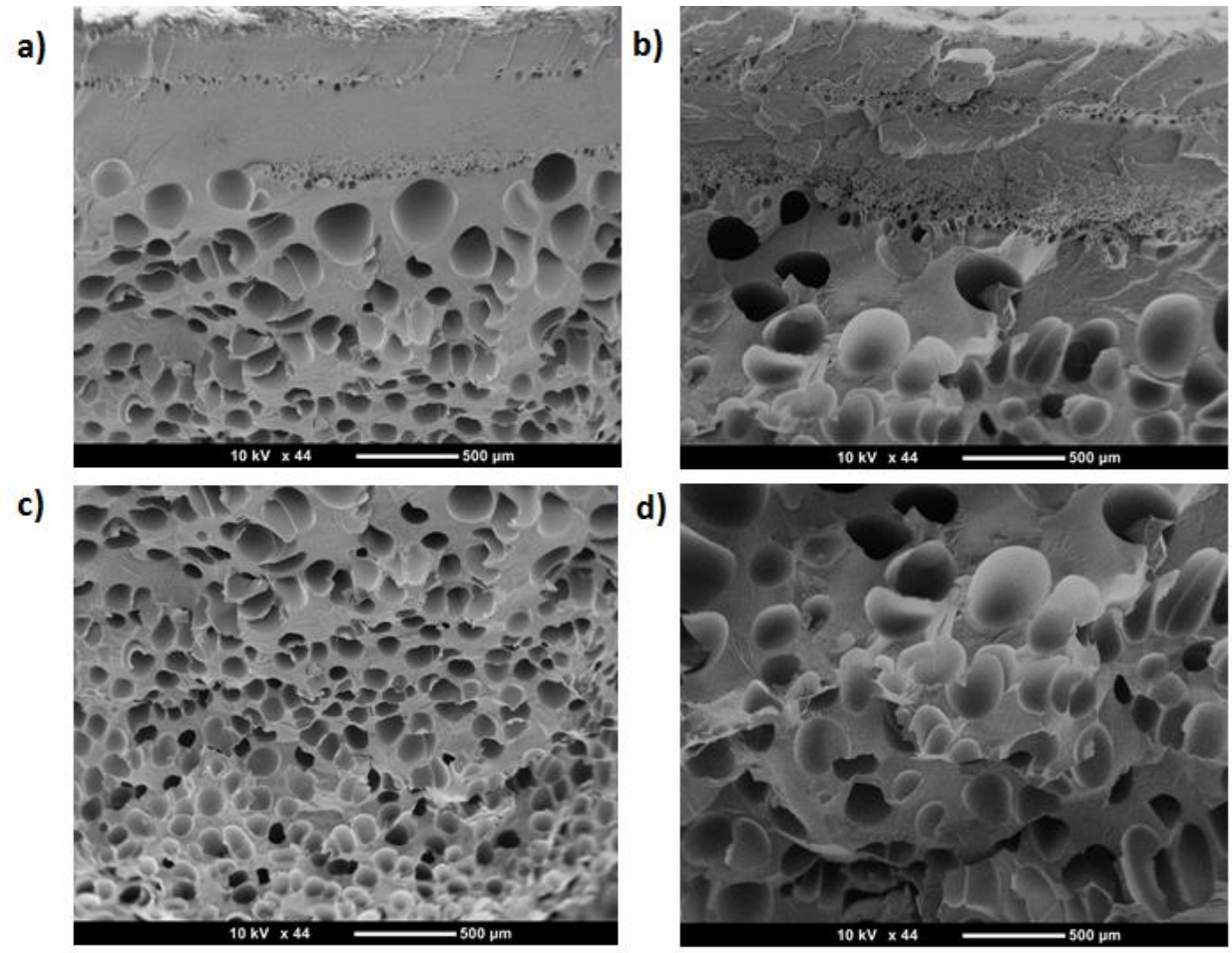

Figure 5.2. SEM images of CR-MIM samples at a 30% density reduction at the edge of the CR-MIM part at (a) 2 s delay and (b) 3.5 s delay ; and at the center of CR-MIM part at (c) 2 s delay and (d) 3.5 s delay. Scale bars are 500 µm.

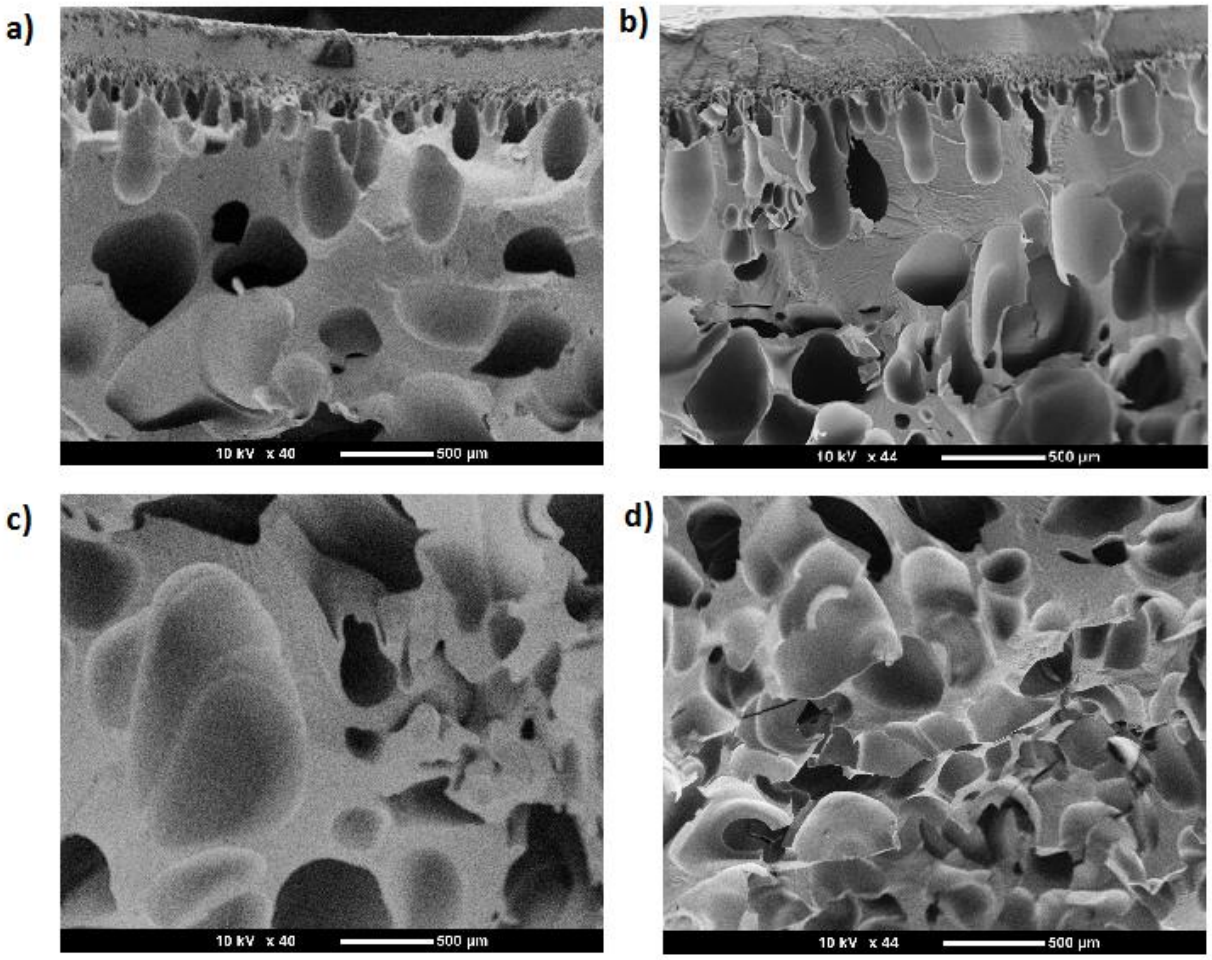

Figure 5.3. SEM images of CR-MIM samples at a 55% density reduction at the edge of the CR-MIM part at (a) 2 s delay and (b) 3.5 s delay ; and at the center of CR-MIM part at (c) 2 s delay and (d) 3.5 s delay. Scale bars are 500 µm.

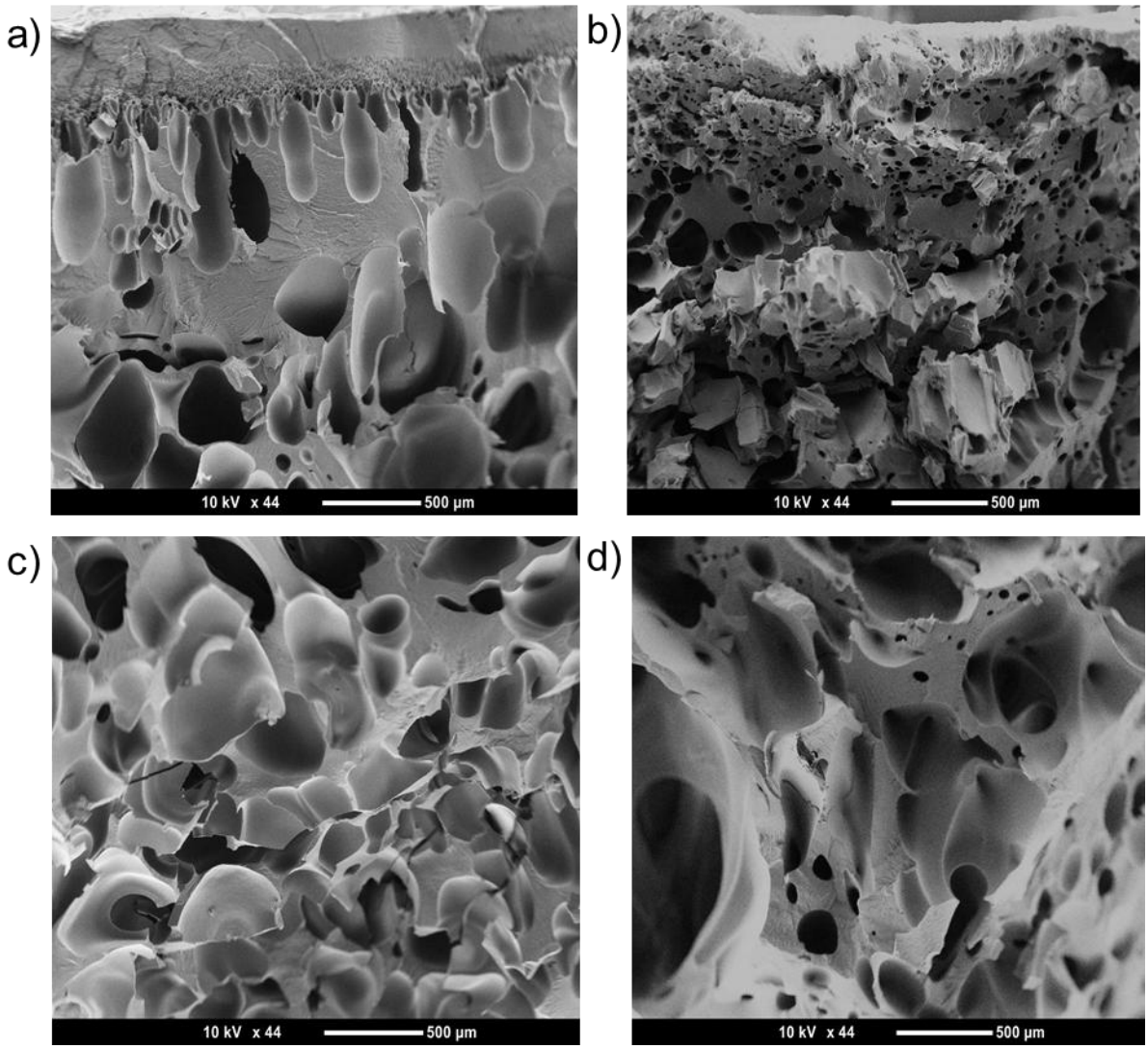

Figure 5.4. SEM images of foamed parts at a 55% density reduction at the edge with (a) CR-MIM process and (b) MIM process; and at the center with (c) CR-MIM process and (d) MIM process. Scale bars are 500 µm.

5.4.2 Rheology

It is well known that temperature affects the rheology of molten polymers.[113] Figure 5.5 shows the complex viscosity data for PP as a function of angular frequency at different temperatures below the processing temperature (210 ˚C). During injection molding, once the molten polymer is injected into the mold it immediately begins to cool, with the polymer touching the metal mold freezing first. In the case of MIM or CR-MIM processes, this can be examined by the solid skin layer that is formed at the mold surface (cf. Figures 5.2 and 5.3). The polymer on the interior of the solid skin layer then begins to cool, during which time the dissolved gas can nucleate for cells to grow. Nucleation and cell growth are both governed by the rheology of the melt, the gas diffusivity, and the solubility/saturation level of the gas. When the temperature decreases, the viscosity will increase and the diffusivity will decrease—both exponentially. In addition, the solubility of N_2 in PP will decrease linearly with temperature.[18, 114]

Melt strength, defined as the resistance to extensional flow in polymers and also referred to as their ability to withstand extension without breaking, is relevant to cell expansion because cell or bubble growth is purely extensional; specifically, equibiaxial extensional flow.[98, 99] Equation 5.3 describes the relationship between equibiaxial extensional viscosity (η_b) and shear viscosity (η) at small strains for Newtonian fluids.[87] Equation 5.4 relates the shear viscosity (η) to the complex viscosity (η^*) via the Cox–Merz Rule over a large range of shear rates, where $\dot{\gamma}$ is the shear rate and ω is the angular frequency.[100]

$$\eta_b = 6\eta \tag{5.3}$$

$$\eta(\dot{\gamma}) = \eta^*(\omega) \tag{5.4}$$

One can easily relate the two, at least in theory, to compare the complex viscosity in shear to the equibiaxial extensional viscosity so that,

$$\eta_b(\dot{\varepsilon}) = 6\eta^*(\omega) \tag{5.5}$$

where $\dot{\varepsilon}$ is the extensional strain rate. However, in foaming, as the cells become larger and larger, the strains and strain rates can quickly increase to a level where strain hardening begins to occur and the above relationship between equibiaxial extensional viscosity and shear viscosity ceases to exist as the extensional viscosity increases unbounded.[87] In this case, the level of damping in the material, measured as *tan δ*, is a better measure of the melt strength and thus its resistance to extensional flow.[99] This relationship exists because damping is a function of entanglement as is melt strength; in this case, as the temperature decreases, the entanglements are less easily disentangled. Figure 5.6 illustrates the measured *tan δ* values at different temperatures and angular frequencies for PP. As the temperature decreases, the damping values also decrease which coincide with an increase in melt strength. During CR-MIM, the core is retracted after the polymer has been cooling for some time, so a higher melt strength can be expected. This increase in melt strength during foaming prevents the cells from growing too large, coalescing, and forming an open cellular structure.

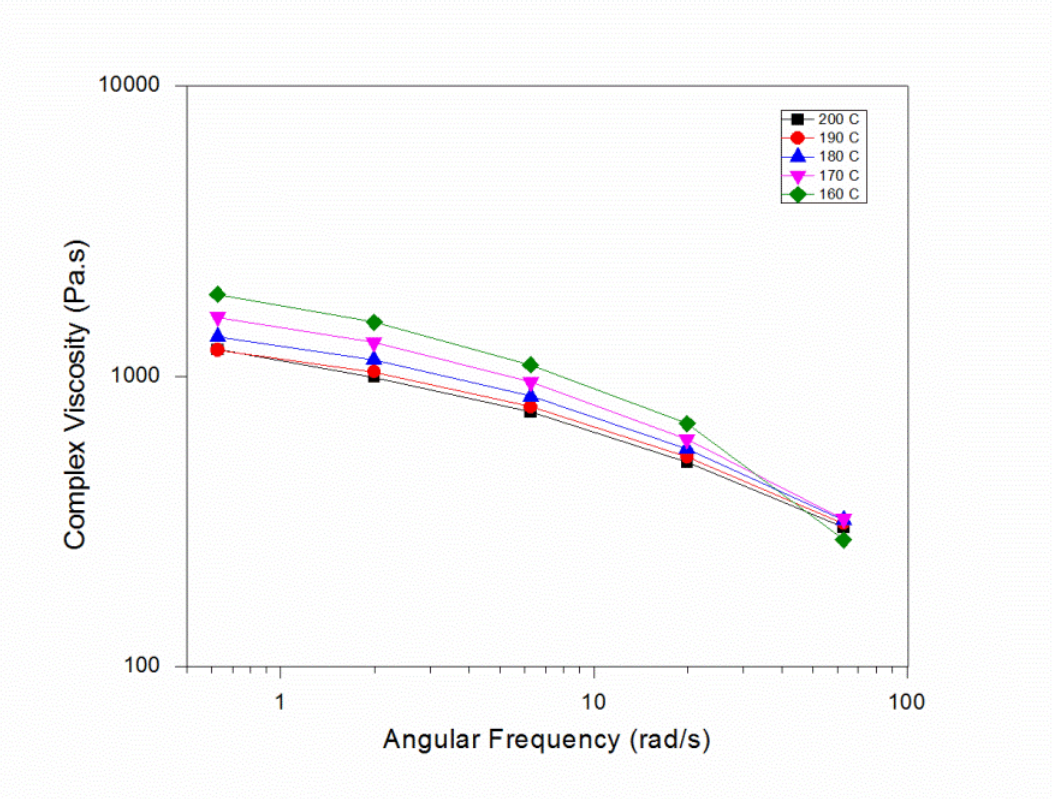

Figure 5.5: Complex viscosity as a function of angular frequency at different temperatures.

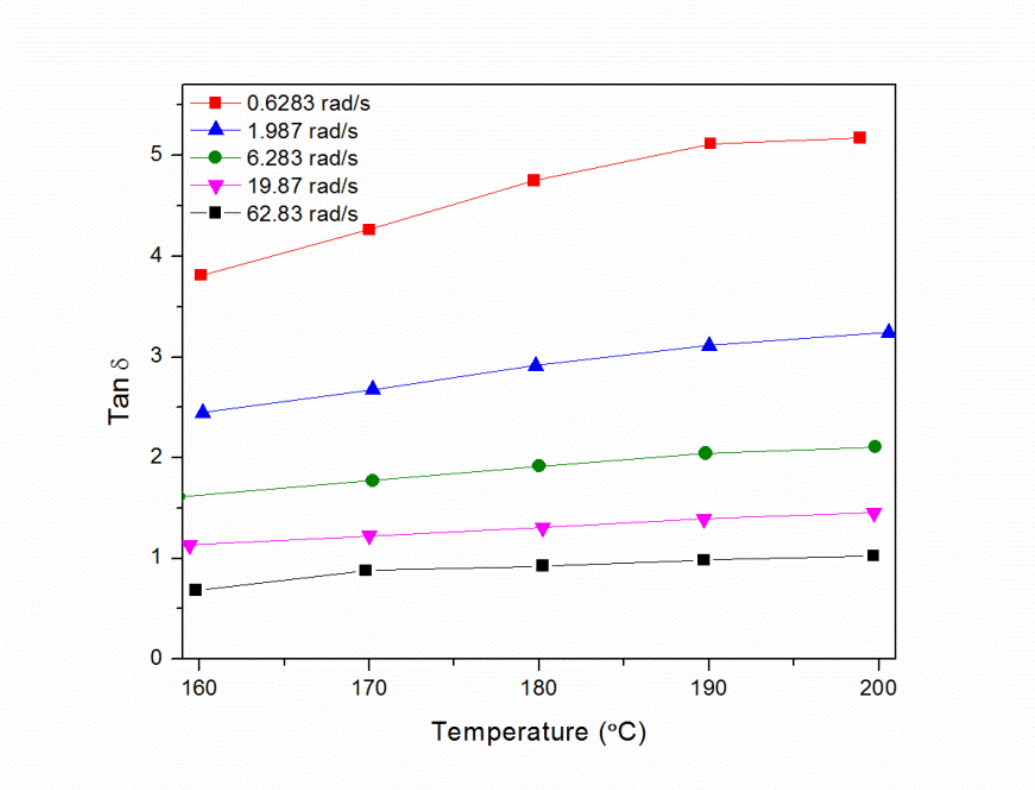

Figure 5.6: Delta versus temperature at different angular frequencies.

5.4.3 Density Variations in Foamed Parts

Dog-bone specimens were laser cut from the foamed parts at approximately 20, 50, and 80 mm from the gate. The densities of the specimens were measured using ASTM D792, which uses Archimedes' buoyancy principles, and is plotted in Figure 5.7. Solid unfoamed parts were also measured for reference. It can be observed from Figure 5.7 that both the 30% and 55% density reduction parts molded with the CR-MIM process showed a more consistent and uniform density along the flow length as compared to conventional MIM parts. It has been shown earlier that MIM foamed parts showed variations in specific density as high as 30% along the flow length.[16] In the conventional MIM process, the cavity is initially partially filled. As the melt containing the blowing agent experiences a pressure drop at the gate, cells nucleate and grow, which leads to complete filling of the mold. There exists a pressure difference along the flow path that results in a non-homogenous density distribution along the flow length. It should be noted that with the conventional MIM process, the 55% density reduction resulted in unfilled regions at the end of the fill. Because of the relatively large cavity thickness, potential jetting and the effect of gravity, amplified by the lower viscosities of the polymer–gas mixture and the large cavity thickness (the mold was positioned downward), it was found that the density actually increased toward the end of the fill in the MIM parts. In the CR-MIM process, the material was initially packed in the thin cavity before nucleation was initiated. As the cavity experienced a more uniform pressure drop during core retraction, the density variations at different locations from the gate decreased.

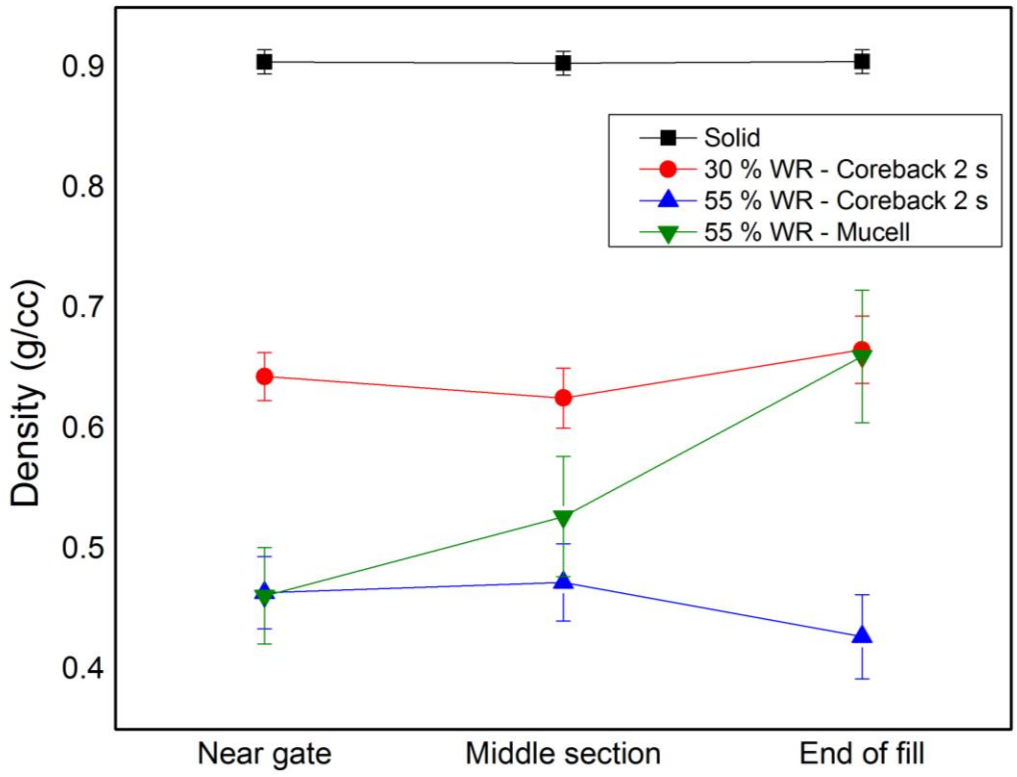

Figure 5.7. Density as a factor of distance from the gate.

5.4.4 Mechanical Testing

Dog-bone specimens were laser cut from the foamed parts at approximately 20, 50, and 80 mm from the gate. Tensile tests were conducted on the tensile bars at an extension rate of 5 mm/min. It should be noted that the weight reduction was achieved by increasing the volume, which means that the cross-sectional area of the tensile bar increased as the density reduction increased, although the amount of plastic remained the same. The Young's moduli at various density reductions are plotted along with unfoamed PP for comparison in Figure 5.8.

As the weight reduction increased, the Young's modulus decreased subsequently at the different distances from the gate. The solid parts also showed a small decrease in Young's modulus as the distance from the gate increased. It is well known that cavity packing pressure decreases from the gate to the end of the fill. The change in cavity pressure changes the density and subsequently affects the Young's modulus. The conventional MIM parts showed a slight increase in modulus with an increase in the distance from the gate. It should be noted that the trend in modulus increase is consistent with the trend in density increase with distance from the gate location with CR-MIM parts. The moduli of the CR-MIM foamed parts are more consistent than the parts foamed with conventional MIM.

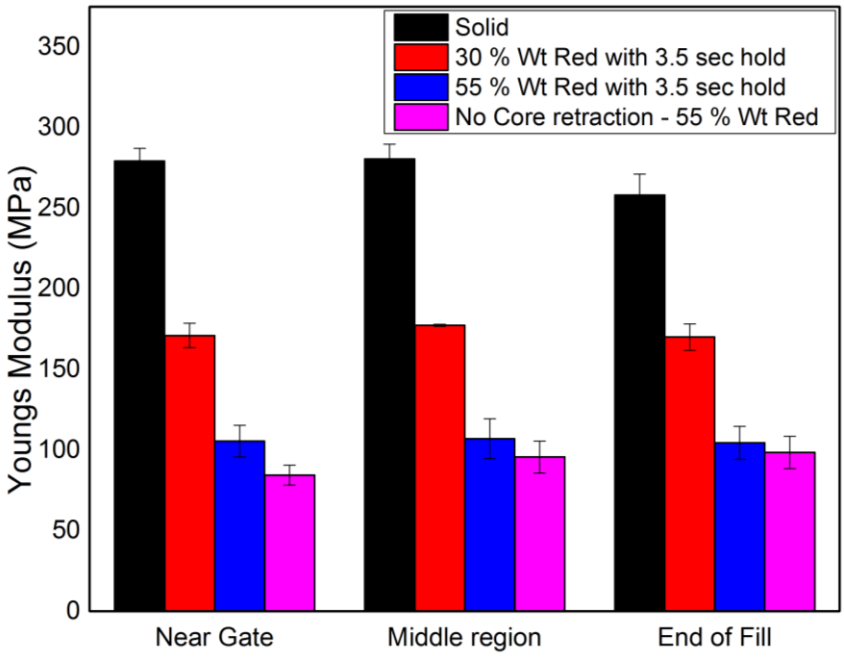

Figure 5.8. Young's modulus as a factor of distance from the gate for different density reductions at a 3.5 s hold time.

5.4.5 Conclusions

Polypropylene could be foamed to a density reduction of 55% in the process of MIM with the use of core retraction. The conventional MIM process with a 55% target weight reduction could not fill the entire cavity and formed short-shot parts. At that targeted weight reduction, microstructures were better with the CR-MIM process. The holding pressure while injecting a full shot was capable of delaying nucleation or even reversing it. The core-retraction process yielded an integral skin layer with little or no foaming that was visibly thicker than the skin layer produced via the conventional MIM process. Delay times and cooling rates can be optimized to achieve the desired level of a polymer-rich region as well as a good surface finish. With an increase in skin layer due to a longer delay time, the cells in the foamed core grew to a larger size to achieve the targeted density reduction. As the delay before nucleation increased, the melt strength increased. By optimizing the melt strength at the time of nucleation and growth, a good closed cell structure can be obtained even at high density reductions. A further increase in delay time, and hence melt strength, increased the energy barrier of nucleation and reduced the nucleation density. Alignment of microcells was possible by cavity opening in the core-retraction direction, and was evident in the transition region between the skin and the core. The core-retraction method of foaming yielded more consistent densities and tensile properties at different distances from the gate. The core-retraction method also yielded a better Young's modulus at the same density reduction as compared to the conventional MIM process. The CR-MIM process can be an advantageous option with aggressive weight reduction targets. Limitations of the MIM process of thickness and weight reduction can be overcome using this method.

6 DEVELOPMENT OF A THREE-STAGE PROCESS TO ACHIEVE CUSTOMIZABLE DENSITIES, MICROSTRUCTURES, AND MECHANICAL PROPERTIES IN TPU FOAMS

6.1 Introduction

Low-density TPU foams show various benefits such as being lightweight, highly flexible, having a great cushioning effect, and fast energy restoration in compression. TPU foams can be easily manufactured in a variety of densities and properties, ranging from highly resilient to highly compressible, with different processing methods. Furthermore, low thermal conductivity, stability over a wide range of temperatures, and good acoustic damping properties make it an ideal material in the heat and noise insulation industry. It is also widely used in furniture, automotive, sportswear, and packaging applications because of its controllable energy management properties. The mechanical and insulation properties of TPU such as softness, viscoelasticity, rebound resilience, noise and thermal insulation, and the ability to damp vibrations and absorb shock depend primarily on the bulk density, cell size, cell density, and open/closed cell structure of the foam.

We have seen in earlier chapters that with proper control of processing parameters, very low density injection molded TPU foams can be manufactured with controllable microstructures. In special applications, it is desirable to have variable properties of the foam in a single product or part. Currently, most of the flexible foam applications use foam created by the reaction injection molding process or a slab-stock process where the foam is later cut and profiled to the required

size and shape by special machining processes. The slab-stock raw material production of foamed sheets is a capital intensive process with limited control over cell structure. Furthermore, OEM manufacturers have to deal with issues such as limited alternatives regarding slab-stock raw materials, waste during the machining process, the cost of extra processes, and reduced design freedom regarding final product aesthetics. In most cases, separate outer coverings and labor-intensive processes are required to improve product appearance and feel. Furthermore, as the number of processes in the manufacturing of a product increase, the costs associated with inventory, labor, space, failure-rate, and administration also increase. Finally, if different foam properties are required in a single component, the process becomes even more challenging and will require the assembly of different foams. There are no options available to the part designer except mechanically joining different parts to achieve the required properties. For example, the soles of athletic shoes, which generally require good energy absorption properties at the heel region and improved resilience at the toe region, require the assembly of different components such as the gel cushion, sock liner, midsole, and outsole to achieve the desired properties. There is a need for a simplified process that can mass-produce foamed parts with customizable mechanical properties, contours, colors, and bulk densities, while reducing the waste, costs, operational expenses, and capital investments associated with existing manufacturing processes.

In this study, a novel process of manufacturing foamed TPU parts with variable properties using the injection molding process has been developed. The aim of this process is to achieve variable mechanical and energy absorbtion properties in a single injection molded part by locally varying the bulk density and cell microstructure within the part.

6.2 Experiment

6.2.1 Materials

TPU (Elastollan® 1180A10, BASF), a flexible polyether-based elastomer, was used as the polymer matrix in this study. Nitrogen gas was purchased from Airgas and used as received as a physical blowing agent in the microcellular injection molding (MIM) process.

6.2.2 Equipment

An injection molding machine (Arburg ALLROUNDER 320S) was used for sample fabrication. The injection molding machine was equipped with microcellular injection molding capability (MuCell® Trexel, Inc.) that enabled precise control of the gas injection weight by adjusting the pressure drop between the gas delivery and the exit, the gas flow rate, and the valve open time. A custom injection mold was manufactured to mold a rectangular cavity with a core that retracts in the thickness direction as shown in Figure 6.1. The retraction of the core was achieved by attaching the moving core to a hydraulic cylinder. The cylinder was activated through the core-pulling function of the injection molding machine. The maximum allowable hydraulic pressure for the cylinder was 20 MPa, which ensured a cavity pressure higher than the critical pressure of the dissolved gas. After the process of injection molding and core retraction, the samples were degated and inserted into a separate aluminum mold. The molds were then immersed in a heated water bath to further expand the parts to their final desired shape in an “out of mold” process. Parts with two profiles, as shown schematically in Figure 6.2, were produced and named (a) Part 1 - with a flat profile and (b) Part 2 - with a varying profile. Both parts were

produced using the same injection mold but different Stage 3 molds. The molds were inserted into a water bath that was maintained at an elevated temperature (higher than the glass transition temperature but below the melting temperature). The densities of the foamed samples were measured using ASTM D792 with Archimedes buoyancy principles. The microstructures of the foamed samples were observed using a scanning electron microscope (SEM) (JCM-5000, NeoScope). Cyclic compressive strengths were studied using a universal testing machine (5967, Instron). Image analysis was conducted using ImageJ software.

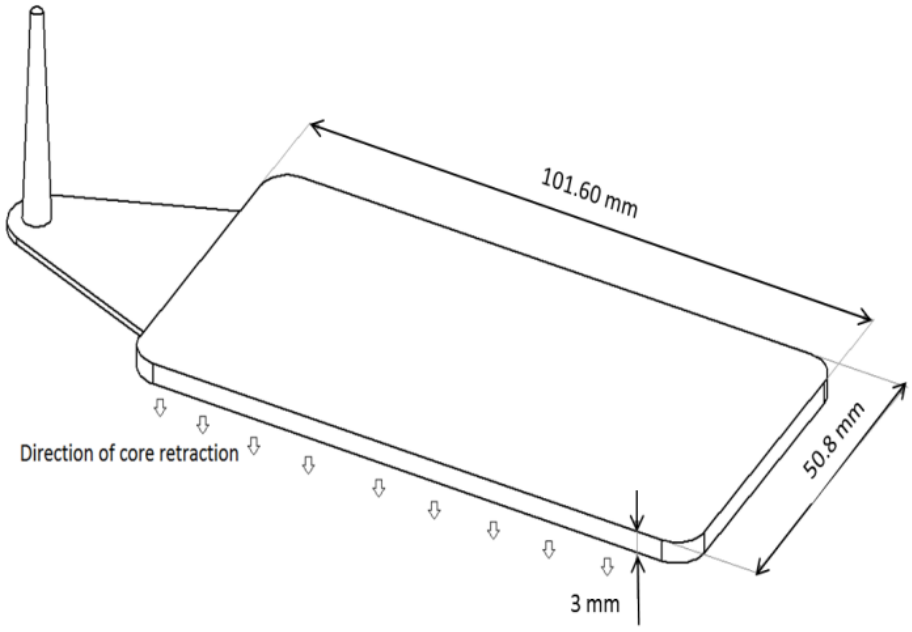

Figure 6.1. Schematic of the injection molded part showing the direction of core retraction.

6.2.3 Experimental Conditions

In this study, a three-stage process has been developed using core retractions and an out of mold expansion to achieve low and/or varying part density within the same part. In particular, after injection of a full shot-volume of TPU/gas solution into a thin cavity, a core-retraction-aided MIM process was used to create injection molded TPU foam with a foam density of 0.42 g/cc through two stages of cavity expansion. The mechanism explaining the process of achieving low density foams with customizable properties in the same injection molded foamed part is explained in Figure 6.2. The process conditions used before and during the injection molding process are tabulated in Table 1. In Stage 1 of the process (cf. Figure 6.2), core retraction enables additional control of the time delay for cell nucleation and growth to achieve a well-controlled microstructure at a density of 0.52 g/cm^3. In Stage 2, the core is further retracted, thus creating extra volume for the cells to grow and occupy. Stage 2 is initiated at a delayed time, and therefore at a higher melt strength of the cell ligaments. In this study, since two-stage core-retraction was not available because of a single stage hydraulic cylinder, the same process was mimicked by intermittent mold opening. A foam density of 0.42 g/cc was achieved at the end of Stage 2. For foamed TPU, Stage 2 was initiated after 60 s into the cooling cycle. At the end of the cooling stage (180 s), the part was ejected and then degated and inserted into one of the two aluminum molds that had the final desired part shape. These molds containing the inserted part were then subjected to a water bath maintained at an elevated temperature to create foamed samples with 2 different profiles using a Stage 3 out-of-mold foaming process, thus yielding the final part shape as depicted in Figure 6.2. In particular, Part 1 with a flat profile was foamed to a low density of 0.25 g/cc using a water bath maintained at 100 ˚C for 5 minutes. The aim of

preparing this profile was to achieve very low density foams without significant degradation of the microstructures at the center of the part. On the other hand, Part 2 was foamed to form a varying profile thickness using a lower water bath temperature of 90 ˚C for 5 minutes. The motivation of creating this profile was to demonstrate that injection molded parts can be created with varying local densities, and therefore varying microstructures and mechanical properties, in the same injection molded part using this 3-stage process. Since Stage 3 occurs outside of the mold after the injection molding process, it does not increase the processing time in the capital intensive injection molding process. Furthermore, since there are no significant pressures associated with this process, investments in elaborate injection molds can be avoided. This can be especially beneficial for molding parts that can use the same pre-forms to form similar Stage 3 parts with slight variations in their final profiles. The out-of-mold aluminum cavity used in Stage 3 has the desired shape of the final part. The purpose of the third, out-of-mold heating process is to promote cell formation in the solid skin layer that quickly solidifies during the mold filing stage without cell nucleation and growth, and to increase the cell size in the center region without significant deterioration of the microstructure.

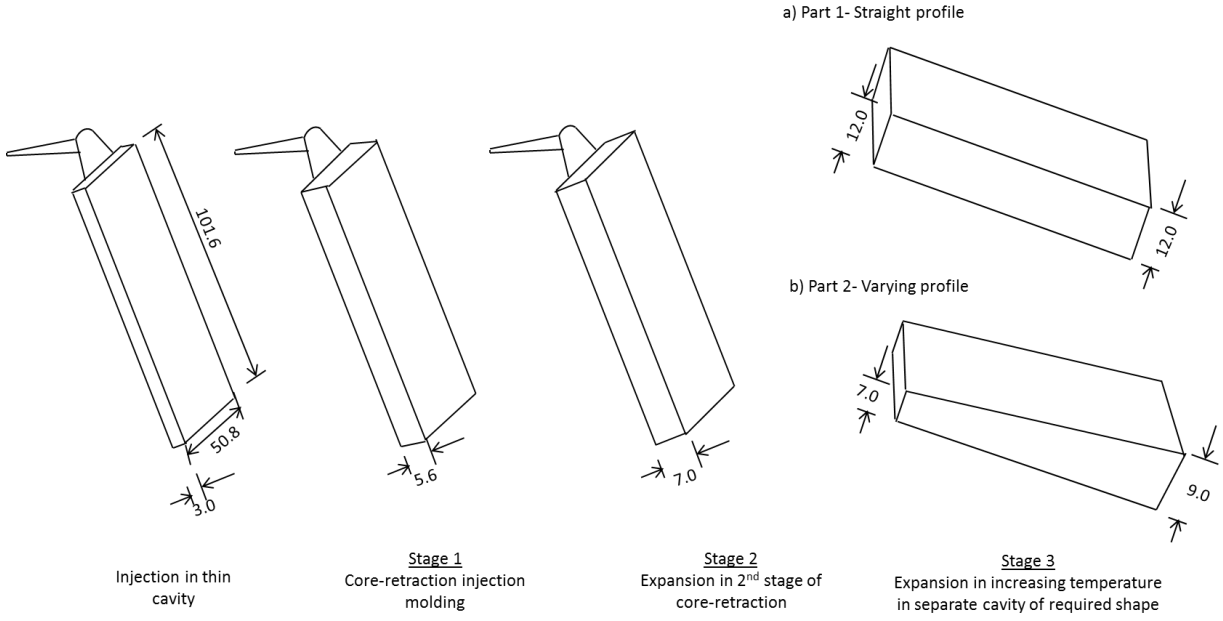

Figure 6.2. Schematic representation of the three-stage process.

Table 6.1. Processing conditions for the molding processes.

Processing Parameters	Units	Value
Drying temperature	°C	80
Drying time	hours	4
Processing temperature	°C	160/180/190/200/205
Loading of SCF	%	0.6
Cooling time	s	165
Initiation of Stage 1 retraction	s	0 s after hold
Initiation of Stage 2 retraction	s	60 s after cooling
Injection pressure	MPa	135
Injection speed	cm^3/s	75
Packing pressure	MPa	80
Packing time	s	4
Back pressure	MPa	8
Mold temperature	°C	25
Shot weight	cm^3	29

6.3 Results and Discussions

6.3.1 Part 1: Foaming to Form a Flat Profile

Scanning electron microscopy

By close examination of Part 1 samples under the microscope, the microstructures of the parts at the end of each stage were documented. Figure 6.3 shows the SEM images at the edge (at 44× magnification) and the center (at 150× magnification) of the part at the end of each stage 50 mm from the gate. The SEM images were analyzed by using ImageJ software. The bulk density and average cell size at the center of the cross-section is reported in Figures 6.4 (a) and (b), respectively. At the end of Stage 1, using the core-retraction technology, the microstructure is controlled and has an average cell size at the center of 8 μm. A distinct solid skin layer is visible. With the second stage of expansion, further cell growth occurs at lower temperatures where the melt strength is higher. The average bulk density at the end of the second stage is 0.42 g/cm^3 and the average cell size in the center region is 44 um. The solid skin is still distinct, and the microstructure is stable. At the end of Stage 3, the solid skin layer is no longer evident and has been replaced by a cellular microstructure. Cell growth occurs due to the temperature rise in the water bath. As the heat is conducted from the outside of the part, a sudden temperature rise occurs at the surface of the part, which is accompanied by a reduction in the polymer melt strength. This enables the growth of nucleated cells near the surface and the nucleation of new cells in the solid skin region. It should be noted that, unlike the regular MIM process, in the CR-MIM process, a full shot-volume is injected into a thin cavity. The nucleation of cells is thwarted during injection until additional space is created by the core retraction. In addition, rapid cooling

in the injection mold prevents bubble nucleation near the solid skin. Foaming is promoted by core retraction at a delayed time, but the cooled material near the mold surfaces does not get a chance to nucleate and grow. In the 3rd stage, cell nucleation and growth can be seen, accompanied by an overall increase in cell size near the center of the part. As the part expands in a specific direction, the cells tend to elongate in the direction of expansion, thus aligning the microcells and polymer walls in that direction. The SEM images at the skin regions are at a lower magnification and show that the microstructures are consistent and lack of any large voids or inconsistencies despite having a density as low as 0.25 g/cm^3. This is important because large coalesced cells can deteriorate the mechanical properties of a part rapidly. Furthermore, in the center region of the part, the open-celled fraction increases with further expansion. The average cell size increases to 73 μm and the final density of the part is 0.25 g/cm^3.

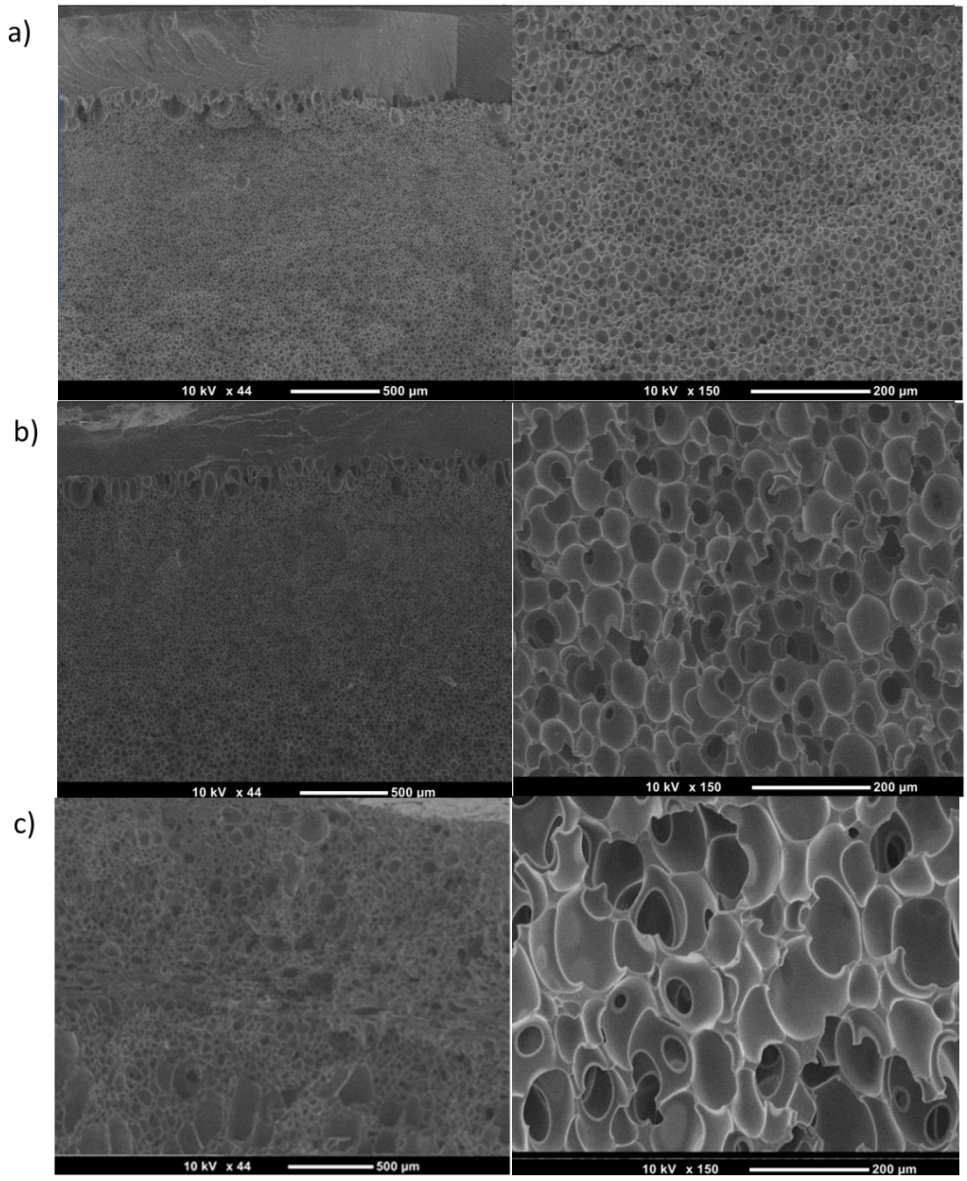

Figure 6.3. SEM images at the edge and the center of the part at the end of (a) Stage 1, (b) Stage 2, and (c) Stage 3.

Uniaxial compression tests

Uniaxial hysteresis compression tests of 100 cyclic loadings and unloadings were conducted on the samples at different stages at a strain rate of 50 mm/min to a fixed value of maximum stress. The resultant stresses were measured against the defined strain during the procedure. The

TPU foams became slightly softer within the first few cycles of loading, and typically stabilized after the initial 3 to 4 cycles. The softening behavior occurs because of the bending/breakage of bonds within the hard segments. The loading and unloading curves of the 5^{th} cycle are shown in Figure 6.4 (c). As shown in the plot, the loading and unloading curves of the foam during the cyclic compression test followed two separate and distinct paths. A typical hysteresis loop of TPU foam has three distinct regions as it is strained. The first and initial small elastic region relates to the energy required for bending the polymer walls between the microcells. As the foam becomes highly expanded, the material (cell ligament) regions become thinner and the elastic region gets smaller. The second stage is described as the polymer walls buckling and the microcells compressing. In this region, the stress does not increase at the same rate as the strain. In the last stage, at high strain, the walls of the polymer start compressing against neighboring walls; this is referred to as the densification region. In this region, the stress rises rapidly with increased strain. As seen in Figure 6.4 (c), the foam becomes softer as the density decreases, with increasing stages of expansion. The strain required to reach the maximum stress value increases as the bulk density decreases. Furthermore, the densification of the foam is delayed due to a higher strain value as the foam becomes softer and more compressible. The unloading paths all follow similar curves, irrespective of the number of loadings, and there is a small amount of residual strain in the sample immediately after the first cycle, which recovers slowly after the test is finished; this is an indication of its viscoelastic behavior [80]. This residual strain is strain rate dependent, and at 50 mm/min, it showed an increasing trend with decreasing density, signifying that the foam's viscoelastic nature increased as the foam became more compressible.

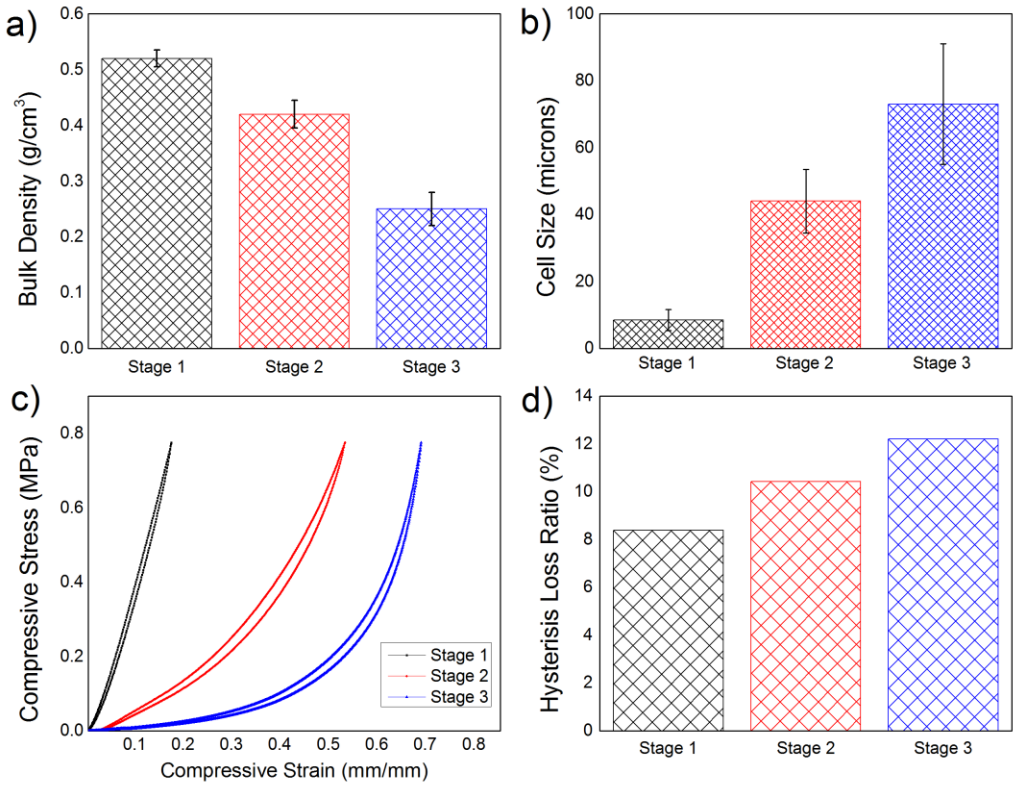

Figure 6.4. Graphical representation of (a) bulk density, (b) cell size, (c) hysteresis loops, and (d) hysteresis loss ratio results at the end of different stages in the three-stage expansion process.

Due to the viscoelastic nature of the foam, the samples are capable of absorbing kinetic energy during the loading cycle and dissipating it as heat. Energy lost during deformation is measured as the difference between the energy required to load the sample and the energy required to unload the sample. The area between the curves is the energy lost during deformation. The ratio of the energy lost to the energy required to compress the sample, known as the

hysteresis loss ratio (HLR)—provides a simple measure of the energy absorbing capability of the foamed material. The lower the ratio, the better the foam performed with respect to returning the energy absorbed during deformation. A higher hysteresis ratio indicates that the foam is more energy absorbent and dissipating, which is ideal for applications where shock absorbing properties are of paramount importance. The HLR is calculated and reported in Figure 6.4 (d). It can be seen that the foam becomes more energy absorbent as it gets softer. In Figure 6.3 (c), it can be seen that the open-cell fraction increases in Stage 3. During the compression of the foam, the gas is compacted inside of the individual cells, and thus the pressurized gas is forced into neighboring cells through a tortuous path, which creates a damping effect and increases the viscoelasticity of the foam. This results in an increased absorption of energy and a higher HLR. An increase in the residual strain at zero stress in the unloading cycle is observed in Figure 6.4 (c) and is also indicative of this.

6.3.2 Part 2: Foaming to Form a Tapered Profile

Scanning electron microscopy

Samples of Part 2, which were expanded to a varying cross-section (cf. Figure 6.2), were quenched in liquid nitrogen and fractured at the locations shown in Figure 6.5. The surfaces were sputter-coated with a thin layer of gold and observed under SEM. Figures 6.6 and 6.7 show the SEM images at the center of the cross-sections of all 4 sections at a magnification of 15× and 200×. It can be seen in Figure 6.6 that the microstructures are consistent throughout the center of the cross-section at all sections along the length of the part. Differences in cell size are not discernable at this magnification, but it can be observed that the cross-sections across all 4

sections are consistent and absent of any large inconsistencies. Figure 6.7 shows higher magnification images at the center locations. It can be seen that as the expansion ratio changes along the length of the part, the microstructure changes gradually.

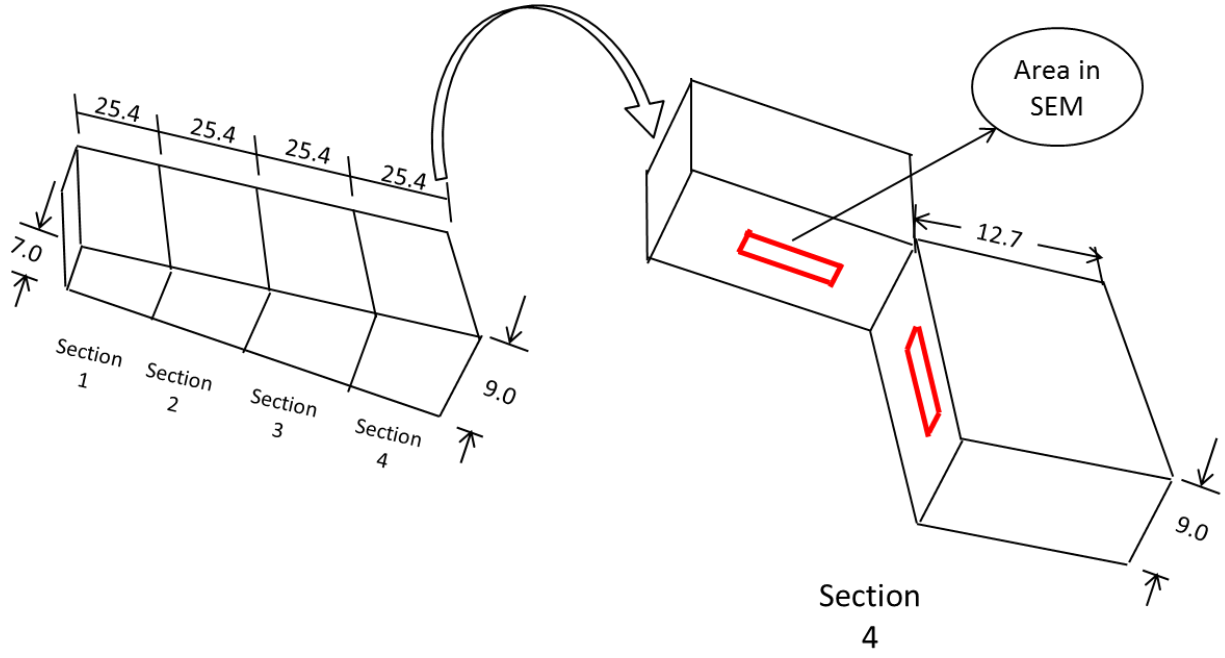

Figure 6.5. Location of SEM samples and uniaxial compression samples for Part 2.

The bulk density measured in the 4 sections is shown in Figure 6.8 (a). As the volume for expansion increases from Section 1 to Section 4, the bulk density decreases from 0.45 to 0.32 g/cc. ImageJ was used to analyze the SEM images and calculate the average cell size and aspect ratio of the cells, which are shown in Figures 6.8 (b) and (c), respectively. As the expansion volume increases, the average cell size (calculated at the thinner cross-section) increases from 23 to 87 µm. The cell structure changes from being predominantly closed cells to having a gradually increasing fraction of open cells. It can also be noted that since the expansion of the part is

uniaxial, the cells are allowed to grow in the direction of the expansion. Therefore, there is a transition from cells being predominantly spherical in Section 1 to having an average aspect ratio of 2.02 in Section 4, as depicted in Figure 6.8 (c). It has been shown in this study that within the same injection molded part, densities as low as 0.32 g/cm^3, and as high as 0.45 g/cm^3, can be obtained with uniform microstructures. Varying densities, accompanied by varying microstructures, such as different cell sizes, cell aspect ratios, and open cell fractions, can be achieved locally in the same injection molded part. Furthermore, by changing the expansion ratio and the parameters of Stage 3, open or closed cell microstructures can be manufactured locally in the same injection molded part as per application requirements.

Uniaxial compression tests

Samples from all 4 sections were cut to a size of 25.4 mm by 25.4 mm. Uniaxial compression tests were conducted on these samples at a strain rate of 10 mm/min for 10 cycles until a maximum load of 45 N with a 50 N load cell. The hysteresis curves of loading and unloading of the 5th cycle are presented in Figure 6.8 (d). A small maximum load and a smaller and more sensitive load cell were selected to be able to test the response of the foam at small deformations.

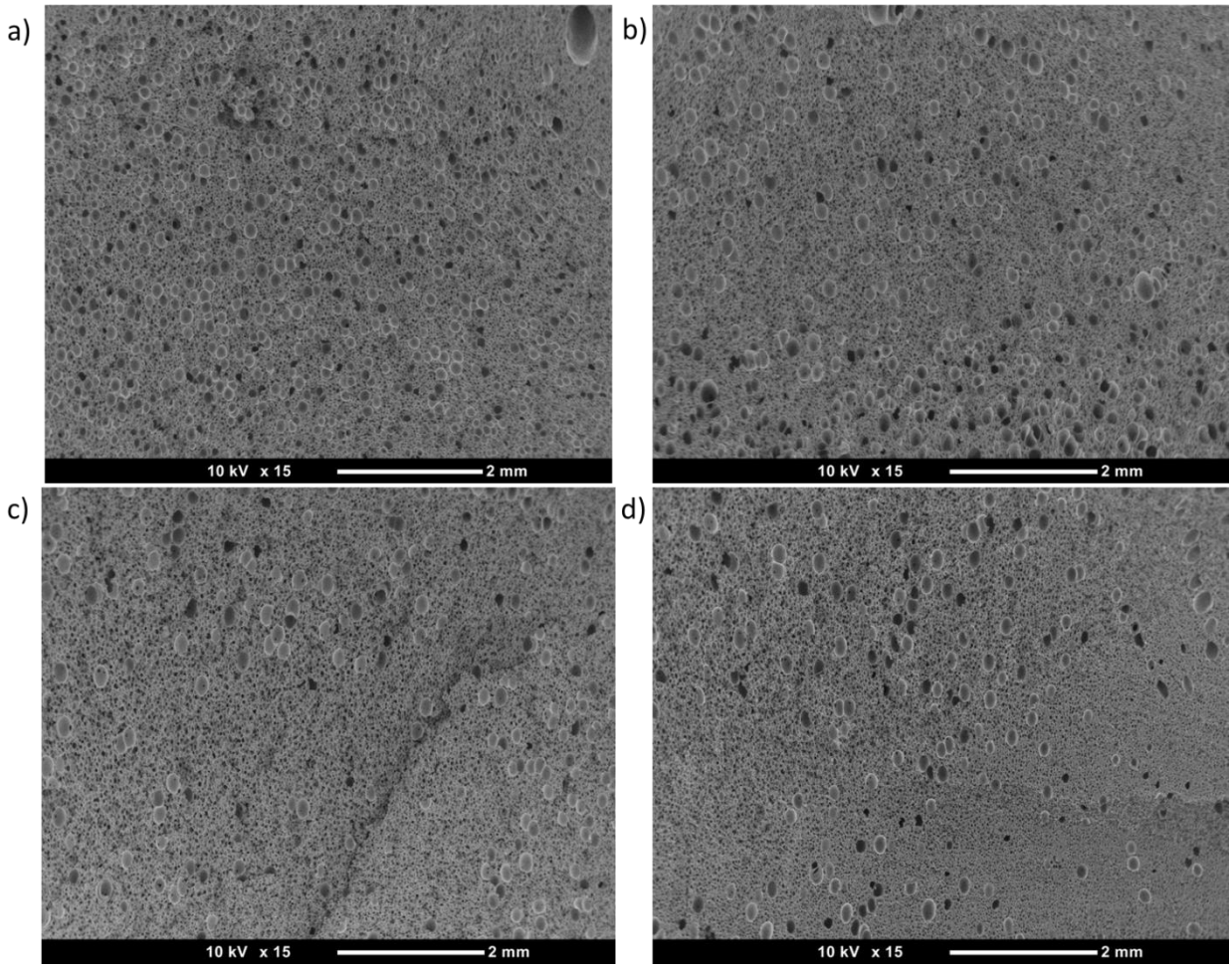

Figure 6.6. SEM images at 15× magnification at the center of cross-sections at (a) Section 1, (b) Section 2, (c) Section 3, and (d) Section 4.

It can be seen that although Section 1 shows a smaller initial compressive modulus, the stress curve rises sharply at around 4% compressive strain. Sections 2 and 3, although they have a lesser bulk density, show a higher initial compressive modulus as compared to Section 1, but do not show any kind of densification at such low strains. It should be noted that during the initial deformation of the foams, the resistance to deformation is provided primarily by the elastic reversible bending of the polymer walls and the compression of the gas inside the cells. Since

Section 1 is a predominantly closed-cell structure with thicker polymer walls, it shows an early increase in the slope of the stress vs. strain curve (cf. Figure 6.8 (d)).

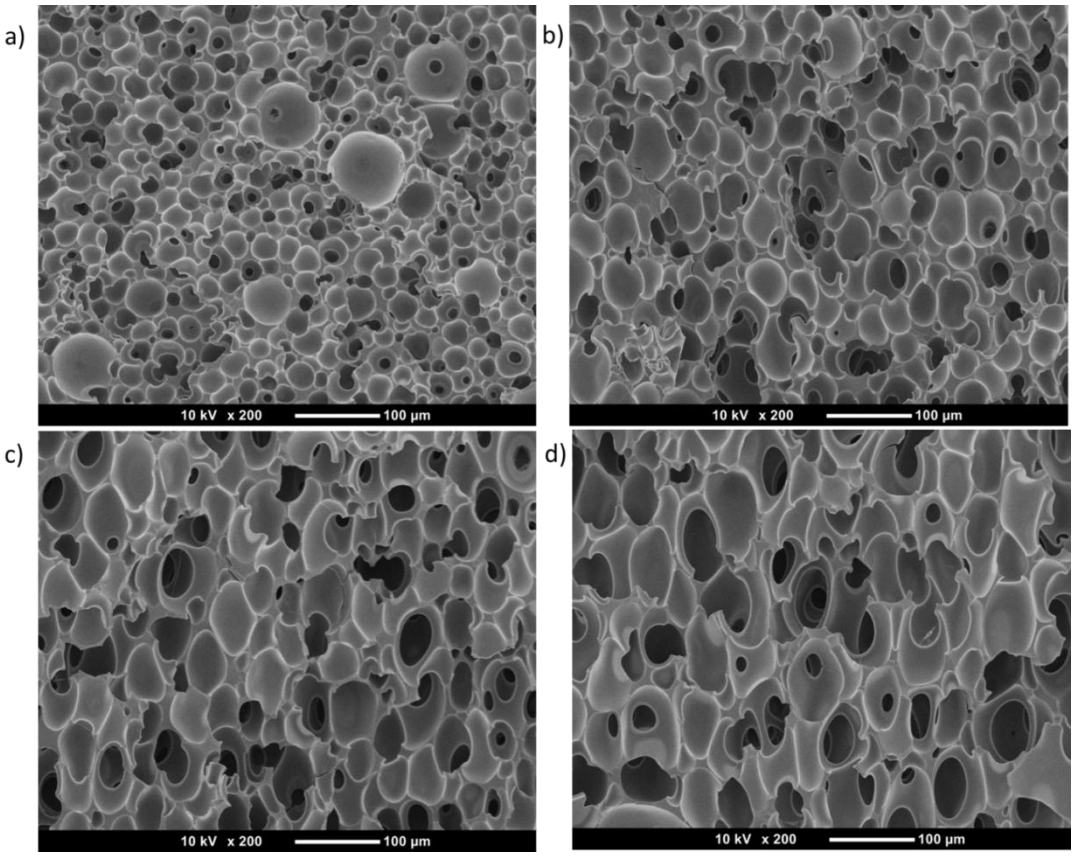

Figure 6.7. SEM images at 200× magnification at the center of cross-sections at (a) Section 1, (b) Section 2, (c) Section 3, and (d) Section 4.

The response to deformation of the foam is dependent on a lot of factors including the strength of the polymer matrix, microstructure, and bulk density. It is generally seen that the compressive modulus of the foam decreases with a reduction in bulk density (as foams get softer). But, in the case of very small deformations, factors such as the cell structure, alignment, and modulus of the matrix material become very important. It has been previously demonstrated

that the nonlinearity in the compressive response of foams at low strain percentages is governed by cell ligament buckling or the quasi-reversible bending of cell ligaments [101]. The foams with anisotropic cells have an increased alignment of polymer ligaments, and furthermore, display increased compressive moduli in the direction in which the cells are elongated. The higher initial modulus seen in Sections 2 and 3 could be because the positive effect of the increased cell aspect ratio and polymer alignment overrode the negative effect of the decreasing bulk density. In Section 4, as the density further decreases, the foam becomes softer.

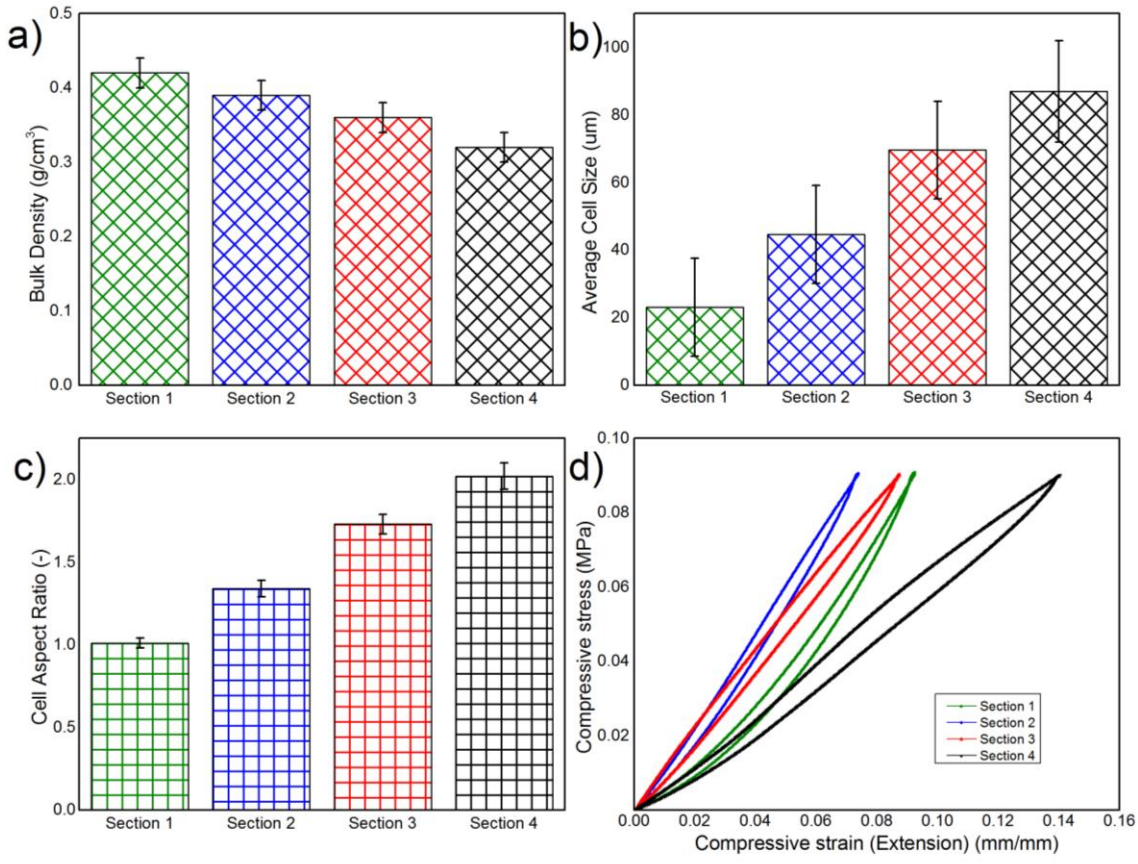

Figure 6.8. Graphical representation of (a) bulk density, (b) cell size, (c) cell aspect ratios, and (d) hysteresis loop results at different sections in Part 2.

In order to study the response of the foam at higher loadings and higher strains, the samples were compressed to a maximum load of 2000 N at a rate of 10 mm/min for 10 cycles. Figure 6.9 (a) shows the loading and unloading curves of the 5^{th} cycle. The onset of densification of the foam occurs at later strains progressively from Section 1 to Section 4. The foam gets more compliant as it moves from Section 1 to Section 4. Furthermore, the residual strain during the unloading cycle also increases from Section 1 to Section 4, signifying that recovery of the foam after compression is slower and that the foam is becoming more viscoelastic. The other characteristic of viscoelastic foams is their increased ability to absorb shock and dampen vibrations. The inset in Figure 6.9 (a) shows a magnified image of the response at low strains. It can be seen that Sections 2 and 3 show a higher initial modulus, as compared to the denser Section 1, showing that at such low stresses factors such as cell aspect ratio and polymer alignment can have a greater effect than that of the decreasing bulk density. Hysteresis loss ratios (HLR) were calculated as the ratios of the energy absorbed and the total energy supplied during the compression test. The HLR as a percentage is shown in Figure 6.9 (b). It can be seen that the HLR progressively increases from Section 1 to Section 4, showing that the energy absorbent and dissipating ability of the foam is increasing. It should be noted that cell sizes and cell openness ratios increased from Sections 1 to 4.

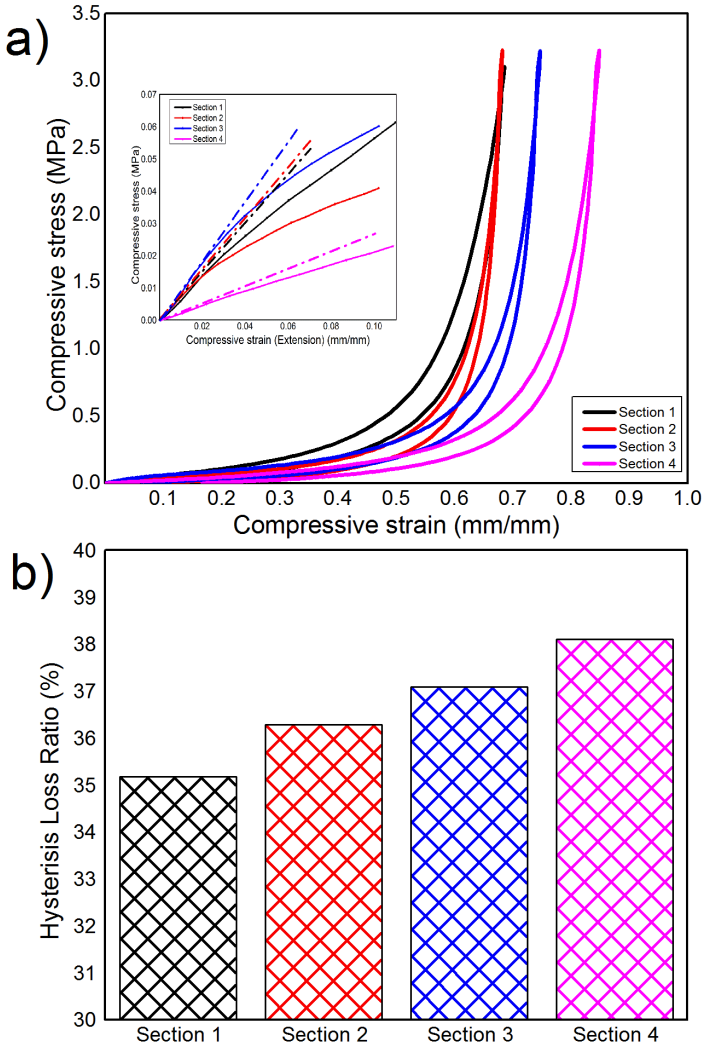

Figure 6.9. Plot of (a) uniaxial compression hysteresis loops and (b) hysteresis loss ratios at different sections in Part 2 with a maximum load of 2000 N.

6.4 Conclusions

A novel process has been invented to manufacture low density foams with customizable local properties in injection molded TPU foams. The process uses out-of-mold expansion to create the

final shape of the part. By controlling the temperature at which the cell growth occurs, higher expansion ratios can be achieved with good, uniform microstructures. Earlier, a core-retraction-assisted microcellular injection molding process was used to achieve foamed TPU parts with a bulk density of 0.42 g/cm^3. Using these foamed parts, they were further expanded in the 3rd stage of this process to achieve (a) a highly expanded part with a flat profile and (b) an expanded part with a variable profile. Analysis of the flat profile part (Part 1) showed that the density progressively increased with each stage to yield a progressively softer foam. Bulk densities as low as 0.25 g/cm3 were achieved while achieving consistent microstructures. Cell size increased progressively with each stage, with cells, and hence polymer walls, being aligned in the direction of foaming. As the density of the foam decreased, and as the open-cell fraction increased, the foam became more viscoelastic with a slower recovery time as the residual strain at zero stress increased. Bulk densities of the 4 sections in the tapered profile part (Part 2) showed that variable densities ranging from as low as 0.25 g/cm3 to 0.42 g/cm3 were achieved in the same injection molded foamed part. The cell size increased progressively along with the cell aspect ratio and the open-cell fraction from Section 1 to Section 4 of the part. Uniaxial compression tests at low loads showed that a higher initial compressive modulus could be obtained for Sections 2 and 3, as compared to Section 1, even though bulk densities were lower. Uniaxial compression tests up to a maximum load of 2000 N showed that the foamed part displayed increased levels of softness and energy absorbing capability as the expansion ratio in the 3rd stage of the process increased. The 3-stage expansion process could be especially beneficial in manufacturing very low density TPU foams with variable microstructures and mechanical properties as per application requirements.

7 FUTURE WORK

The research presented in this manuscript was focused on achieving very low density foams with controllable microstructures and mechanical properties via novel injection molding foaming process. Several improvements and further validation need to be done with technologies presented herein for accelerated implementation in real world applications.

First of all, work needs to be done on researching the benefits of using co-blowing agents in improving the foamability of plastics. Results from our research are promising and it is clear that co-blowing agents can create synergistic benefits to create low density foams with smaller cell sizes and higher cell densities. Since the two co-blowing agents usually have different critical pressures, they cannot be combined together in the commercially available MuCell process with one compressing unit. The Supercritical Gas-Laden Pellets Injection Molding Foaming Technology (SIFT) technology can be a cost effective way of achieving this objective effectively. The optimal ratio of co-blowing agents that can yield desirable properties such as small cell sizes and high cell densities, specifically for foaming TPU via the injection molding process, needs to be further studied and reported.

Second, SIFT has proven to be a good method for creating thermoplastic foamed parts using injection molding without being too capital intensive. One major limitation of the SIFT process is that the gas content is limited and slowly degrades over time via diffusion. Several studies regarding die geometry and quenching of the extrudate using liquid nitrogen have been conducted during the course of this research, which are not presented in this thesis. Initial results

are encouraging and the initial gas content and shelf life have been significant increased by these methods. Further work needs to be carried out in this area to propel SIFT toward faster acceptance in industry. Furthermore, it is known that for most thermoplastics, the solubility of gas increases with an increase in pressure and a decrease in temperature. An under-water pelletizer system for SIFT that can operate at high pressures can effectively cool and pelletize the extrudate without the gas coming out of solution at the end of the die. A system designed for this purpose could significantly overcome the short-comings of this novel process. Furthermore, pressurized canisters at room temperature have been previously shown to be able to maintain the dissolved gas in solution. Research in this area, with a practical outlook to its feasibility and acceptance by industry, can help propel SIFT as a favored technology for thermoplastic foaming in injection molding.

The use of core retraction to aid microcellular injection molding has shown tangible advantages in controlling cell nucleation and growth, as well as increasing the benefits of micro-cellular injection molding. Instead of a concurrent process of cell growth and melt strengthening, a sequential process of melt strengthening, followed by allowing the cells to grow, would enable control of the size of the microcells, especially at very high density reductions. Strengthening the melt at the time of nucleation and growth has been achieved in this research by different means such as by the incorporation of a cross-linking agent or nanoclay, or by lowering the melt temperature using core-retraction-aided processing. A pilot core-retraction mold was designed and manufactured in this research. Improvements and modifications to this mold, such as adding pressure and temperature sensors, a cavity viewing window, and a more accurate speed control

system for controlling the speed of core pull-back, would improve our understanding of this process and help realize the many benefits that it has to offer.

Finally, a novel 3-stage expansion process was invented to enable variable mechanical properties in a foamed injection molded TPU part by locally changing the density and microstructure within the part. This novel process is capable of creating parts with extremely low densities, while maintaining a desirable microstructure even at high density reductions. These benefits can be extremely useful for flexible foam OEM manufacturers where current manufacturing options entail tedious and elaborate processes of profiling from slab-stock or reaction injection molding. Proving the sturdiness and repeatability of this process for several real-life products can help propel this research further and make it commercially more attractive to OEM manufacturers.

It is hoped that the aforementioned approaches will help to increase the understanding of foaming TPU while highlighting strategies to effectively control the microstructure and mechanical properties in very low density foam-injection-molded TPU parts.

8 REFERENCES

1. SPI website. *The plastics industry trade association*. 2014 [cited 2014; Available from: http://www.plasticsindustry.org/AboutPlastics/.
2. Osswald, T.A., L.-S. Turng, and P.J. Gramann, *Injection molding handbook*. 2008: Hanser Verlag.
3. Website, S. 2014 [cited 2014; Available from: http://www.sprayfoam.com/newsarchives/.
4. Bledzki, A.K. and O. Faruk, Journal of Cellular Plastics, 2006. **42**(1): p. 63-76.
5. Colton, J.S.S., N. P.,, Polymer Engineering and Science, 1987. **27**(7): p. 3.
6. Colton, J.S.a.S., N. P.,, Polymer Engineering and Science. **27**(7): p. 485-492.
7. Heck, R.L., Journal of Vinyl and Additive Technology, 1998. **4**(2): p. 113-116.
8. Mizumoto, T., et al., Macromolecules, 2000. **33**(18): p. 6757-6763.
9. Sumarno, et al., Journal of Applied Polymer Science, 2000. **77**(11): p. 2383-2395.
10. Throne, J.L., *Thermoplastic foam extrusion: an introduction*. 2004: Hanser Verlag.
11. Heck, R.L. and W.J. Peascoe, Encyclopedia of Polymer Science and Technology, 2002.
12. Michaeli, W., et al. in *ANTEC Conference Proceedings*. 2008.
13. Sauceau, M., et al., Progress in Polymer Science, 2011. **36**(6): p. 749-766.
14. Kim, S., et al., Cellular polymers, 2006. **25**(1): p. 19-33.
15. Gale, M. in *ANTEC Conference Proceedings*. 2000.
16. Oliver Pfannschmidt, W.M. in *ANTEC Conference Proceedings*. 1999.
17. Peng, J., L.-S. Turng, and X.-F. Peng, Polymer Engineering & Science, 2012. **52**(7): p. 1464-1473.
18. Xu, J., *Microcellular injection molding*. Vol. 9. 2011: John Wiley & Sons.
19. Yeh, S.-K., et al., Polymer Engineering & Science, 2010. **50**(8): p. 1577-1584.
20. Wissinger, R.G. and M.E. Paulaitis, Journal of Polymer Science Part B: Polymer Physics, 1987. **25**(12): p. 2497-2510.
21. Seeler, K.A. and V. Kumar, Journal of Reinforced Plastics and Composites, 1993. **12**(3): p. 359-376.
22. Han, X., et al., Polymer Engineering & Science, 2003. **43**(6): p. 1261-1275.
23. Moon, Y., S.W. Cha, and J.-h. Seo, Polymer-Plastics Technology and Engineering, 2008. **47**(4): p. 420-426.
24. Park, C.B., *The role of polymer/gas solutions in continuous processing of microcellular polymers*, 1993, Massachusetts Institute of Technology: UMI Dissertations Publishing.
25. Di Maio, E., et al., Polymer Engineering & Science, 2005. **45**(3): p. 432-441.

26. Lee, J.W.S. and C.B. Park, Macromolecular Materials and Engineering, 2006. **291**(10): p. 1233-1244.
27. Mi, H.-Y., et al., Polymer Engineering & Science, 2014: p. n/a-n/a.
28. Nadella, K., V. Kumar, and W. Li, Advances in Building Technology, 2002. **1**: p. 121-128.
29. Costeux, S., Journal of Applied Polymer Science, 2014. **131**(23): p. n/a-n/a.
30. Gong, S., et al., International Polymer Processing, 2005. **20**(2): p. 202-214.
31. Kramschuster, A., et al., Polymer Engineering & Science, 2005. **45**(10): p. 1408-1418.
32. Kharbas, H.A., *Developments in microcellular injection molding technology*, 2003, University of Wisconsin--Madison.
33. Sun, X., *Novel injection molding foaming approaches using gas-laden pellets*, 2013, The University of Wisconsin-Madison.
34. Elkovitch, M.D., L.J. Lee, and D.L. Tomasko, Polymer Engineering & Science, 2001. **41**(12): p. 2108-2125.
35. Kwag, C., C.W. Manke, and E. Gulari, Journal of Polymer Science Part B: Polymer Physics, 1999. **37**(19): p. 2771-2781.
36. Trexel Inc. *Trexel Inc*. 2013 [cited 2014; Available from: http://www.trexel.com/en/.
37. Suh, N., *Innovation in Polymer Processing*. Hanser, Cincinnati. 1996.
38. Zhang, Z. and Y.P. Handa, Journal of Polymer Science Part B: Polymer Physics, 1998. **36**(6): p. 977-982.
39. Colton, J.S.a.S., N. P.,, Polymer Engineering & Science, 1987. **27**(7): p. 6.
40. Yeh, S.-K., et al., Journal of Cellular Plastics, 2013. **49**(2): p. 119-130.
41. Kun Chang Lin, C.-H.C., Hsin-Chih Peng, Chen-Feng Kuan, Hsu-Chiang Kuan. in *ANTEC Conference Proceedings*. 2012. SPE.
42. Kharbas, H., et al., Polymer Composites, 2003. **24**(6): p. 655-671.
43. Turng, L.S. and H. Kharbas, Polymer Engineering & Science, 2003. **43**(1): p. 157-168.
44. Turng, L.-S. and H. Kharbas. in *ANTEC Conference Proceedings*. 2004.
45. Lee, J., et al., Polymer, 2011. **52**(6): p. 1436-1446.
46. Sun, X., et al., Manufacturing Letters, 2014. **2**(2): p. 64-68.
47. Lee, J.a.T., L.-S.,. in *ANTEC Conference Proceedings*. 2009.
48. Sun, X. and L.-S. Turng *Foam injection molding using nitrogen and carbon dioxide as co-blowing agents*. Plastics Research Online, 2013.
49. Sun, X., H. Kharbas, and L.S. Turng, Polymer Engineering & Science, 2015. **55**(11): p. 2643-2652.
50. Hossieny, N.J., et al., Polymer, 2014. **55**(2): p. 651-662.
51. Mi, H.-Y., Jing, X., Turng, L.-S. and Peng, X.-F. in *ANTEC Conference Proceedings*. 2013.
52. Engels, H.W., et al., Angewandte Chemie International Edition, 2013. **52**(36): p. 9422-9441.

53. Maccari, B. and S. Mussini. in *Polyurethane World Congress*. 1999.
54. Ames, K.A., Rubber chemistry and technology, 2004. **77**(3): p. 413-475.
55. ASICS. *http://www.asics.no/running/knowledge/anatomy-of-a-running-shoe/*. 2015 2015 [cited 2015 2015]; Anatomy of running shoe].
56. O'Leary, K., K.A. Vorpahl, and B. Heiderscheit, Journal of the American Podiatric Medical Association, 2008. **98**(1): p. 36-41.
57. Hreljac, A., Medicine and Science in Sports and Exercise, 2004. **36**(5): p. 845-849.
58. Ito, S., et al., Journal of Applied Polymer Science, 2007. **106**(6): p. 3581-3586.
59. Nemat Hossieny, M.N., Mohamad Reza Barzegari, Chul Park. in *70th Annual Techical Conference of the Society of Plastics Engineers*. 2012. SPE.
60. Li, S., G. Gaudet, and J. Nair, ECS Journal of Solid State Science and Technology, 2013. **2**(3): p. P97-P103.
61. Prasad, A., G. Fotou, and S. Li, Journal of Materials Research, 2013. **28**(17): p. 2380-2393.
62. Michaeli, W. and R. Heinz, Macromolecular Materials and Engineering, 2000. **284-285**(1): p. 35-39.
63. Dai, C., et al., Polymer Engineering & Science, 2013. **53**(11): p. 2360-2369.
64. Nema, A.K., et al., Journal of Cellular Plastics, 2008. **44**(4): p. 277-292.
65. Mi, H.-Y., et al., Materials Science and Engineering: C, 2013. **33**(8): p. 4767-4776.
66. Tomasko, D.L., et al., The Journal of Supercritical Fluids, 2009. **47**(3): p. 493-499.
67. Michaeli, W., et al., Journal of Cellular Plastics, 2009. **45**(4): p. 321-351.
68. Yeh, S.-K. in *ANTEC Conference Proceedings*. 2015. Orlando, FL,.
69. Lin, K., et al., Society of Plastics Engineers Technical Papers, 2012. **78**: p. 155.
70. Mi, H.-Y., et al., Journal of Cellular Plastics, 2013. **49**(5): p. 439-458.
71. Mark, L., et al., Society of Plastics Engineers Technical Papers, 2015.
72. Lee, J., et al., Polymer Engineering & Science, 2011. **51**(11): p. 2295-2303.
73. Li, Q. and L.M. Matuana, Journal of applied polymer science, 2003. **88**(14): p. 3139-3150.
74. Martin, D.J., et al., Journal of applied polymer science, 1997. **64**(4): p. 803-817.
75. Eceiza, A., et al., Polymer Engineering & Science, 2008. **48**(2): p. 297-306.
76. Saniei, M., Hossieny, N.J., Ameli, A., Jahani, D. and Park, C.B. in *ANTEC Conference Proceedings*. 2013.
77. Sun, X. and L.S. Turng, Polymer Engineering & Science, 2014. **54**(4): p. 899-913.
78. Fleming, O.S. and S.G. Kazarian, *Polymer Processing with Supercritical Fluids*, in *Supercritical Carbon Dioxide*. 2006, Wiley-VCH Verlag GmbH & Co. KGaA. p. 205-238.
79. Wong, A., et al., The Journal of Supercritical Fluids, 2014. **90**: p. 35-43.
80. Qi, H.J. and M.C. Boyce, Mechanics of Materials, 2005. **37**(8): p. 817-839.

81. Silva, J., et al., Journal of Non-Newtonian Fluid Mechanics, 2014. **222**: p. 96-103.
82. Nasirzadeh, R. and A.R. Sabet, Journal of Cellular Plastics, 2014.
83. Voda, A., et al., Polymer Testing, 2006. **25**(2): p. 203-213.
84. Lu, Q.-W. and C.W. Macosko, Polymer, 2004. **45**(6): p. 1981-1991.
85. Rashmi, B.J., et al., Journal of Applied Polymer Science, 2013. **128**(1): p. 292-303.
86. Jing, X., et al., Journal of Cellular Plastics, 2014. **50**(4): p. 361-379.
87. Meissner, J., Polymer Engineering & Science, 1987. **27**(8): p. 537-546.
88. Rizvi, S., et al., Journal of Cellular Plastics, 2014. **50**(3): p. 199-219.
89. Lakes, R.S., *Viscoelastic materials*. 2009: Cambridge University Press.
90. Osswald, T.A. and G. Menges, *Materials science of polymers for engineers*. 3rd ed. 2012: Carl Hanser Verlag GmbH Co KG.
91. Wong, A. and C.B. Park, Chemical Engineering Science, 2012. **75**(0): p. 49-62.
92. Leung, S.N., et al., The Journal of Supercritical Fluids, 2012. **63**(0): p. 187-198.
93. Bhattacharya, S., et al., Polymer Engineering & Science, 2009. **49**(10): p. 2070-2084.
94. Lee, L.J., et al., Composites Science and Technology, 2005. **65**(15–16): p. 2344-2363.
95. Cao, X., et al., Polymer, 2005. **46**(3): p. 775-783.
96. Barick, A.K. and D.K. Tripathy, Applied Clay Science, 2011. **52**(3): p. 312-321.
97. Wang, X.-C., et al., Polymer Engineering & Science, 2016. **56**(3): p. 319-327.
98. Chaudhary, A.K., *Rheology modification and foaming of polypropylene- clay nanocomposites with coupling agents*, 2010.
99. Zwynenburg, J., *Predicting polyolefin foamability using melt rheology*, 2008.
100. Cox, W. and E. Merz, Journal of Polymer Science, 1958. **28**(118): p. 619-622.
101. Gong, L., S. Kyriakides, and N. Triantafyllidis, Journal of the Mechanics and Physics of Solids, 2005. **53**(4): p. 771-794.
102. Turng, L.-S. and H. Kharbas, International Polymer Processing, 2004. **19**(1): p. 77-86.
103. Kishbaugh, L. in *ANTEC* 2015. Orlando, FL.
104. Hyde, L. and L. Kishbaugh, International institute of connector and interconnection technology, Inc, 2003.
105. Nam, P.H., et al., Polymer Engineering and Science, 2002. **42**(9): p. 1907.
106. Sun, X., et al., Polymer, 2015. **56**(0): p. 102-110.
107. Doroudiani, S., C.B. Park, and M.T. Kortschot, Polymer Engineering & Science, 1998. **38**(7): p. 1205-1215.
108. Taki, K., et al., Polymer Engineering and Science, 2004. **44**(6): p. 1004-1011.
109. Naguib, H.E., et al., Polymer Engineering and Science, 2002. **42**(7): p. 1481.

110. Park, C.B. and L.K. Cheung, Polymer Engineering and Science, 1997. **37**(1): p. 1.

111. Ishikawa, T. and M. Ohshima, Polymer Engineering & Science, 2011. **51**(8): p. 1617-1625.

112. Ishikawa, T., K. Taki, and M. Ohshima, Polymer Engineering & Science, 2012. **52**(4): p. 875-883.

113. Rudolph, N. and T.A. Osswald, *Polymer Rheology: Fundamentals and Applications*. 2014: Carl Hanser Verlag GmbH Co KG.

114. Baird, D.G. and D.I. Collias, *Polymer processing: principles and design*. 2nd ed. 2014: John Wiley & Sons.